Author:
Tovey, S. N

Title:
A Study of the production of high energy Pi-mesons

A Study of the Production of High Energy Pi-mesons.

by

S.N.Tovey, B.A.

H.H.Wills Physics Laboratory,

University of Bristol.

A thesis submitted

to the

University of Bristol

for the

Degree of Doctor of Philosophy.

March 1964.

Preface.

This thesis describes a study of the production of π-mesons in the interactions of energetic cosmic rays. Most of the data presented in this thesis has been obtained from a direct study of interactions occuring in the detector or its surroundings. This method is complementary to the indirect method which has been carried out in this laboratory over the past six years and which involves the measurement of the energy spectra of γ-rays and nuclear particles at different heights in the atmosphere.

Chapter I contains a review of the theory of electromagnetic cascades which is essential for an understanding of the methods of energy measurement employed. The main experimental evidence presented in this thesis concerns the observation of γ-rays from the decay of π^{o}-mesons produced in high energy interactions. Chapter II describes the assembly in which these measurements were made, the methods by which the events were detected and by which their energies were estimated and the manner in which the rates of production of events were calculated. Chapter III presents a detailed analysis of the data on π^{o}-meson production which is examined interms of a simple phenomenological model proposed by Cocconi, Koester and Perkins.

The first part of Chapter IV describes measurements made on nuclear interactions occuring in the photographic emulsion of a number of detecting assemblies. In these interactions

the production of charged particles is studied in terms of the same model as above. A method of estimating the energy carried by these charged particles is derived. In the second part of Chapter IV possible production channels of the π-mesons are considered.

Finally Chapter V presents a brief survey of the theories of high energy inelastic interactions.

Contents.

List of Figures.

List of Plates.

List of Tables.

CHAPTER I.

The Interaction of Electromagnetic Radiation with Matter.

§ 1.1 Introduction

In this chapter the interactions of high energy electrons and γ-rays with matter are discussed. These occur between the incident γ-ray or electron and the coulomb fields of the nuclei and atomic electrons present in matter. The physics of these processes is discussed in detail, since an understanding of the theory of electromagnetic cascades is necessary to the developement of this thesis. The dominant processes at relativistic electron energies are the production of electron pairs by γ-rays and the production of γ-rays by the Bremsstrahlung of electrons. An electromagnetic cascade is generated by successive processes of pair production and Bremsstrahlung, the number of electrons and γ-rays in the cascade multiplying until their mean energy is so low that collision losses become important and prevent further developement.

The cross section for pair production and Bremsstrahlung have been calculated by Bethe and Heitler (1934), whose theory is discussed in § 1.2 - 1.7. The one-dimensional theory of cascades, as described by Rossi and Greisen (1941) and Rossi (1952), is given in § 1.8. This theory is later used to estimate the degradation in the energy of γ-rays between their production in the atmosphere and their detection by our assembly at a lower point in the atmosphere.

The three-dimensional theory of cascades, Nishimura and Kamata (1958), is described in § 1.9; this theory is utilised in determining the energy of electromagnetic cascades occuring in our detector.

§ 1.2 The Fundamental Processes.

γ-rays and electrons passing through matter interact with the coulomb fields of the nuclei and electrons present.

(a) In the processes of pair production and Bremsstrahlung the recoil momentum is taken up by the whole atom; these processes which dominate at high energies, are described in detail below.

(b) In the processes of electron-electron scattering and γ-ray-electron scattering the recoil momentum is given to a single electron which is ejected from its atom. The first of these interactions causes the well known ionization loss suffered by all charged particles in matter; the second interaction is known as Compton scattering. Both of these interactions can be neglected at energies $\gtrsim$ 1 Gev in air or $\gtrsim$ 100 Mev in lead. This is illustrated in Fig. 1.2 (a) which compares the total cross sections for pair production and Compton scattering of a γ-ray, and in Fig. 1.2 (b) which compares the rates of energy loss of an electron due to the processes of Bremsstrahlung and ionisation. The cross section for Crompton scattering was taken from the theory of Klein and Nishina (1929). The ionisation loss was calculated from the formulae of Møller (1932) for electron-electron

scattering and Bhabha (1936) for positron-electron scattering.

§ 1.3 Differential Cross Sections.

The first order diagrams representing the processes of pair production and Bremsstrahlung are given in Fig. 1.1 (a) and (b) respectively.

Fig. 1.1

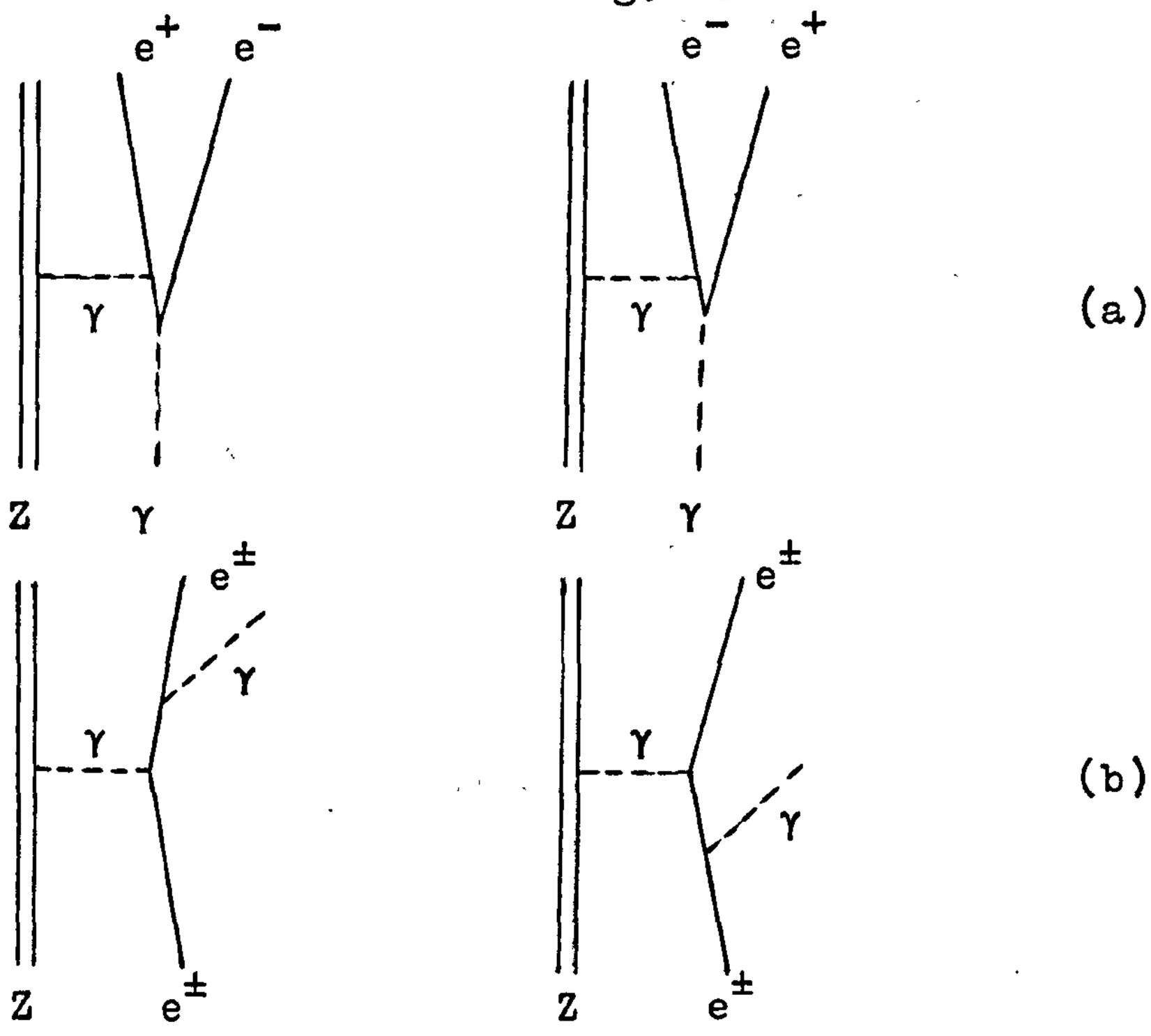

Both processes involve the exchange of a virtual photon between a heavy nucleus Z and an electron, and their cross sections are closely related. These cross sections have been calculated using first order perturbation theory in quantum electrodynamics by Bethe and Heitler (1934). The notation used below is that of Rossi (1952).

N = Avagadro's number.

A = Atomic weight of the material.

Z = Atomic number of the material.

m = Mass of the electron.

r_e = Classical radius of the electron (e^2/mc^2).

α = Fine structure constant ($e^2/\hbar c$).

The cross sections $\varphi(E,E')$ represent the differential probability that the incident particle, energy E, radiates a particle in the energy range (E',dE') per gram per square centimeter of material. They have been calculated assuming the validity of the Born approximation. This is a good approximation provided that $Z \ll 1/\alpha$; a correction for high values of Z is discussed later (§ 1.6)

(a) Bremsstrahlung

$$\varphi_{rad.}(E,E') = 4\alpha \frac{N}{A} Z^2 r_e^2 \frac{dE'}{E'} F(E,v) \qquad (1.1)$$

where E = Energy of incident electron

E' = Energy of radiated γ-ray

$v = E'/E$

(b) Pair production

$$\varphi_{pair}(E,E') = 4\alpha \frac{N}{A} Z^2 r_e^2 \frac{dE'}{E} G(E,v) \qquad (1.2)$$

where E = Energy of incident γ-ray

E' = Energy of one of the electrons

$v = E'/E$

The functions $F(E,v)$ and $G(E,v)$ are calculated taking into account the screening of the nuclear charge by the surrounding atomic electrons.

§ 1.4 Effects of Screening.

At large distances from the nucleus the electric field differs from that due to a point charge. Bethe and Heitler (1934) replaced the charge Z by the expression $(Z - F(\underline{q}))$ where $F(\underline{q})$ is the well known atomic form factor:

$$F(\underline{q}) = \int \rho(\underline{r})\, e^{\frac{i}{\hbar c}\, \underline{q}\cdot\underline{r}}\, d\underline{r} \qquad (1.3)$$

$\underline{q}$ = Momentum transfered in the collision

$\rho(\underline{r})$ = Density of electrons at radius $\underline{r}$,

$F(\underline{q})$ becomes comparable to Z when $\underline{q}/\hbar c$ is of the order of (or smaller than) the reciprocal atomic radius. In the Fermi theory of the atom the atomic radius is given approximately by $a_o Z^{-1/3}$, $a_o = \frac{\hbar^2}{me^2}$ being the radius of the hydrogen atom. The screening of the nuclear charge is therefore effective if

$$q \lesssim Z^{1/3}\, \frac{mce^2}{\hbar} = (mc^2)\, Z^{1/3} \alpha \qquad (1.4)$$

Consider now the processes of pair production and Bremsstrahlung.

E_o = Energy of γ-rays.

E_1, E_2 = Energies of the two electrons.

It is easily shown that the minimum momentum transfer is

$$q_{min} = (mc^2)^2\, \frac{E_o}{2E_1 E_2}$$

For equipartition of energy this becomes

$$q_{min} \approx \frac{(mc^2)^2}{E}$$

where E is the energy of the incident γ-ray in pair production or of the incident electron in Bremsstrahlung. For $E \gg m$ the processes of pair production and Bremsstrahlung take place almost spontaneously and the momentum transfer is negligible. The condition (1.4) for complete screening now becomes

$$E \gg \frac{(mc^2)}{\alpha Z^{1/3}} \qquad (1.5)$$

Classically the significance of this relation is that large incident energies produce small momentum transfers, which correspond to large impact parameters; at these large distances from the nucleus the screening by the atomic electrons is effective. Numerically condition (1.5) corresponds to

$$E \gg 35 \text{ Mev for air}$$

$$E \gg 17 \text{ Mev for Lead or Tungsten}$$

for complete screening, according to Bethe and Heitler, the functions F(E,v) and G(E,v) of § 1.3 are both independent of E.

$$F(E,v) = \left[1 + (1-v)^2 - \frac{2}{3}(1-v)\right] \ln(183Z^{-1/3}) + \frac{1}{9}(1-v)$$

$$G(E,v) = \left[v^2 + (1-v)^2 + \frac{2}{3}v(1-v)\right] \ln(183Z^{-1/3}) - \frac{1}{9}v(1-v)$$

(1.6)

§ 1.5 Total Cross Sections.

(a) Pair production.

From equations (1.2) and (1.6) the total cross section for pair production per gm./cm^2. of matter is given in the asymptotic limit of complete screening by

$$\mu_{pair} = 4\alpha \frac{N}{A} Z^2 r_e^2 \frac{1}{E} \int_0^{E-2mc^2} G(E,v)dE'$$

$$\therefore \quad \mu_{pair} = 4\alpha \frac{N}{A} Z^2 r_e^2 \left[\frac{7}{9} \ln(183Z^{-1/3}) - \frac{1}{54}\right] \qquad (1.7)$$

It is convenient to measure lengths in units of the radiation length, X_o, which is defined by

$$\frac{1}{X_o} = 4\alpha \frac{N}{A} Z^2 r_e^2 \ln (183Z^{-1/3}) \qquad (1.8)$$

The total probability of pair production per radiation length is

$$\mu_o = \frac{7}{9} - \frac{b}{3}$$

where $b = \dfrac{1}{18 \ln (183Z^{-1/3})}$ is a very slowly varying function of Z, which may be taken as 0.0135 for all elements with $Z \geqslant 4$.

Fig 1.2(a) shows the total cross section for pair production per radiation length in lead. Note how it approaches the asymptotic limit of $\mu_o \approx \frac{7}{9}$ for the case of complete screening. The conversion length for γ-rays

Fig 1.2(a).

The total cross sections per radiation length for Compton scattering and pair production by a γ-ray in lead are shown as a function of the γ-rays energy.

Fig 1.2(b).

The curves show the variation with energy of the fractional energy loss per radiation length through electron-electron scattering and Bremsstrahlung for an electron traversing lead and air.

Both these figures are taken from Rossi (1952).

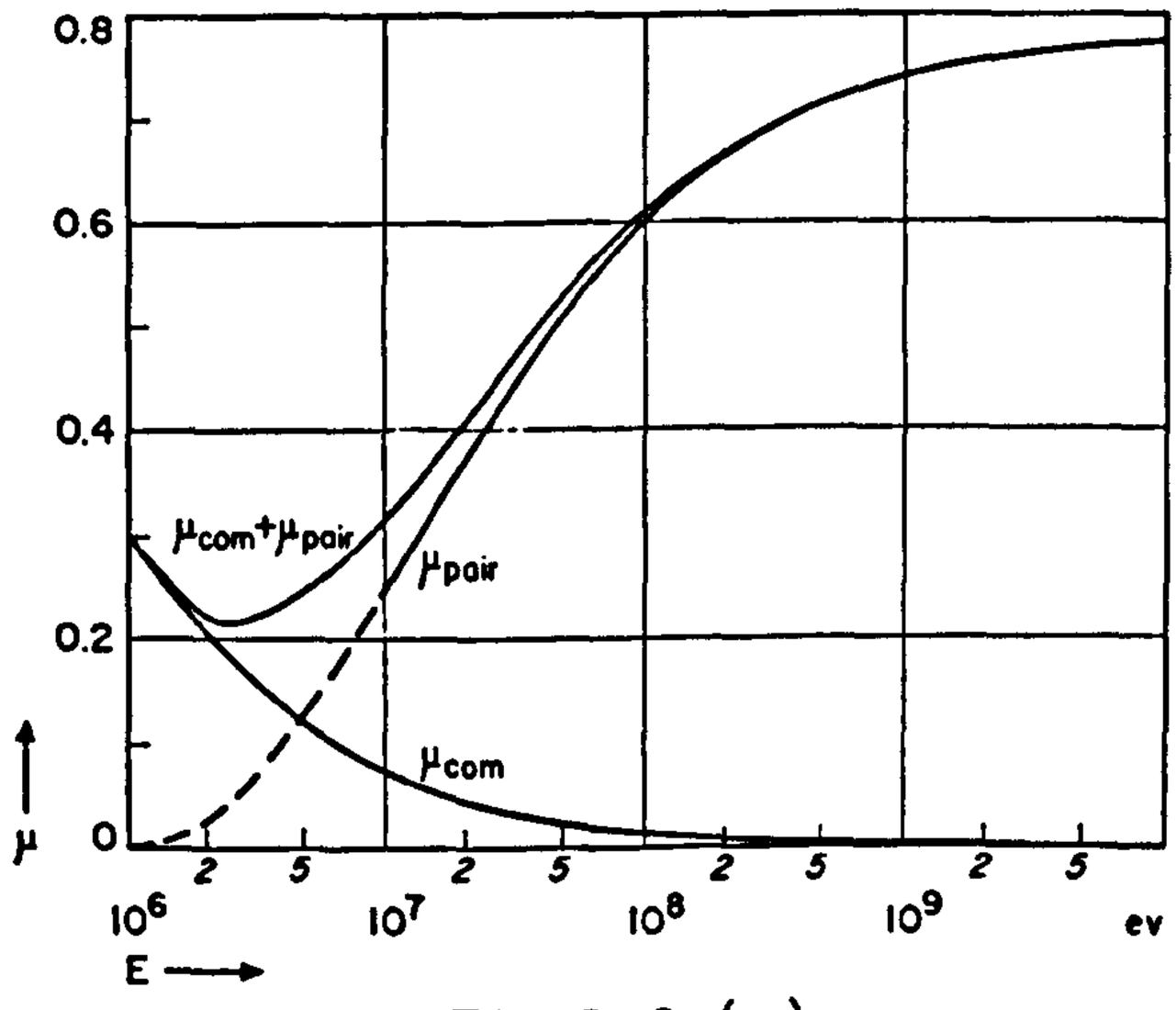

Fig 1.2 (a)

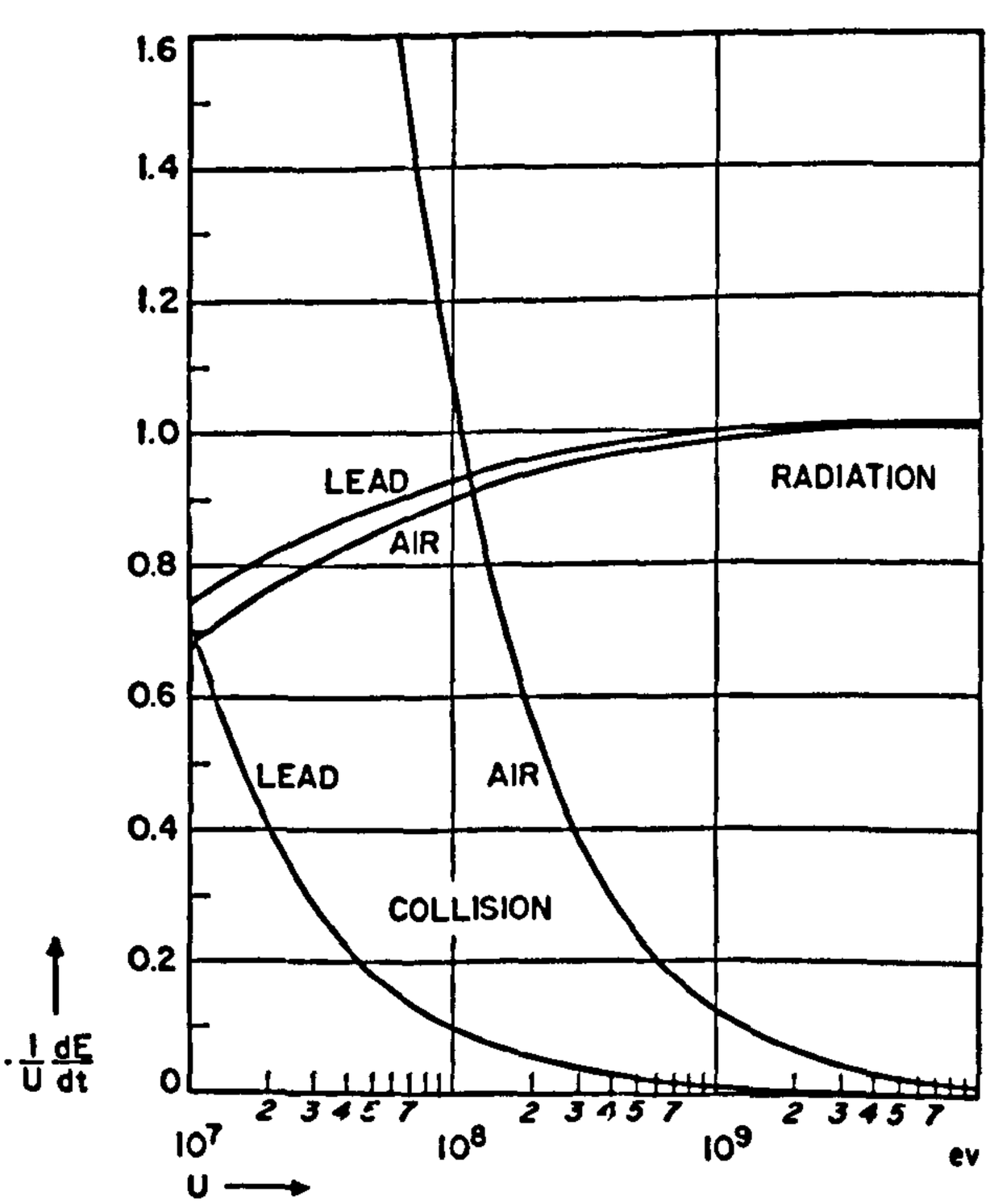

Fig 1.2 (b)

is

$$X_c = \frac{X_o}{\frac{7}{9} - \frac{b}{3}} \approx \frac{9}{7} X_o$$

A beam of high energy γ-rays passing through matter is attenuated exponentially by pair production with a characteristic length equal to the conversion length.

For comparison the total cross section for Compton scattering is also shown in Fig 1.2(a).

(b) Bremsstrahlung

From equations (1.1) and (1.6) the total energy radiated by a relativistic electron per gm./cm.^{2} of matter is

$$-\left(\frac{dE}{dx}\right) = 4\alpha \frac{N}{A} Z^2 r_e^2 \int_o^E F(E,v)dE'$$

$$= 4\alpha \frac{N}{A} Z^2 r_e^2 \, E\left[\ln(183Z^{-1/3}) + \frac{1}{18}\right] \qquad (1.9)$$

If we measure lengths in terms of the radiation length, X_o defined in (1.8) above, then the energy loss becomes

$$-\left(\frac{dE}{dt}\right) = E(1 + b) \qquad (1.10)$$

Fig 1.2(b) shows the fractional energy loss per radiation length for an electron of energy E traversing lead or air. At high energies the condition for complete screening is satisfied and both curves approach the asymptotic limit, which is close to unity. The rates of energy loss by collision processes are shown for comparison.

§ 1.6 Corrections to the above formulae.

Two corrections are necessary to the formulae given above.

(a) In deriving the differential cross sections the validity of the Born approximation was assumed, i.e. the incoming and outgoing electrons were represented as plane waves, the atomic field being considered as a perturbation. This approximation is valid provided $\frac{Ze^2}{\hbar c} < 1$. When $Z \sim 137$ second order terms must be considered. Recently Bethe and Maximon (1954) and Handel Davies et al (1959) have performed new calculations without making use of Borns approximation. These calculations were checked by Malamud (1959) in an experiment on the absorption of 1 Gev γ-rays in various elements and the results were in agreement. According to these results the radiation length, X_o, should be increased by a factor

$$(1 + 0.12(\frac{Z}{82})^2)$$

(b) Wheeler and Lamb (1934) have shown that the processes of pair production and Bremsstrahlung can take place in the field of an atomic electron, with the recoil momentum being taken up by the whole atom. This can occur only if the momentum transfered to the electron is insufficient to eject the electron from its atom. It was shown, § 1.4, that the momentum transfer at high energies is $q \sim \frac{m^2}{E}$. If the electron were free this would correspond to a kinetic energy of $\frac{m}{2}(\frac{m}{E})^2$ which, for $E \sim 1$ Gev, is approximately 0.05 ev. This energy is much less than the ionisation potential of all atoms, and so the recoil momentum will be taken up by the

whole atom. This effect can be allowed for by replacing Z^2 with $Z(Z+1)$ in the expressions for the differential cross sections per gm./cm^2 of matter, (1.1) and (1.2). More conveniently, Z^2 may be replaced by $Z(Z+1)$ in expression (1.8) for the radiation length; the cross sections per radiation length calculated above are then left unchanged.

The amended value of the radiation length after both these corrections have been applied is

$$\frac{1}{X_o} = 4\alpha \frac{N}{A} Z(Z+1) r_e^2 \ln(183Z^{-1/3})\left[1+0.12\left(\frac{Z}{82}\right)^2\right]^{-1} \qquad (1.11)$$

The radiation length in a composite material is given by

$$\frac{1}{X_o} = \sum_i \frac{p_i}{X_i} \qquad (1.12)$$

p_i, X_i are the fractional weight and radiation length of each element present.

§ 1.7 Summary.

It will be useful here to summarize the theory presented above.

(a) In the limit of high energies and complete screening the processes of pair production may be represented by single cross sections, independent of the nature of the medium, provided that distances are measured in units of the radiation length, X_o, defined by equation (1.11).

(b) The radiation length can be thought of as that distance in which the energy of an electron and the intensity of a

γ-ray beam are attenuated by a factor ≈ e.

(c) The differential probabilities per radiation length that an electron with energy E radiate a γ-ray of energy vE, or that a γ-ray of energy E produce an electron of energy vE, are both independent of E and are given by

$$\varphi_{rad}(v)\,dv = \frac{1}{v}\left\{ 1 + (1-v)^2 - \left(\frac{2}{3}-2b\right)(1-v) \right\} dv$$

$$\varphi_{pair}(v)\,dv = \left\{ v^2 + (1-v)^2 + \left(\frac{2}{3}-2b\right)v(1-v) \right\} dv \qquad (1.13)$$

§ 1.8 Electromagnetic Cascades in One Dimension

The equations describing the one-dimensional developement of electromagnetic cascades have been solved by several authors. The notation used here is that given by Rossi (1952). Under Approximation A, losses of energy by collision processes and the Compton effect are neglected and pair production and Bremsstrahlung are treated under the approximation of complete screening. Degradation of energy continues until the individual γ-ray and electron energies are so low that the approximation is no longer valid. The assumption of complete screening imposes the condition that $E > \frac{(mc^2)}{\alpha Z^{1/3}}$ but in practice the approximation is considered to be valid for $E > \frac{mc^2}{2\alpha Z} = \frac{35}{Z}$ Mev since above this energy the screening is almost complete and the departure of the cross sections from the asymptotic limit is slow, see Fig 1.2. Since the cascades considered in this thesis have energies usually

well in excess of 50 Gev, this approximation is clearly valid.

Let $\pi(E,t)$ and $\gamma(E,t)$ be the differential energy spectra of electrons and γ-rays respectively at a distance t(r.l.) from the origin of the cascade. π and γ are related to the cross sections for pair production and Bremsstrahlung by the equations

$$\frac{\partial \pi(E,t)}{\partial t} = -\pi(E,t) \int_0^E \varphi_{rad}(E,E')dE' + \int_E^\infty \pi(E',t)\, \varphi_{rad}(E,E'-E)dE'$$

$$+ 2 \int_E^\infty \gamma(E',t)\, \varphi_{pair}(E',E)dE' \qquad (1.14a)$$

$$\frac{\partial \gamma(E,t)}{\partial t} = -\gamma(E,t) \int_0^E \varphi_{pair}(E,E')dE' + \int_E^\infty \pi(E',t)\, \varphi_{rad}(E',E)dE' \qquad (1.14b)$$

These equations form a set of linear integro-differential equations, often refered to as the diffusion equations.

They may be written as

$$\frac{\partial \pi}{\partial t} = A\pi + B\gamma$$

$$\frac{\partial \gamma}{\partial t} = C\pi + D\gamma \qquad (1.15)$$

A,B,C,D are linear integral operators, operating on the energy variable of the functions $\pi(E,t)$ and $\gamma(E,t)$. The

equations (1.15) have seperable stationary solutions of the form

$$\pi(E,t) = aE^{-(s+1)}\, e^{\lambda(s)t} \;,\; \gamma(E,t) = bE^{-(s+1)}\, e^{\lambda(s)t}$$

Substituting in equations (1.14) we obtain

$$\lambda a = -A(s)a + B(s)b$$

$$\lambda b = C(s)a - \mu_o b \qquad (1.16)$$

where $A(s) = \int_0^1 \left[1 - (1-v)^s\right] \varphi_{rad}(v)dv$

$$B(s) = 2\int_0^1 v^s\, \varphi_{pair}(v)dv$$

$$C(s) = \int_0^1 v^s\, \varphi_{rad}(v)dv$$

$$\mu_o = \int_0^1 \varphi_{pair}(v)dv$$

A(s), B(s), C(s) and μ_o may be simply found using the expressions for the differential cross sections given above in equation (1.13). To obtain a solution of the simultaneous equations (1.16) λ must satisfy the quadratic equation

$$\left[\lambda + A(s)\right]\left[\lambda + \mu_o\right] - B(s)C(s) = 0.$$

Hence, for every value of the exponent s, there exist two values of the attenuation length, λ, and two values of the ratio a/b given by

$$\frac{a_1}{b_1} = \frac{\mu_o + \lambda_1(s)}{c(s)}$$

$$\frac{a_2}{b_2} = \frac{\mu_o + \lambda_2(s)}{c(s)}$$

Tables of A(s), B(s), C(s), μ_o, $\lambda_1(s)$ and $\lambda_2(s)$ are given by Rossi (1952). C(s) is always positive and $\lambda_1(s) > -\mu_o > \lambda_2(s)$ so that a_1/b_1 is always positive; a_2/b_2 is always negative and cannot alone represent a physical solution.

The most general solution of this form is a linear combination

$$\pi(E,t) = E^{-(s+1)} \left\{ a_1 e^{\lambda_1(s)t} + a_2 e^{\lambda_2(s)t} \right\}$$

$$\gamma(E,t) = E^{-(s+1)} \left\{ \frac{a_1 C(s)}{\mu_o+\lambda_1(s)} e^{\lambda_1(s)t} + \frac{a_2 C(s)}{\mu_o+\lambda_2(s)} e^{\lambda_2(s)t} \right\} \qquad (1.17)$$

a_1 and a_2 may be chosen to satisfy the boundary conditions.

This is a solution of the one-dimentional shower problem under Approximation A for an incident radiation consisting of γ-rays and/or electrons distributed in energy according to the same power law. Since $\lambda_1(s) > -\mu_o > \lambda_2(s)$ the term in a_2 is attenuated more rapidly than that in a_1 so that at large depths, t, the attenuation is exponential and the ratio of γ-rays to electrons is constant and independent of their initial proportions.

Two special cases are of interest:

(a) $a_2 = 0$; the cascade is attenuated exponentially at all depths and the initial ratio of γ-rays to electrons is preserved throughout

$$\frac{\gamma(E,t)}{\pi(E,t)} = \frac{\gamma(E,0)}{\pi(E,0)} = \frac{C(s)}{\mu_0+\lambda_1(s)}$$

(b) $a_1 = -a_2$; equation (1.17) then describes a cascade initiated by a source of γ-rays only. This solution will be of use later (Chapter 2).

Solutions of this type cannot describe the case when the cascade is initiated by a single γ-ray or electron. A solution can be obtained by summing over many such stationary solutions

$$\pi(E,t) = \int_s n(s)\pi(E,t,s)ds \quad \text{etc.}$$

where $\pi(E,t,s)$ is the stationary solution with index s. This problem is solved by considering the diffusion equations in the Mellin Transforms of $\pi(E,t), \gamma(E,t)$ given by

$$m_\pi(s,t) = \int_0^\infty E^s\pi(E,t)dE \qquad \text{etc.}$$

where s is a complex parameter.

§1.9 Electromagnetic Cascades in Three Dimensions.

Calculations on the structure of cascades in three dimensions have been made by Nishimura and Kamata (1952,1958) and Pinkau (1958). Electrons in a shower traversing matter suffer deflections in the Coulomb fields of the nuclei and atomic electrons. Except at the very beginning of the shower, deflections due to the processes of pair production and Bremsstrahlung are negligible compared with those from Coulomb scattering. Three-dimensional cascade theory can be constructed from the one-dimensional theory described in §1.8 by the addition of two hypotheses.

(a) The electrons suffer a constant energy loss due to ionization, which is independent of the energy of the electron and is equal to ϵ Mev per radiation length. ϵ is called the critical energy and is defined as that electron energy at which the rate of energy loss per radiation length is equal to electrons energy. ϵ is approximately 8 Mev in lead and 80 Mev in air.

(b) The probability per radiation length that an electron be scattered through an angle $\underline{\theta}$ is $\sigma(\underline{\theta})d\underline{\theta}$.

The one-dimensional diffusion equations (1.15) are modified to give

$$\frac{\partial \pi}{\partial t} + \underline{\theta}\cdot\frac{\partial \pi}{\partial \underline{r}} = A\pi + B\gamma + G\pi - \epsilon\frac{\partial \pi}{\partial E}$$

$$\frac{\partial \gamma}{\partial t} + \underline{\theta}\cdot\frac{\partial \gamma}{\partial \underline{r}} = C\pi + D\gamma \qquad (1.18)$$

$\pi(E,\underline{r},\underline{\theta},t)dE\ d\underline{r}\ d\underline{\theta}$ and $\gamma(E,\underline{r},\underline{\theta},t)dE\ d\underline{r}\ d\underline{\theta}$ are the average number of electrons and γ-rays respectively with energy in the range (E,dE), travelling at a distance $(\underline{r},d\underline{r})$ and at an angle $(\underline{\theta},d\underline{\theta})$ from the cascade axis at a depth t from the origin of the shower.

A,B,C and D are the same integral energy operators which appeared in equation (1.15); the term in ϵ represents the constant ionisation loss; the terms in $\underline{\theta}.\frac{\partial}{\partial \underline{r}}$ represent the constant drift from the axis of a particle at angle $\underline{\theta}$; the term $G\pi$ describes the electron scattering and is discussed below.

G is an integral operator, operating on the variable $\underline{\theta}$ of $\pi(E,\underline{r},\underline{\theta},t)$ and given by

$$G\pi = \int_{-\infty}^{\infty} \sigma(\underline{\theta}-\underline{\theta}')\pi(\underline{\theta}')d\underline{\theta}' - \int_{-\infty}^{\infty} \sigma(\underline{\theta}')\pi(\underline{\theta})d\underline{\theta}' \qquad (1.19)$$

Williams (1939) made the approximation that $\sigma(\underline{\theta})$ is given by the Rutherford formula, (1.20), within the limits $\theta_{min}<\theta<\theta_{max}$ and is zero outside these limits.

$$\sigma(\underline{\theta})d\underline{\theta} = \frac{1}{4\pi\ \ln(183Z^{-1/3})}\left(\frac{E_s}{E}\right)^2 \frac{d\underline{\theta}}{\underline{\theta}^4} \qquad (1.20)$$

where $E_s^2 = 4\pi\frac{(mc^2)^2}{\alpha}$, $E_s = 21$ Mev.

He estimated θ_{min}, θ_{max} from considerations of shielding and of the size of the nucleus, and by expanding the integrals in equation (1.19) as Taylor series and neglecting second

order terms, obtained the relation

$$G\pi \approx \frac{E_s^2}{4E^2} \nabla_\theta^2 \pi$$

This approximation is known in cascade theory as the Landau approximation. Higher moments of the Rutherford cross section have been neglected and thus the contributions from plural and single scattering have not been included. Solutions derived under this approximation may be in error at both small and large angles.

Nishimura and Kamata (1958) succeeded in solving the diffusion equations without invoking the Landau approximation. They took Mellin transforms in E and Fourier transforms in $\underline{r}$ and $\underline{\theta}$ and employed the scattering theory of Molière (1948). As above $\sigma(\underline{\theta})$ was taken to equal the Rutherford formula, (1.20), within the limits $\theta_{min}<\theta<\theta_{max}$ but the cross section outside these limits was not set equal to zero but was calculated from the Thomas-Fermi model of the atom. Their solution for the total number of electrons, of all energies, within a radius $R\mu$ from the axis of a cascade initiated by a single γ-ray was expressed as a series.

$$N(E_o,R,t) = \frac{1}{2\pi i}\int_{-i\infty}^{i\infty} ds \frac{\Gamma(1-1/2s)}{s} \left(\frac{E_o R}{KX_o}\right)^s M(-1/2s,0,0,s,t) + \ldots. \qquad (1.21)$$

E_o = Energy of initiating γ-ray

X_o = Radiation length of the medium.

K is a very slowly varying function of the medium and is closely related to E_s in the Rutherford formula (1.20). It is equal to 19.1 for lead and 19.3 for air.

M is a slowly varying function obeying a difference relation which may be solved using the 'saddle-point' method. The solution is valid for $R \ll X_o$. Very recently Pinkau (1964) has estimated the upper limit of R for which this solution is valid. This limit depends on the energy and age of the cascade. For cascades initiated by γ-rays with energies of about $10^3 - 10^4$ Gev, at depths of 6 - 10 radiation lengths from their origin, the upper limit is estimated as $R \approx 2.10^{-2}X_o$.

The first term in the series given above is, except for the small difference between K and E_s, the solution obtained using the Landau approximation. The second term in the series is the contribution from single scattering and some of the plural scattering. Additional terms are contributed to by the remainder of the plural scattering. It should be especially noted that the solution is a function only of the variables t and $Z_o = {}^{E_o R}/_{X_o}$; this property is extremely valuable since it allows solutions for different values of E_o, X_o etc. to be found by using a simple scaling procedure.

Numerical values derived from equation (1.21) have been given in the tables of Nishimura and Kidd (1960). These calculations were made so that the results were accurate to within a few percent, even for small values of t; the results are summarized in Figs. 1.3 and 1.4. Fig. 1.3 shows the number of electrons within a radius $R(\mu)$ plotted as a

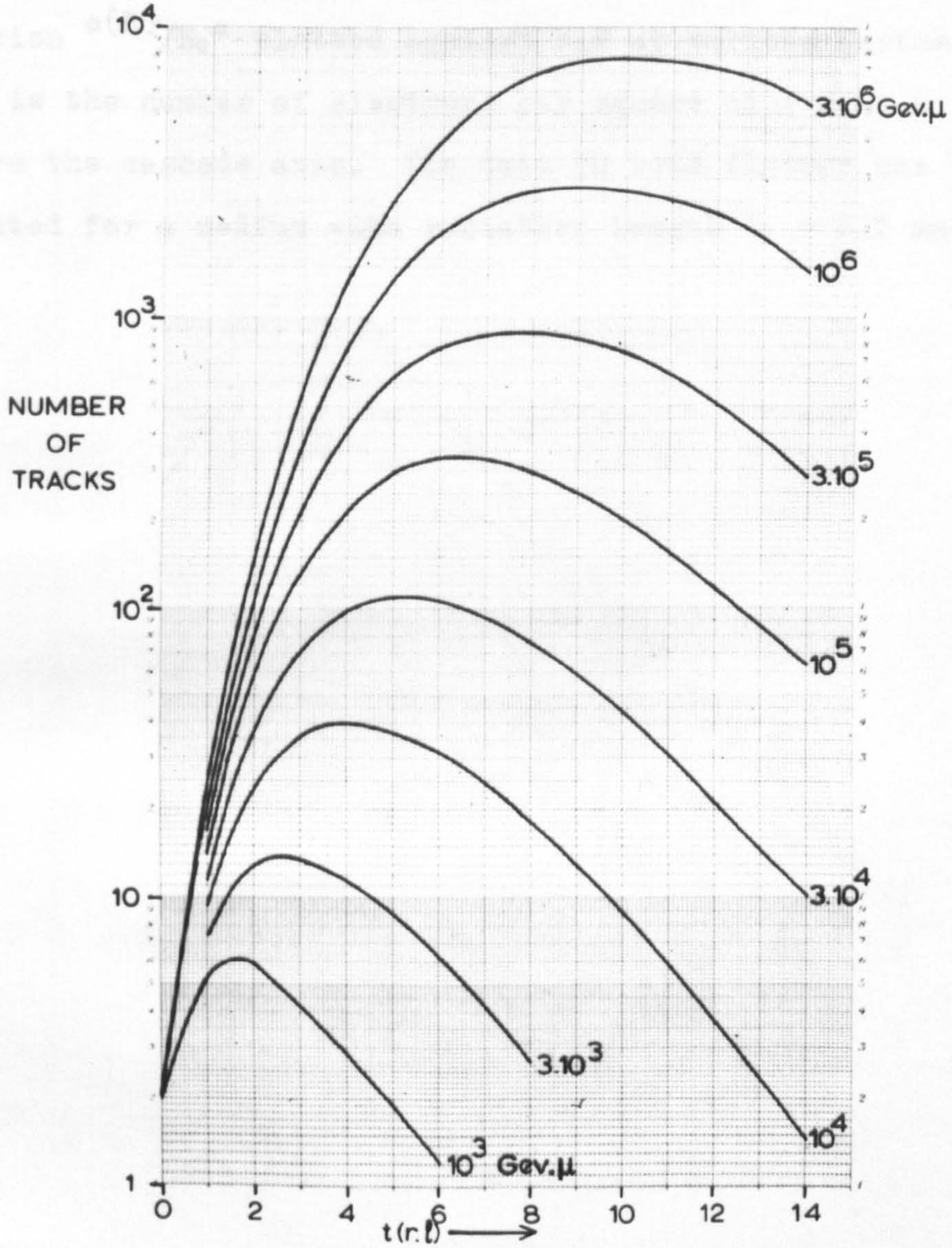

Fig 1.3.

The Integral Lateral Distribution of Electrons in an Electromagnetic Cascade for various values of $E_o.R$ (X_o = 6.2 mm.).

function of the depth t (r.l.) for various values of $E_o.R$ (Gev.μ). Fig 1.4 shows the electron lateral distribution function $\rho(R)/E_o^2$ plotted against E_oR at various depths. $\rho(R)$ is the number of electrons per square micron at a radius R from the cascade axis. The data in both figures has been computed for a medium with radiation length X_o = 6.2 mm.

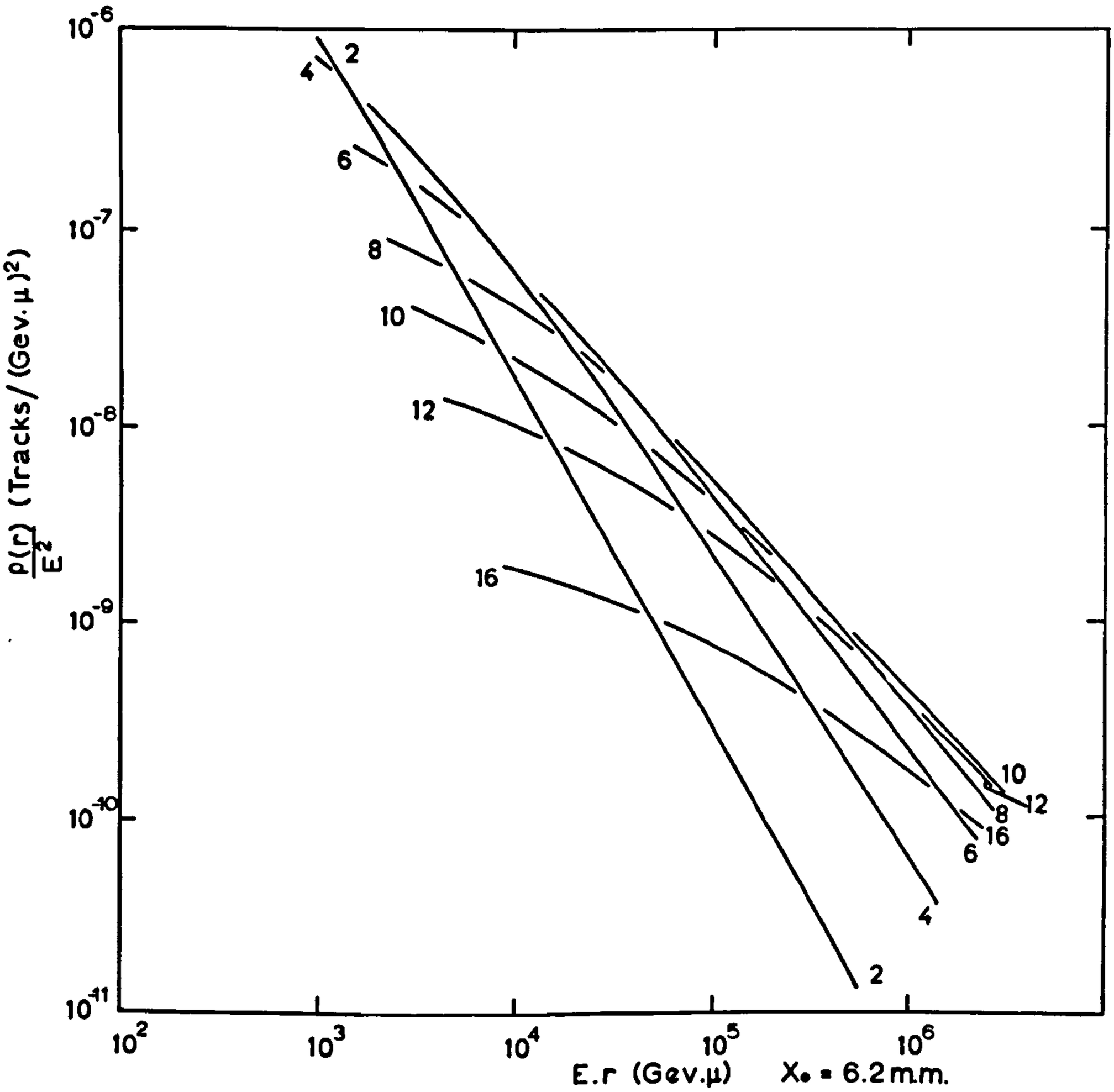

Fig 1.4.

The Differential Lateral Distribution of Electrons as a function of $E_o.R$ for various depths (radiation lengths) from the origin of the cascade.

CHAPTER II

The Analysis of the Indian Stack.

§ 2.1 Introduction.

The measurements which are described in the next two chapters were made in an assembly known as the Indian Stack which was flown on a polythene balloon near the top of the atmosphere. In this chapter the design and exposure of the assembly and the initial stages of its analysis will be discussed in detail.

This experiment was one of a series performed in this laboratory to study the interactions of high energy cosmic ray particles in the atmosphere. Previous assemblies have been exposed at balloon and aircraft altitudes and another exposure in an aircraft is being undertaken at the present time. The detectors used in these experiments, although differing in detail, have a common basic design. They employ alternate layers of photographic emulsion and a heavy metal to detect, and measure the energies of, high energy γ-rays arising from nuclear interactions both in the detector and in the atmosphere above it. γ-rays passing through the detector initiate electromagnetic cascades consisting of large numbers of electrons and γ-rays; the cascade is detected by means of the tracks in the photographic emulsion caused by these electrons. As was described in chapter I, the rapidity of developement of electromagnetic cascades is governed by the radiation length, equation (1.11), of the medium. The layers of emulsion are interleaved with sheets of metal, such as

lead or tungsten, in order to shorten the overall radiation length in the detector. The developement of the cascades is correspondingly condensed which renders them easier to detect and analyse.

The purpose of the Indian Stack was to study high energy interactions in two ways:

(1) By measureing the fluxes of γ-rays and nuclear active particles near the top of the atmosphere and by comparing these fluxes with each other and with other data, such as the fluxes at different altitudes or the flux of μ-mesons at sea level.

(2) By studying in detail individual nuclear interactions occuring in a thin layer of graphite, which surrounded the detector and was separated from it by about 12 cms. γ-rays from interactions in this producing layer arrived at the detector with sufficient spatial separation for their energies to be individually determined.

This thesis will be concerned mainly with the latter method; a discussion of the former method is being presented by another author (Miss V.M.Mayes).

§ 2.2 Design of the Detector

The detector was made up of 20 vertical sheets of photographic emulsion and 20 sheets of heavy metal, arranged alternately. The face area was 122 cm. x 61 cm.. Each emulsion layer consisted of Ilford G-5 stripped emulsions, 600μ thick. The central 18 metal sheets consisted of 1.60 mm. thick sheets of G.E.C. Heavy Metal Alloy (90% Tungsten, 7.5% Nickel, 2.5%

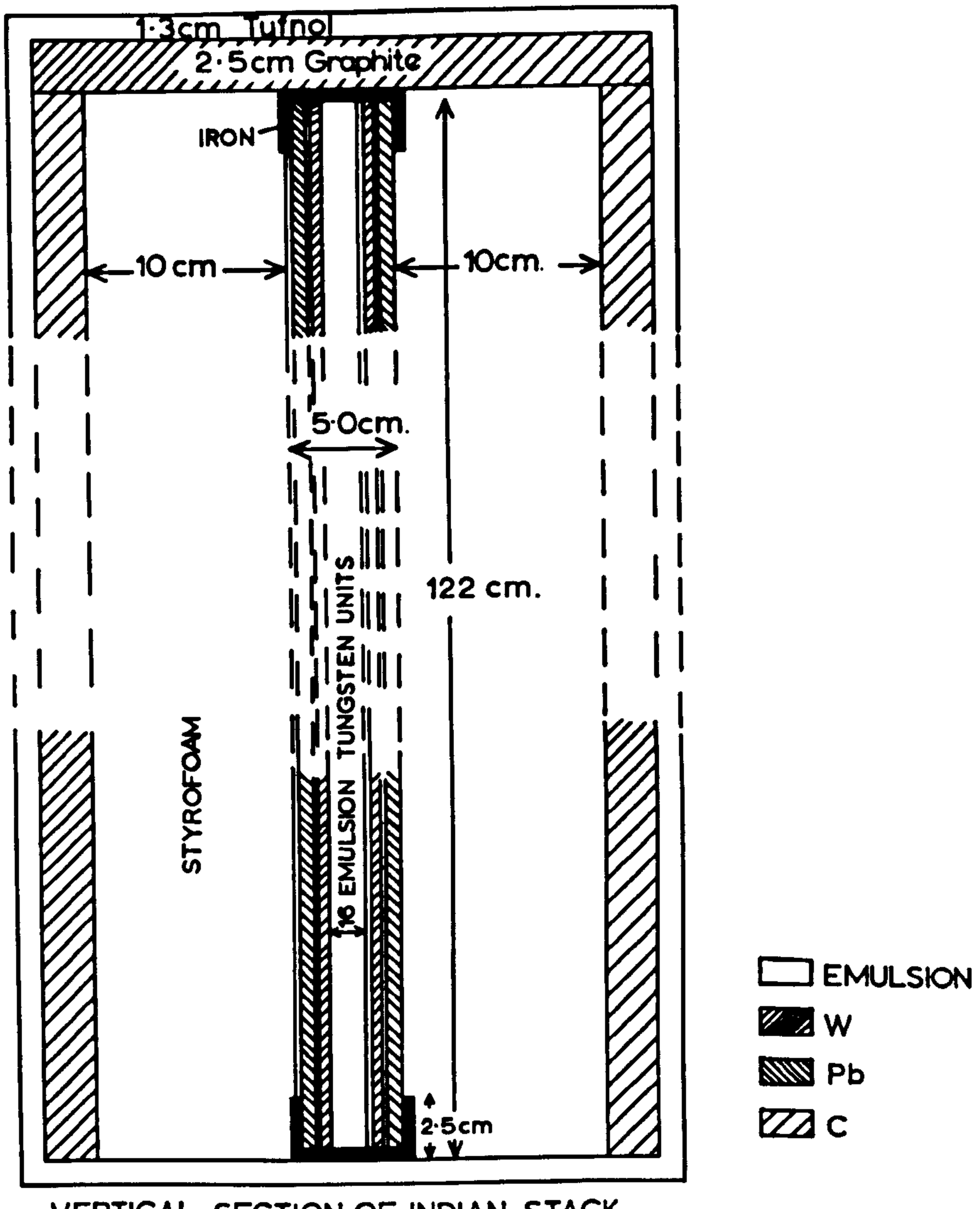

VERTICAL SECTION OF INDIAN STACK

Fig 2.1.

Copper) while the outermost metal layer on either side of the detector was made of lead, 2.5 mm. thick. The metal and emulsion layers were separated by thin polythene sheets, 60μ thick; because of a small packing loss the repeat distance in the central section of the detector was 2.4 mm.. The layers of the detector were held in position by an iron 'picture frame' which overlapped the face by 2.5 cm. on all sides, see Fig 2.1.

Using equations (1.11) and (1.12) values of the electromagnetic radiation length, X_o, were computed for the detector. These values are given in Table 2.1.

Also shown in Table 2.1 are values of the geometrical interaction length in the detector. These have been calculated using the relation

$$\lambda_i = \frac{A}{N\sigma_i} \quad \text{gm./cm.}^2$$

where N is Avagradro's Number, A is the atomic weight of the material and $\sigma_i = \pi R^2$ where R is the radius of the nucleus, which is given in the uniform density model as $R = r_o A^{1/3}$. r_o was taken as 1.28×10^{-13} cm. after several authors, especially Williams (1955).[7]

Values of the interaction length can also be calculated allowing for the transparency of nuclear matter; these values are a little higher than the geometrical values. The difference is too small to be detected experimentally except for $A < 4$. Duthie et al (1961) give an interaction length of 15 cm. for a detector of similar composition and this value has been used in the remainder of this analysis.

Table 2.1

Medium	Density $gm.cm.^{-3}$	Radiation Length $gm.cm.^{-2}$	Length cm.	Interaction Length $gm.cm.^{-2}$	Length cm.
Tungsten	18.80	6.90	0.37	183	9.7
Nickel	8.75	12.90	1.47	125	14.3
Copper	8.89	13.0	1.46	128	14.4
GEC Heavy Alloy	16.80	7.25	0.433	175	10.4
G5 Emulsion	3.82	11.10	2.90	133	34.8
Detector	12.10	7.52	0.62	170	14.0
Lead	11.34	6.50	0.57	190	16.8
Graphite	-	44.5	-	74	-
Tufnol CH_2O	-	40.0	-	71	-

§2.3 The Graphite Producing Layer.

The detector was surrounded, see Fig 2.1, by a thin graphite producing layer. This layer was separated from the face of the detector by a layer of expanded polystyrene 10 cm. thick; this material was chosen on account of its low density ($\approx$0.020 gm./$cm.^3$). The graphite layer was adjacent to the detector at the top and sides. The graphite layer was 2.5 cms thick and it was surrounded by a 1.2 cm thick sheet of Tufnol. Tufnol is a commercial plastic available in rigid sheets; It

consists of paper impregnated with a synthetic resin formed from the organic compound phenol formaldehyde; its atomic proportions are approximately CH_2O. The interaction and radiation lengths of graphite and Tufnol are given in Table 2.1. The densities of graphite and Tufnol are not given since neither is a constant. The graphite producing layer was weighed after the experiment; its thickness was 6.5 gm./cm.^{2} which corresponds to 0.09 nuclear interaction lengths.

§ 2.4 Exposure of the Assembly

The assembly was flown on a polythene balloon and spent 30 hours at approximately 27 km. above sea level. The flight took place in April 1961 from Hyderabad, India and the altitude-time curve for the flight is shown in Fig 2.2. The mean vertical depth of the assembly in the atmosphere was 20 gm./cm.^{2}.

After exposure the emulsions were processed at the Tata Institute of Fundamental Research, Bombay. The stack was subsequently divided between the Tata Institute and Bristol, half the stack being analysed in each laboratory. The upper half of each emulsion layer, of face area 61 x 61 cm., was analysed in Bristol and it is the analysis of this section which is reported here.

§ 2.5 Examination and Classification of Events.

The processed emulsions were examined by viewing them against an illuminated ground glass screen with the unaided eye. This method has been described by Duthie et al (1961). Approximately 1900 cascades were found in the Bristol section

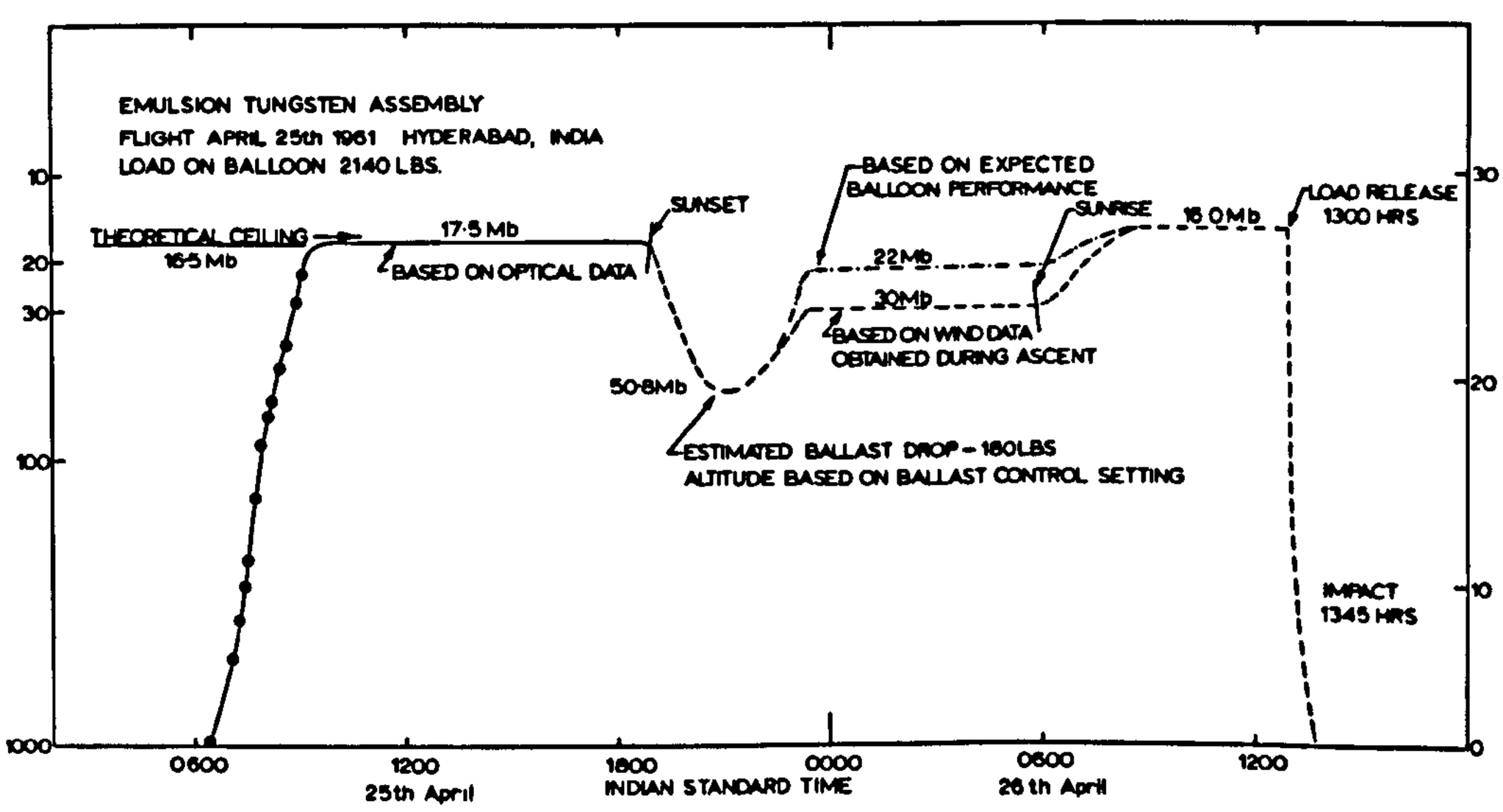

Fig 2.2.

Exposure of the Indian Stack.

of the detector and subsequently inspected under the microscope. Each cascade was examined in successive emulsion layers, particular attention being given to their early developement. The cascades were classified according to their origins as Electro-magnetic Events, or as Nuclear Events originating in either the detector or the graphite producing layer.

(i) Electro-magnetic Events

The cascade was followed back to a single electron pair originating in an emulsion layer, or to a small number of tracks emerging from a metal sheet, with no neighbouring associated tracks and no evidence of a nuclear interaction. In addition four events were classified as electromagnetic in which a number of γ-rays and/or electrons entered the stack within 100μ of each other. In these events there was no measureable convergence between the individual members and hence no evidence for their having originated in the producing layer.

(ii) Nuclear Events.

(a) Origins in the Detector.

The cascade was followed back to either a nuclear interaction in one of the emulsion layers or, more frequently, to a number of tracks emerging from a presumed nuclear interaction in a metal sheet. In the latter case the tracks showed measureable convergence to a point inside the metal sheet and the cascade was missing in the earlier emulsion, although occasionally the primary particle was found. Nuclear events originating in the metal sheets were almost always distinguishable from

electro-magnetic events.

Distinctive features of the nuclear events are the possibility of seeing secondary interactions, the high average multiplicity of charged particles and electron pairs and their convergence to a point inside the adjacent metal sheet, and their greater depth of origin. This last factor results from the large difference between the interaction length of protons in the detector (15 cm.) and the conversion length of γ-rays (0.8 cm.), and is illustrated by Fig 2.3 which shows the distance inside the detector for origins which were classified as nuclear or electro-magnetic. This ability to distinguish between γ-rays from the overlying atmosphere and local interactions in the detector is an important feature of this experimental technique.

(b) Origins in the Producing Layer.

The event consisted of several γ-rays and/or electrons entering the detector from outside, with typical separations of hundreds of microns. Careful convergence measurements were performed in every case to ensure that these γ-rays had a common origin in the graphite producing layer. In two events, a low energy interaction in the graphite layer was followed by a higher energy secondary nuclear interaction in the detector. These events were both detected on account of their secondary interactions and were classified as origins in the detector.

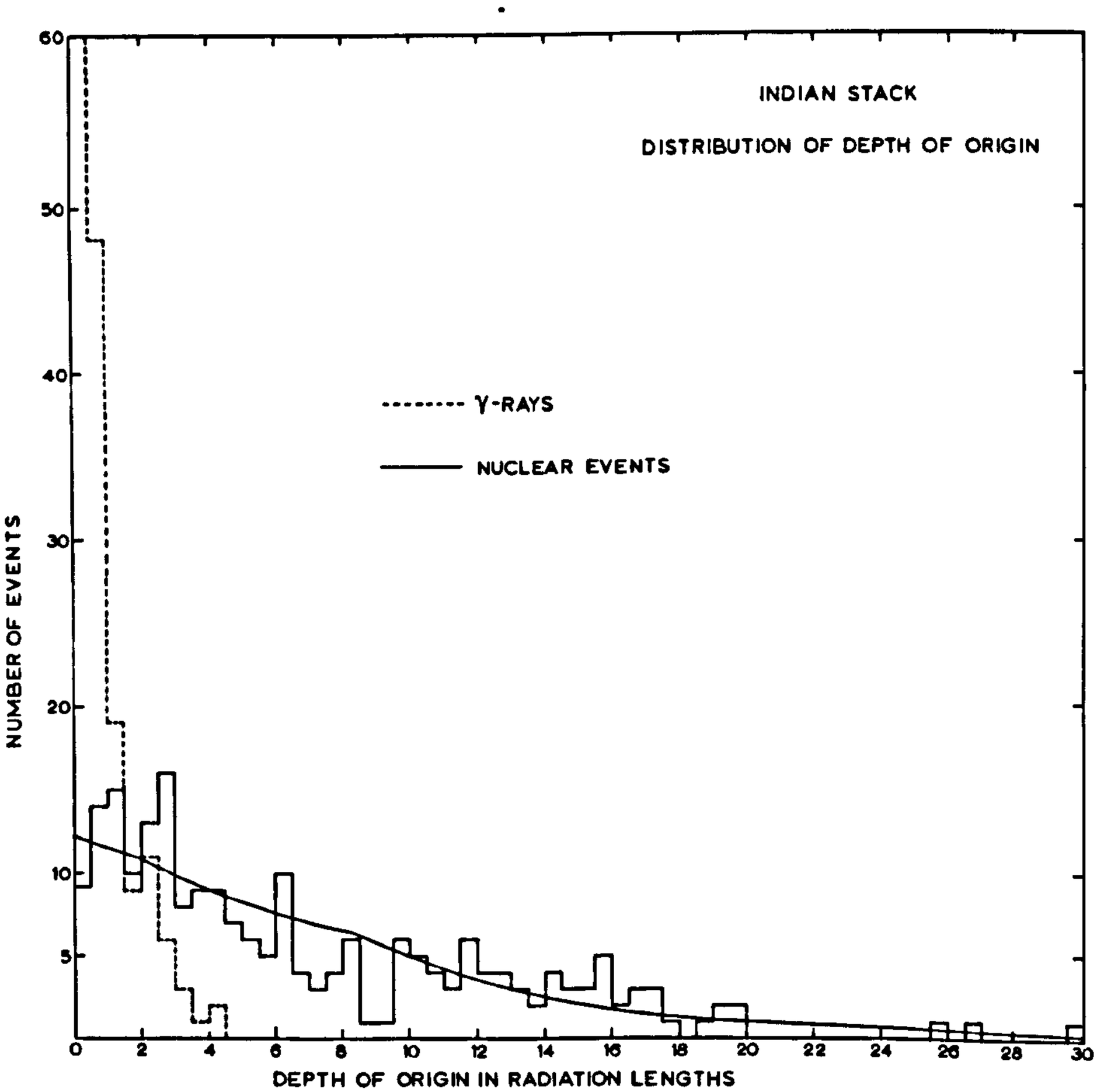

Fig 2.3.

The solid curve shows the expected distribution of nuclear origins for an interaction length in the detector of 15 cm.

§2.6 Selection Criteria.

Events were accepted for analysis if they satisfied certain geometrical selection criteria. These were applied to ensure (i) that the detection and recognition of events was efficient and (ii) that there was sufficient path length in the detector available for the methods of energy measurement described below to be applied.

(a) Electromagnetic Events and Nuclear Origins in the Detector.

For these events the efficiency of the scanning procedure described in §2.5 will depend on the maximum central density, D_m, and the dip angle, δ, of the cascade relative to the emulsion plane. We examined our scanning efficiency and found it to be unity for events with $D_m \geqslant 0.7$ ($E \geqslant 1200$ Gev) and with dip angles in the range $0.15 < \sin \delta < 0.92$. For the more favourable flat events with $0.15 < \sin \delta < 0.51$ the efficiency was unity for $D_m \geqslant 0.2$ ($E \geqslant 300$ Gev). Fig 2.4 shows a comparison between the observed and expected numbers of nuclear events in both ranges of dip angle; the total number expected has been normalized to the total actually found. Such a comparison is less informative for electromagnetic events since (i) the numbers seen at various angles are correlated due to the occurence of high energy interactions in the air above the detector and (ii) there may be a contamination of γ-rays from the graphite layer whose origin was not recognised; this last point is discussed later. The above restriction on dip angles ensured that all events had a path length in the

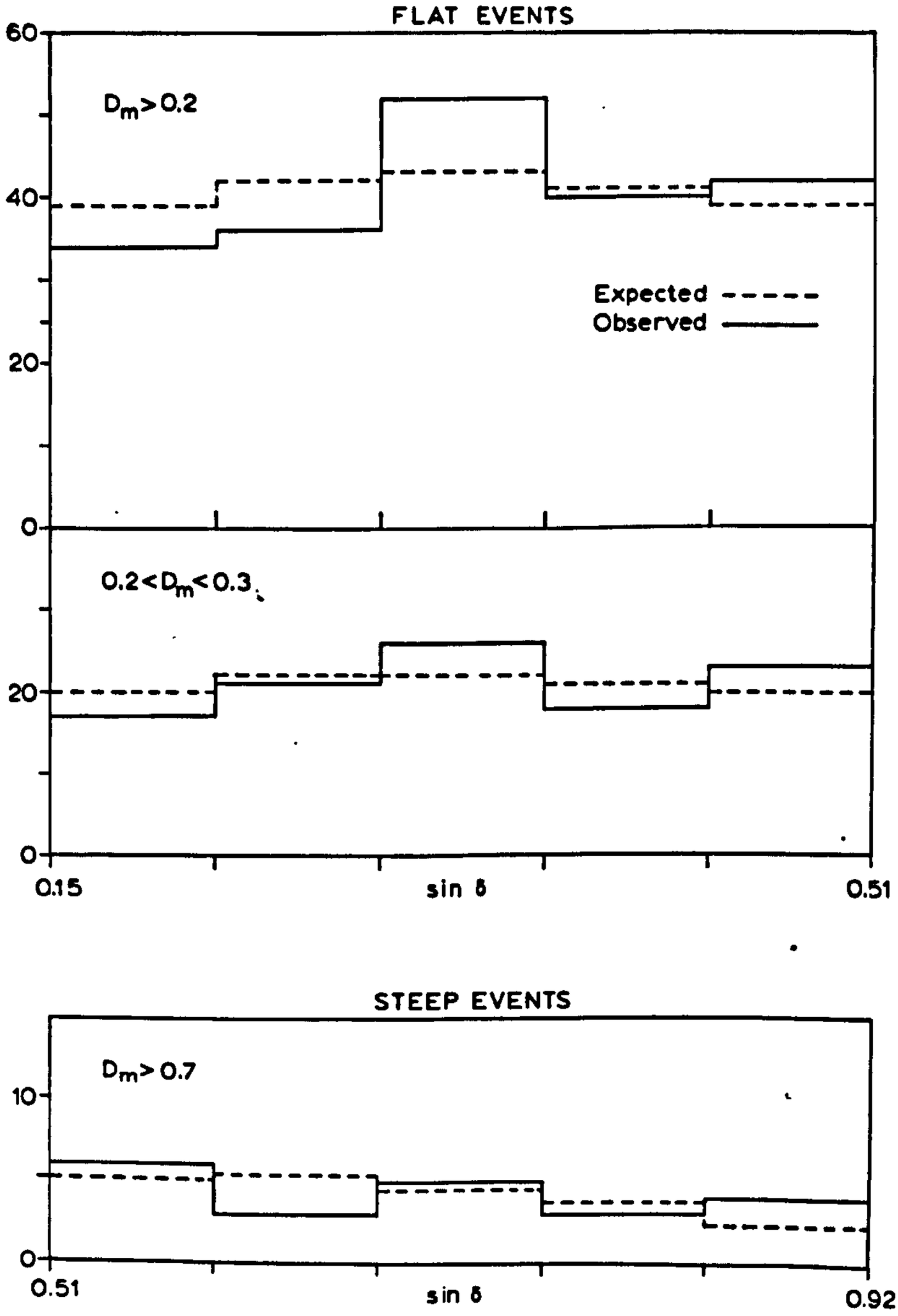

Fig 2.4.

The observed and expected distribution in angle of nuclear origins in the detector for various ranges of energy.

detector of at least 9 radiation lengths. For γ-rays this length is almost always sufficient for the maximum of cascade developement to be contained; in 3 of the 80 high energy γ-rays observed the cascade left the detector close to its maximum developement and the energy estimate for these 3 events was based on the growth of the cascade over several radiation lengths prior to leaving the detector. For nuclear events, the origins of which are distributed fairly uniformly throughout the detector, the extra requirement was made, that there should be at least 6 r.l. of detector available after the interaction. Again in a few cases (5 out of 220) the maximum central density was not reached in the detector and their growth was used to determine their energy.

Some areas of the detector were shielded by the metal frame supporting the emulsions. Electro-magnetic events were accepted only if they entered an un-shielded face but nuclear events entering through the shielding were accepted provided that the particle initiating the cascade traversed at least 4 r.l. of detector before interacting.

(b) Nuclear Origins in the Graphite Producing Layer.

For these events we must consider the probability both that the event be detected and it be recognised as having originated in the graphite producing layer. Graphite events will certainly be detected in the scanning procedure if they possess at least one γ-ray satisfying the requirements of the previous section for electro-magnetic events, i.e. $E > 1200$ Gev with $0.51 > \sin\delta > 0.92$ or $E > 300$ Gev with $0.15 < \sin\delta < 0.51$.

However some of these events, with low energy and low γ-ray multiplicity, may be mistakenly classified as electromagnetic events.

Consider an event with a total radiated energy, ΣE_γ, of 1200 Gev and dip angle in the range $0.15 < \sin \delta < 0.92$ and let the cascade consist of only one π^o, which decays into 2 γ-rays. When examined in detail under the microscope such an event will be recognised as being of graphitic origin providing both γ-rays have energies > 50 Gev, i.e. in approximately 90% of the cases. Events with more than one π^o or with higher energies are even more likely to be recognised. It can be concluded with confidence that graphite events with $\Sigma E_\gamma \geq 1200$ Gev are recognised with a high probability. Of the 25 events found with $\Sigma E_\gamma \geq 1200$ Gev, only 2 had a multiplicity of γ-rays, $N_\gamma(E \geq 50)$ as low as 2; there were in all 5 events with $N_\gamma(E \geq 50 \text{ Gev}) < 5$. It is therefore likely that at most one graphite event with, $\Sigma E_\gamma \approx 1200$ Gev and a low multiplicity, was not recognised as such due to a high disparity between the energies of its γ-rays.

For lower energies the probability of recognising that an event has originated in the graphite layer, will fall. The analysis of nuclear events was therefore restricted to events with $\Sigma E_\gamma \geq 1200$ Gev and $0.15 < \sin \delta < 0.92$.

However all γ-rays satisfying the requirements described above for electromagnetic events will have been <u>detected</u>. For γ-rays with $E_\gamma \geq 1200$ Gev and $0.15 < \sin \delta < 0.92$ the region of production, i.e. in the air or in the graphite, will be

Table 2.2 Numbers of Events.

Class of Event	Energy (Gev)	Dip Angle (sin δ)	Number	Number of Independent Events
γ-rays from Atmosphere	$E_\gamma \geqslant 1200$	0.15 - 0.92	56	33
γ-rays from Graphite	$E_\gamma \geqslant 1200$	0.15 - 0.92	24	14
γ-rays from Atmos. and Graphite	$300 \leqslant E_\gamma < 1200$	0.15 - 0.51	175	152
Nuclear Origins in Graphite	$\Sigma E_\gamma \geqslant 1200$	0.15 - 0.92	25	22
Nuclear Origins in Detector	$\Sigma E_\gamma \geqslant 1200$	0.15 - 0.92	39	39
Nuclear Origins in Detector	$300 \leqslant \Sigma E_\gamma < 1200$	0.15 - 0.51	180	178

the number of independent events from which this number is derived. These numbers differ for two reasons:

(i) A high energy interaction in the graphite may contribute several γ-rays

(ii) Families of cascades are sometimes observed from a single high energy nuclear interaction in the overlying air. The members of such families are predominantly γ-rays but may also be nuclear interaction in the graphite or in the detector.

The solid angle subtended by the assembly at a point in the overlying air is small and consequently groups of secondaries from such a single interaction will only be

detected if they are highly collimated. Hence, because the degree of collimation increases with increasing primary energy, such air families are observed only from very high energy interactions. Such interactions are rare; consequently the occurence or non-occurence of a single high energy interaction in the atmosphere above the assembly can drastically alter the flux of high energy γ-rays, from that which would be seen if averaged over a long period of time.

Five air families were recorded in this exposure, three of them of high energy. Many of the highest energy events seen were associated with these three families (i.e. 23 of the 56 γ-rays from the overlying air with $E_\gamma \geq 1200$ Gev). The main details of the families are presented in Table 2.3.

Table 2.3.

High Energy Air Families

	F_1	F_2	F_3
Total Energy Collected (Gev)	94,000	43,000	32,500
γ's from Air $E_\gamma \geq 1200$	18	5	-
γ's from Graphite $E_\gamma \geq 1200$	2	1	10
Nuclears in Detector $\Sigma E_\gamma \geq 1200$	-	3	1
Nuclears in Graphite $\Sigma E_\gamma \geq 1200$	2	1	3

§ 2.8 Measurement of Energies.

The energy of each event was measured. The method used was to compare the density of electron tracks in the cascade with the theoretical calculations of Nishimura and Kamata (1958). The density of electron tracks was either counted under a high power microscope objective or, more usually, was measured photometrically. The photometric method used in this laboratory has been described in detail by several authors, Duthie et al (1961), Duthie (1961), Kaddoura (1961), Bowler (1962), and will be given here only in outline for the sake of completeness.

The photometer used in this experiment consisted of a Cooke 4000 microscope which was modified so that the image formed by the objective could be either viewed in the normal manner through the microscope eyepieces or deflected to fall on the cathode of a photomultiplier tube, EMI 9524B. The image of a lower defining slit is focussed in the plane of the cascade, Fig 2.5, while the image formed by the objective is focussed on an upper slit close to the cathode of the photomultiplier. This image was scanned across the upper slit, using a rotating glass cuboid with two faces blackened, which was driven by a 2-phase a.c. motor at 1,000 r.p.m. The width of the lower slit was a little greater than that of the upper slit.

All slits and the axis of the cascade were aligned with the y-motion of the microscope stage; the x-motion was used to examine regions at different distances from the cascade

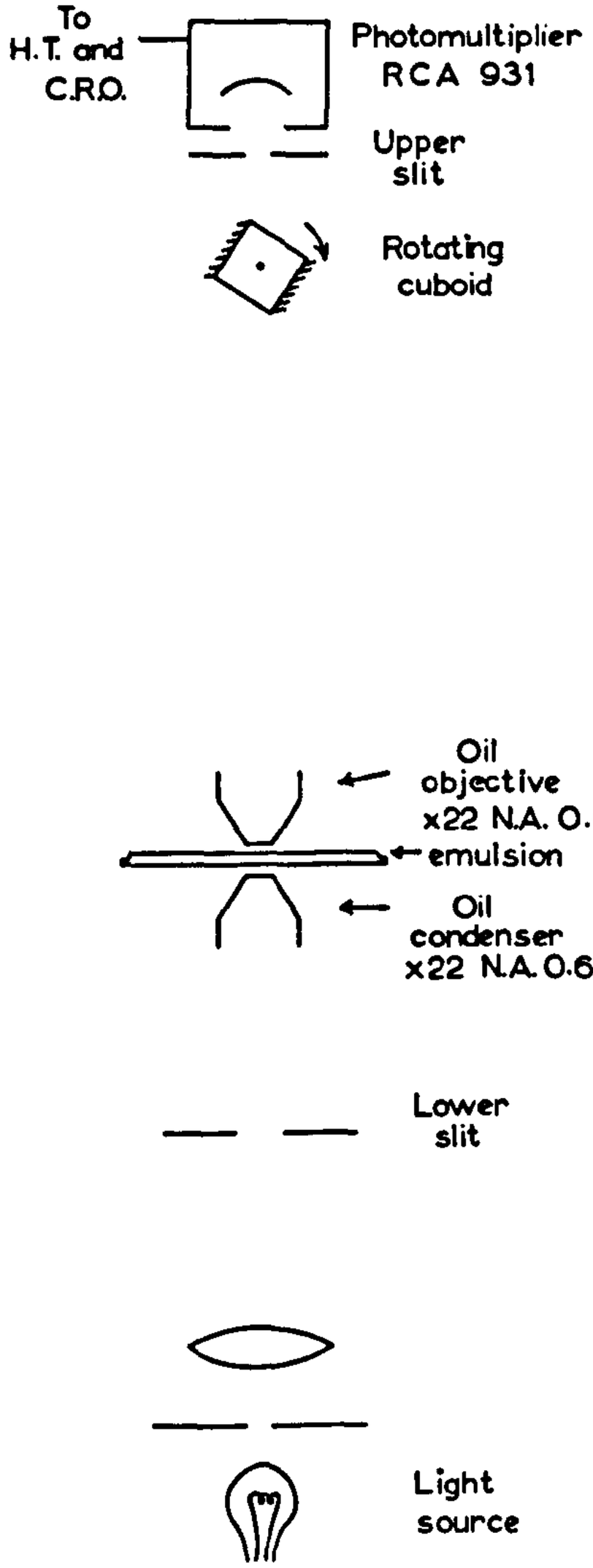

Fig 2.5.

The optical system of the photometer. (The photomultiplier was replaced by an EMI 9524B).

axis. The output of the photomultiplier was displayed on a C.R.O. and the density of tracks obtained by comparing the intensity of light in the region of the cascade with that in a 'background' region sufficiently removed from the cascade.

§ 2.9 Electromagnetic Events.

The photometer was used to measure the average density of electron tracks in a slit 10μ wide centered on the cascade axis; this measurement was made at several positions in each emulsion and a mean value taken. The quantity known as the central density was defined by the relation $D = \ln^{J_o}/J$ where J_o, J are the intensities of transmitted light in the regions of the 'background' and cascade respectively. The expected value of the central density was computed numerically from the lateral density functions (Fig 1.4) for different values of the primary energy, E_o, and the depth, t, of the cascade from its origin.

Firstly, let us consider a cascade in the plane of the emulsion and assume that the photometer measures the attenuation of a parallel beam of light. We must compute the number of electron tracks in a rectangle 10μ wide (the width of the upper defining slit) by 600μ (the thickness of the unprocessed emulsion) centred on the cascade axis. Let (x, z) be directions perpendicular to the cascade and respectively in the plane of the emulsion and normal to it; then the intensity of light incident upon the photomultiplier is given by

$$J = J_o \int_{-5\mu}^{+5\mu} e^{-An\tau(x)} \frac{dx}{10} \qquad (2.1)$$

$$\tau(x) = \int_{-300\mu}^{+300\mu} \rho(x,z)dz \qquad (2.2)$$

where $\rho(x,z)$ is the density of tracks per μ^2, A is the average area of a developed grain and n is the mean number of grains per micron of relativistic electron track.

Let $\bar{\tau}$ be the mean track density in the slit and write

$$\tau(x) = \bar{\tau} + g(x) \qquad (2.3)$$

$$\text{so that } \int_{-5}^{+5} g(x)\frac{dx}{10} = 0$$

We can now write equation (2.1) as

$$J = J_o\ e^{-An\bar{\tau}} \int_{-5}^{+5} e^{-Ang(x)}\ \frac{dx}{10} \qquad (2.4)$$

Provided that the gradient of track density across the slit is small, i.e. $Ang(x) < 1$, then

$$\int_{-5}^{+5} e^{-Ang(x)}\ \frac{dx}{10} = 1$$

and the central cascade density, D, is given by

$$D = \ln(J_o/J) = An\bar{\tau} \qquad (2.5)$$

The dip angle, δ, of the cascade relative to the emulsion plane, effects this estimate in several ways:

(1) The projected grain density is proportional to sec δ.

(2) The limits of the integral in equation (2.2) become $\pm$ 300 cos δ μ.

(3) Since the slit views a region of the emulsion about 140μ long, then only part of the cascade is in focus in the slit; this effect is only present when a non-parallel beam of light is considered.

In computing D, allowance was made for the finite angle of the cone of light, for the three effects dependent upon δ described above and for the non-uniformity of track density across the slit. This last correction is important only when An sec δ g(x) > 1; i.e. for high energies and large dip angles. The magnitude of the correction is 10% for a cascade with $E_o = 10^4$ Gev and sec δ = 1.5, at a depth of 6 r.l.

Empirically it was found that, for cascades close to their maximum developement and with energies E_o < 5000 Gev, where the correction for non-uniformity is small, the corrections for the dip angle could be represented by a single expression, (0.24 + 0.76 cos δ). The computed values of the quantity (0.24 + 0.76 cos δ).D are shown in Fig 2.6; these are independent of δ except at the highest energies.

These values were computed from the theory of Nishimura

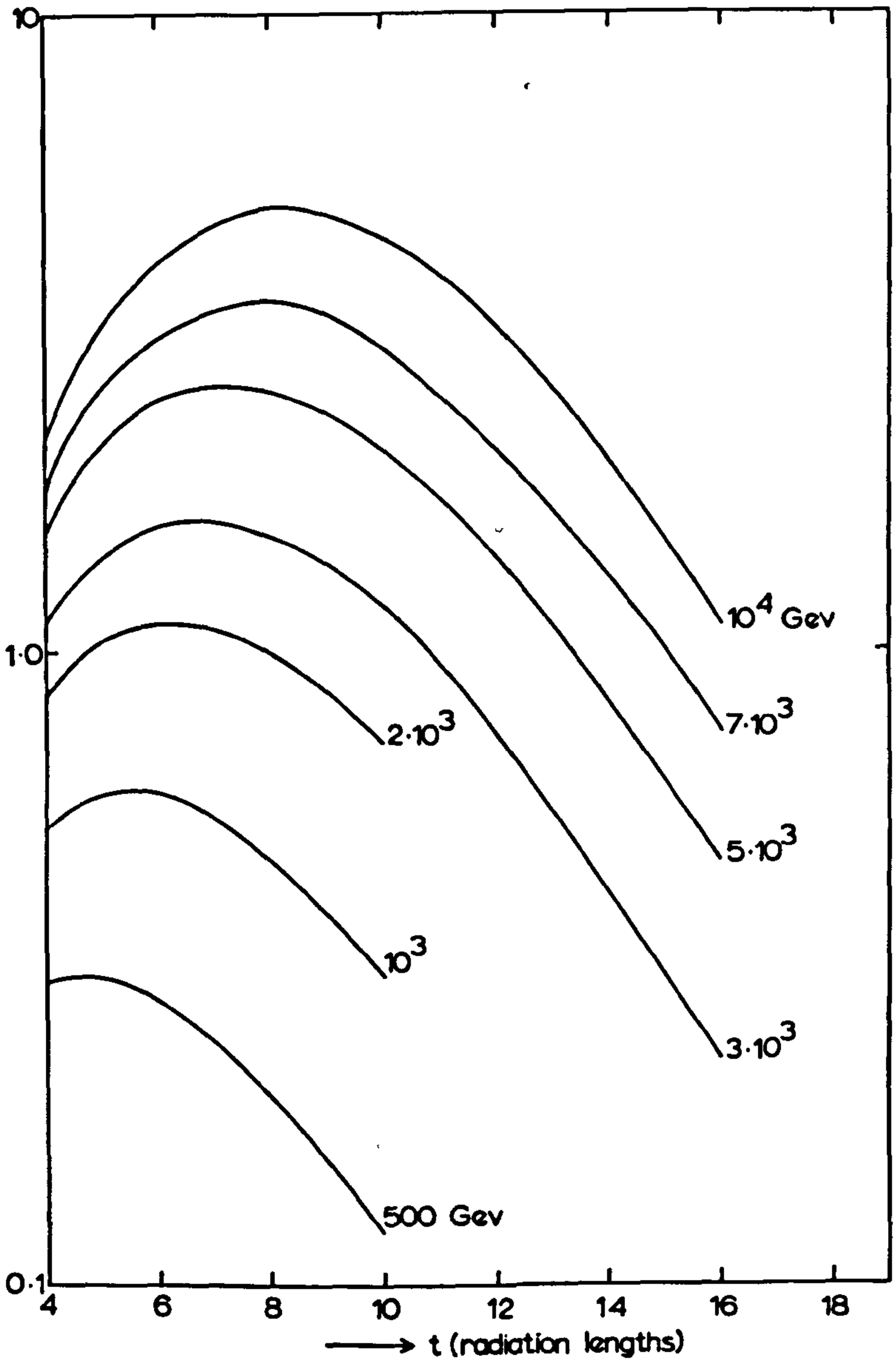

Fig 2.6.

Curves showing the corrected Central Density as a function of age for various primary energies.

and Kamata described in § 1.9. According to Pinkau (1964) their results are strictly valid for $R \lesssim 2.10^{-2}X_o = 120\mu$. However the errors introduced at distances $\approx 300\mu$ are small and in any case the major contribution to the integral in equation (2.2) is from points close to the axis.

The value of the grain density n used in these calculations was found by counting the numbers of grains on selected electron tracks occuring in cascades. The mean value in many emulsions was $n = 0.225 \pm 0.004$ grains/μ; a 5% correction was added to this figure to allow for the contribution to the central density of δ-rays from the electron track. The grain area A was found from a gap count on the track of a slow proton using the method of Fowler and Perkins (1955). The mean value was $A = \left(0.42 \pm 0.02\right)\mu^2$. Hence

$$An = \left(0.100 \pm 0.006\right)\mu$$

The energy of a cascade was estimated by comparing its maximum central density, D_{max}, with that predicted by the above theory. This method has several advantages:

(i) It is rapid

(ii) It reduces the effect of fluctuations early in the cascade developement.

(iii) Close to its maximum, the density is most sensitive to the primary energy, E_o.

Fig 2.7, in which D_{max}, the maximum value of $(0.24 + 0.76 \cos \delta).D$, is plotted against E_o, is simply obtained from Fig 2.6. Except for very steep cascades (sec $\delta \approx 2.0$) the relation

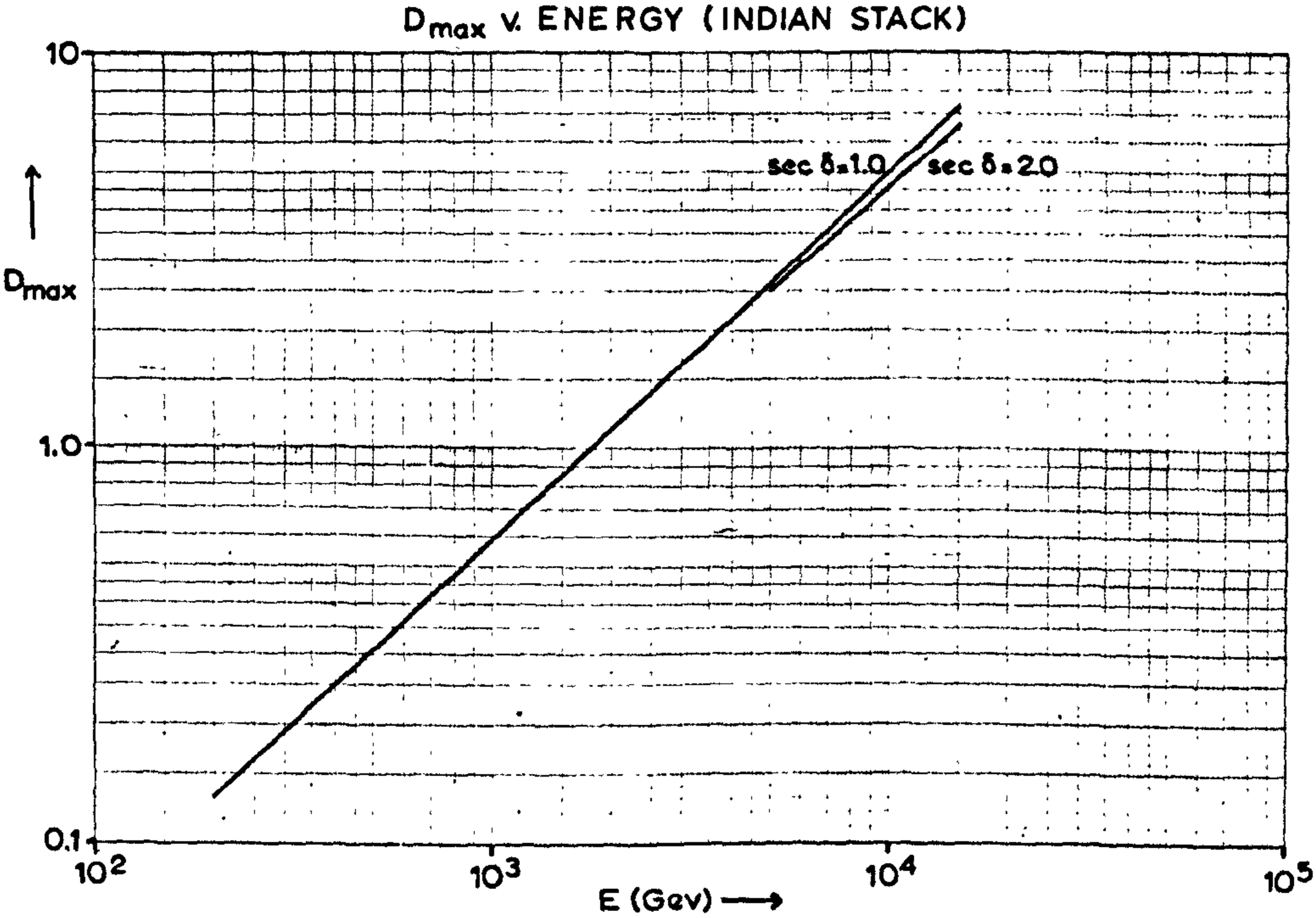
D_{max} v. ENERGY (INDIAN STACK)
10
1.0
0.1
D_{max}
sec δ=1.0
sec δ=2.0
10^2
10^3
10^4
10^5
E (Gev) ⟶

Fig 2.7.

between E_o and D_{max} has the simple empirical expression

$$E_o = 1750\ D_{max}^{1.08} \qquad (2.6)$$

To reduce the effects due to errors of measurement, and of cascade fluctuations, D_{max} was determined experimentally by measuring the central density, D, in successive emulsions close to the maximum and then by computing the average, $\bar{D}$, in those three adjacent emulsions which gave the highest value of $\bar{D}$. Then

$$D_{max} = (0.24 + 0.76 \cos \delta).f(\delta).\bar{D} \qquad (2.7)$$

where $f(\delta) = (1 + {}^{0.006}/_{\sin^2 \delta})$ is a small correction, computed from Fig 2.5, to allow for the finite range of depths from the origin over which the average $\bar{D}$ was taken. Some events with small dip angles traversed distances of 1.5 r.l. or more between successive emulsions. For these very flat events $\bar{D}$ was obtained by averaging over only two adjacent emulsions and the correction term $f(\delta)$ was modified accordingly,

$$f(\delta) = 1 + \frac{0.003}{\sin^2 \delta} \qquad (2.8)$$

As explained above, at high energies, E > 5000 Gev, D_{max} contains a large correction ($\approx$ 10%) for the non-uniformity of track density across the slit. The energy of these cascades was therefore also determined by a measurement of the electron density at positions 50μ on either side of the cascade axis;

at these positions the variation in optical density across the width of the slit was small. There was close agreement between these two methods and a mean value was taken in each case.

§2.10 Nuclear Origins in the Detector.

Cascades caused by nuclear interactions in the detector differ from 'pure electromagnetic' cascades in three respects:

(i) They are initiated by several γ-rays, distributed in energy; this effect alone would lead to a small underestimation of the energy. The maximum central density is almost linear in energy, equation (2.6), but the average age at which the maximum occurs increases slowly with energy, so that the measured maximum central density would be less than the sum of those of its component γ-rays.

(ii) The transverse momenta of the γ-rays (typically 250 Mev/c) causes their axes to diverge, thereby reducing the central density. The magnitude of this effect will depend upon the radiation length of the detector, it being more severe for large radiation lengths.

(iii) Secondary interactions may occur which reinforce the cascade from the original interaction; the importance of this effect will depend on the ratio of the interaction length to the radiation length in the material of the detector.

Effects (ii) and (iii) will occasionally be the subject of large fluctuations, due to the production of a single π^{o}-meson with high transverse momentum or the occurence of a single high energy secondary interaction.

Duthie et al (1961) and Bowler (1962) have studied the effect of these differences on the central density by estimating the energies of cascades in two ways:

(i) By counting photometrically the number of electrons inside a radius so large that the divergence of the γ-rays can be neglected; they chose a square box of side 600μ which is almost equivalent to a disc of radius 340μ. This measurement should be directly comparable to one carried out on an 'electromagnetic' cascade since the number of tracks is linear in total energy.

(ii) By measuring the central density and treating the cascade as if it were of electromagnetic origin.

The parameter R is defined to be the ratio of these energy estimates; both estimates are liable to be effected by secondary interactions but only the second method will be effected by the divergence of the γ-rays. In both methods the maximum was estimated by averaging over the three highest successive plates but it should be noted that this maximum will occur at a different depth from the origin in each method.

R was measured for cascades of various energies, initiated by both γ-rays and nuclear interactions. For the former R has a mean value of 1.0 and a standard deviation of ≈ 0.15; this spread is accounted for in terms of cascade fluctuations. For cascades of nuclear origin R had a mean of 1.12 and a standard deviation of ≈ 0.25; these values did not change significantly over the range of energies 500 to 3,000 Gev. The greater spread of values is to be expected since, as well

as cascade fluctuations, there occur fluctuations in the number of secondary interactions and in the transverse momenta of the γ-rays. The expected mean value of R has been calculated, Bowler (1962), taking into account only the divergence of the γ-rays. The result is not very sensitive to the model of pion production used and gives $R \approx 1.3$. The difference between this and the experimental value of 1.12 indicates the effect of secondary interactions, which are more important in the case of the central density. Thus it may be concluded that the average of the ratio between the energy as estimated from the maximum central density and the total energy radiated in the primary interaction is close to unity, and does not vary with energy.

In the Indian stack the energies of cascades of nuclear origin were estimated from the maximum central density, exactly as if they were of 'electromagnetic origin' (see § 2.9). Whereas the absolute energy values obtained may be systematically wrong by ≈ 5%, the relative values should be accurate.

§ 2.11 Nuclear Events Originating in the Graphite.

In events originating in the graphite producing layer, a number of γ-rays entered the detector with a wide variation of energies and with separations varying between tens of microns and millimeters. In these events we were able to measure the individual γ-ray energies, E_γ, and, by addition, the total radiated energy, ΣE_γ. In some events the overall energy was checked by a determination of the total track

number.

The exact method used to determine the individual γ-ray energies depended on the energy of the γ-ray and the proximity of its neighbours.

(a) $0 < E_\gamma < 250$ Gev.

For γ-rays in this energy range the track density was low enough for the electrons to be counted individually under a high power microscope objective. The number of electrons inside a square centred on the cascade axis was counted; this is very nearly the same as the number inside a circle of the same area.

The count was repeated in successive emulsions ranging from approximately 1.5 r.l. to 5 r.l. from the point of conversion of the γ-ray. The energy was determined by comparing the sum of these numbers with that computed from the theoretical calculations, using Fig 1.3. The choice of the cell size used depended on the distance of the γ-ray from its neighbours. Usually γ-rays of this low energy were millimeters from the main axis and hundreds of microns from their nearest neighbour. In this case a cell size corresponding to a radius of 19μ was chosen. However, if two γ-rays were close enough together to interfere significantly, smaller radii of 11μ or 5.5μ were used, and corrections for this interference were applied if necessary.

This method becomes unreliable at γ-ray energies $\lesssim$ 30 Gev when the number of tracks is low ($\approx$4) and the effect of fluctuations becomes increasingly important.

(b) $200 < E_\gamma < 2000$ Gev.

In this energy range the electron density near the axis is too high to be counted by eye and was determined photometrically. γ-rays of this energy usually occur near the centre of the event and may have several neighbours within 50 - 100μ. The method used was to measure photometrically the transmission of light through an area of the emulsion 10μ square centered (i) on the axis of the γ-ray and (ii) at 10μ on either side of the axis. The difference in these readings represents the number of extra tracks within the central cell; this is approximately equal to the numbers of tracks inside a disc of radius 5μ centered on the γ-ray axis. This method has the great advantage that, since it involves a difference measurement, the effect of 'background' tracks due to neighbouring γ-rays is entirely removed, providing only that their density changes linearly over the region considered, a proviso which is always satisfied at core separations of greater than a few microns (see Fig 1.4).

From the lateral density functions, Fig 1.4, numerical integrations to find the expected numbers of excess tracks were performed for a number of primary energies and depths from the origin. These calculations are summarized in Fig 2.8, which shows the expected difference in track density as measured by slits 10μ wide centered on the cascade axis and 10μ off the axis. These differences are plotted as functions of the primary energy for various distances from the origin of the cascade. In preparing these curves, allowance was

made for the non-uniformity of track density over the area considered; at a depth of 3 r.l. this correction amounted to $\approx$ 10% for E_γ = 1000 Gev and $\approx$ 20% for 1500 Gev. As usual, these curves have been prepared for a medium of radiation length X_o = 6.2 mm.

The measurement described above was repeated in as many emulsions as possible; these measurements were summed to give a total value for the excess tracks over a range of depths from the origin. The energy of the γ-ray was estimated by comparing this sum with a summation from the theoretical curves of Fig 2.8 over the same range of depths.

The method was not used for γ-rays with energies > 2000 Gev on account of the large corrections for non-uniformity at these energies.

(c) E_γ > 1500 Gev.

For the highest energy γ-rays the photometer was used to measure the transmission of light through an area 1.5μ wide by 5μ long centered (i) on the cascade axis, (ii) at 2.5μ on either side of the axis and (iii) at 5μ on either side of the axis, and the differences between the track densities at these points obtained. Since it uses a difference measurement, this method retains the advantage that the effect of background tracks is eliminated; however by employing a narrower slit the correction due to the non-uniformity of track densities is greatly reduced. Three sets of theoretical curves were prepared showing the expected difference in track density between points 0 and 2.5μ from the axis, o - 5μ

Figs 2.8 and 2.9.

The expected differences between the densities of tracks near the axis of a pure electromagnetic cascade. These are shown as a function of energy for various radiation lengths. The curves have been corrected for the non-uniformity of track density across the photometer slit.

Fig 2.8 The difference as seen by a 10μ wide slit centered on the axis and 10μ off the axis.

Fig 2.9. The differences as seen by a 1.5μ wide slit centered

(a) 2.5 and 5μ from the axis.

(b) 0 and 5μ from the axis.

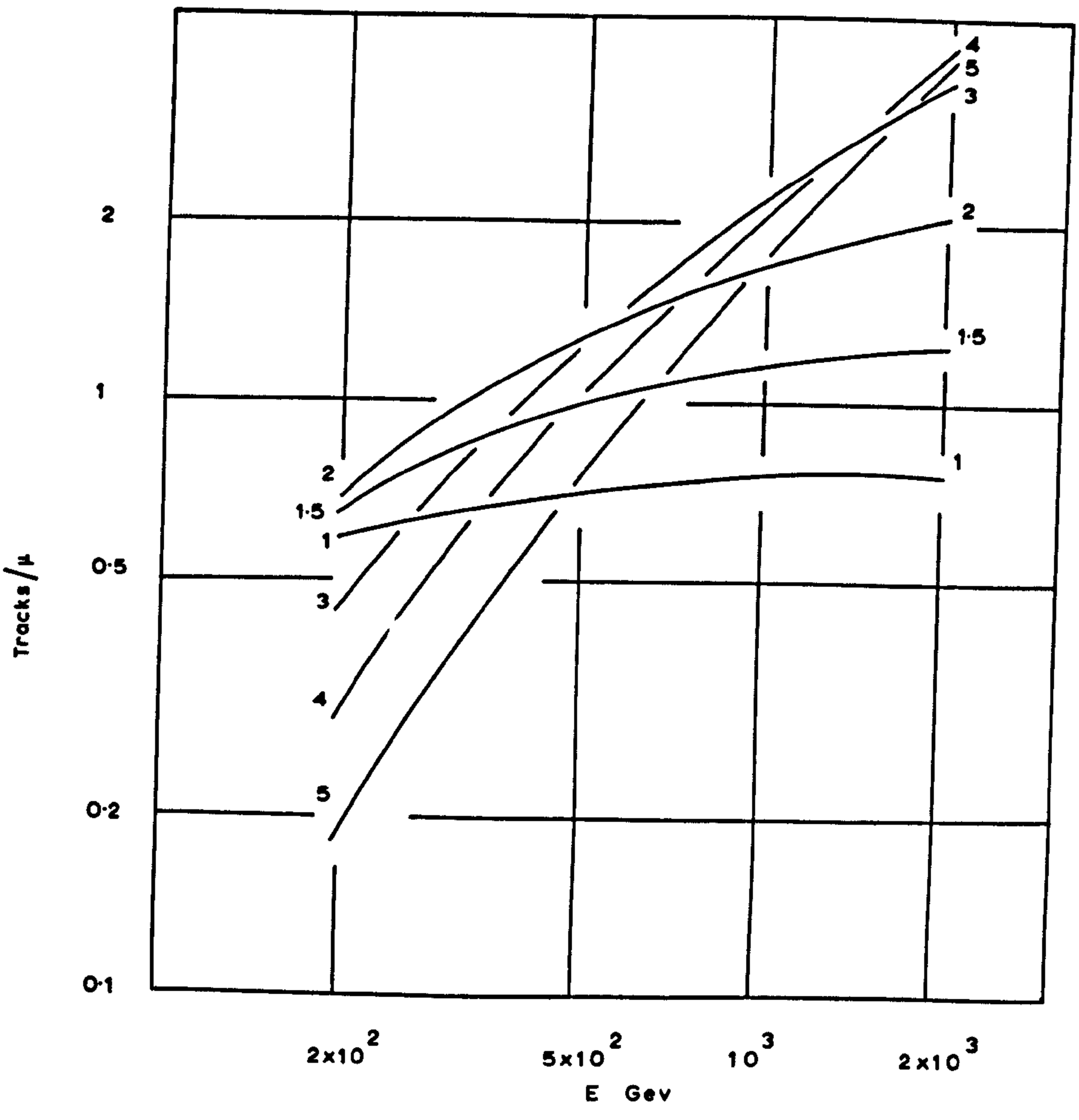
Tracks/μ
2
1
0·5
0·2
0·1
4
5
3
2
1·5
1
2
1·5
1
3
4
5
2x10²
5x10²
10³
2x10³
E Gev

Fig 2.8.

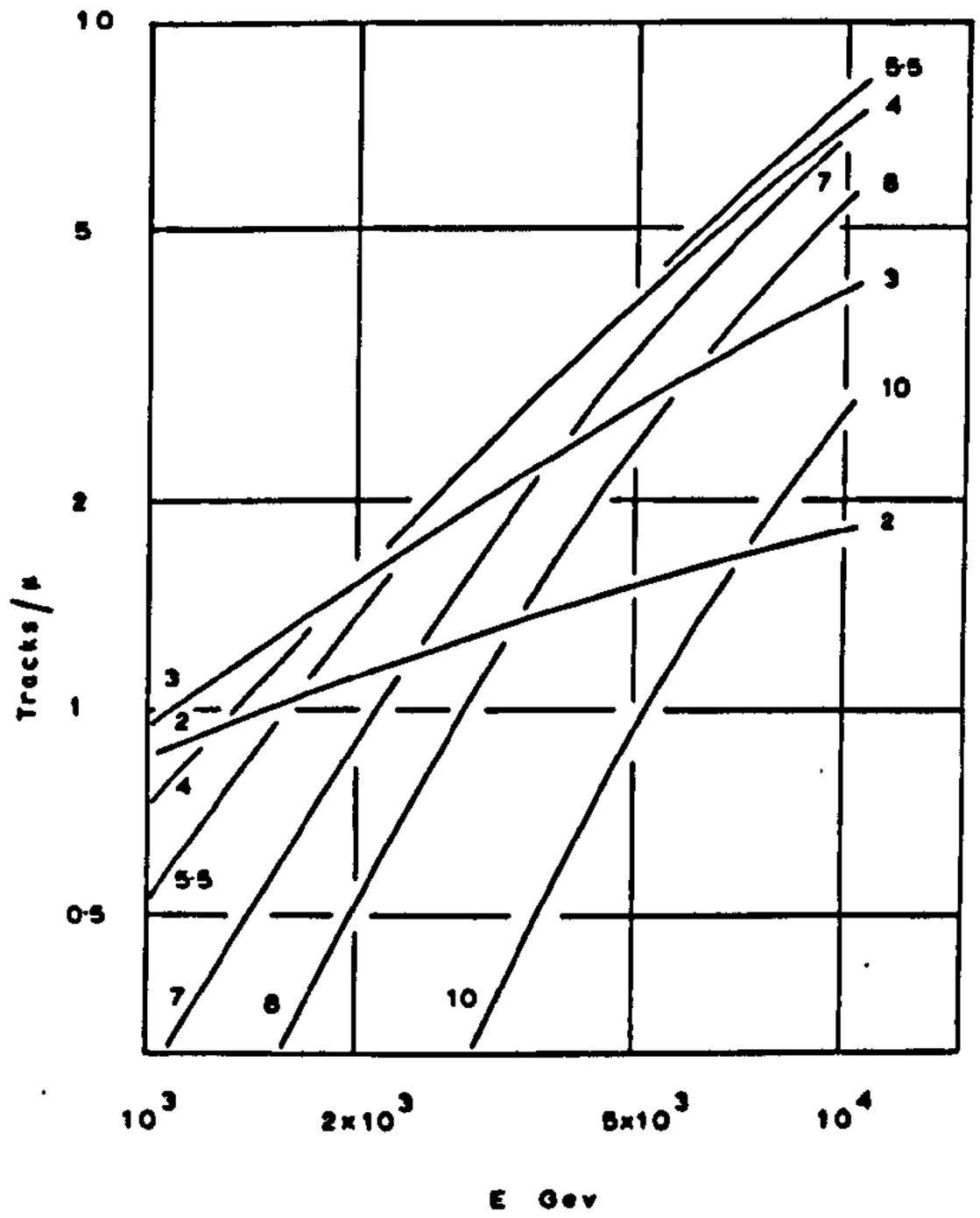

Fig 2.9 (a)

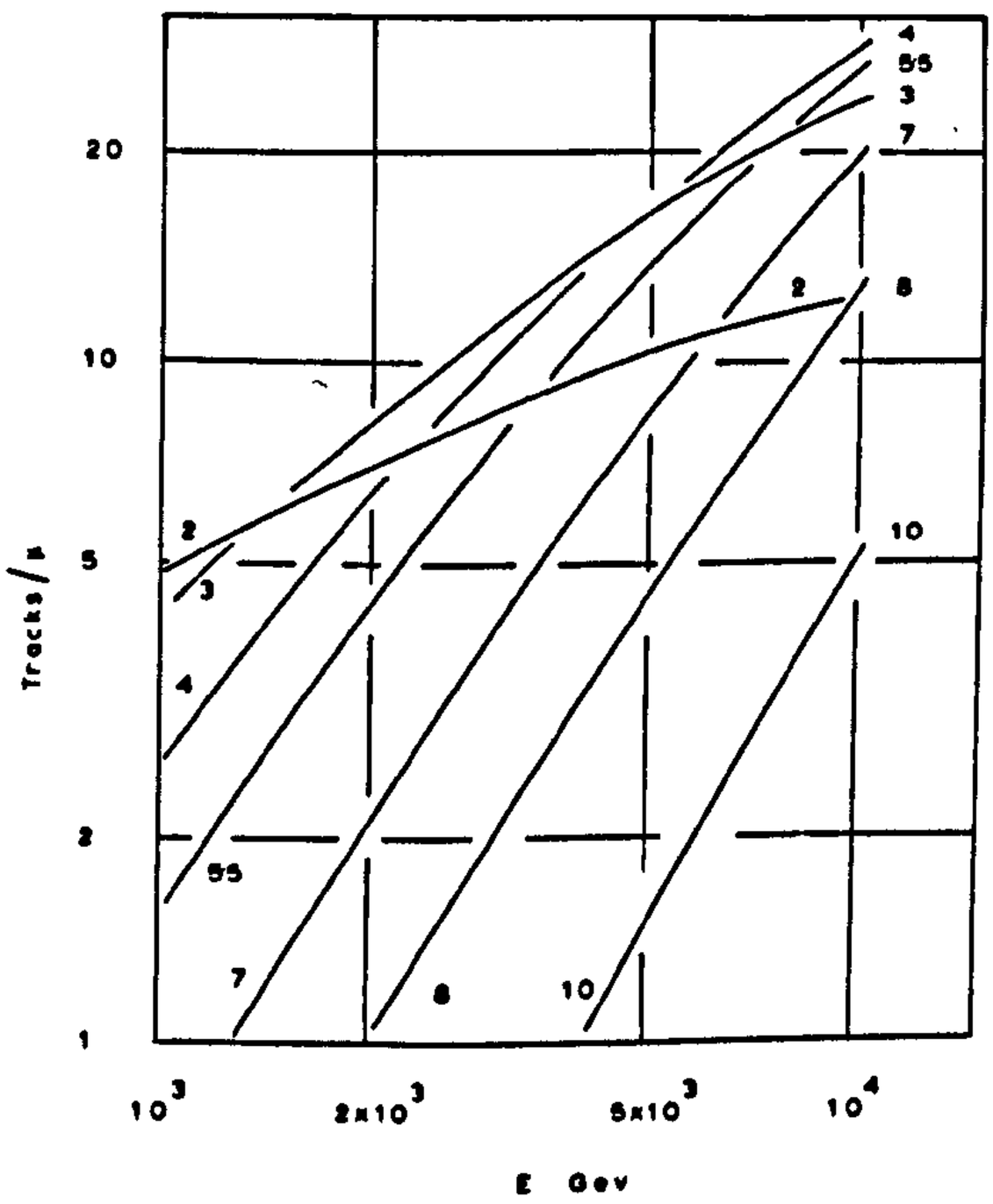

Fig 2.9 (b)

from the axis and $2\frac{1}{2}$ - 5μ from the axis; some of these curves are shown in Fig 2.9. As in the previous section the energy, was estimated by comparing the track difference, summed over many emulsions, with its theoretical value.

It was found that for cascades with energy > 5,000 Gev the energy as estimated from the 0 - $2\frac{1}{2}$μ or 0 - 5μ track differences was systematically a little lower than the energy as estimated by the $2\frac{1}{2}$ - 5μ difference. This inconsistency was examined, Bowler (1962), and it appeared that the amount of light penetrating the central regions of cascades of energy ≈ 5,000 Gev is no longer exponentially dependent on the track density. The reason for this was not obvious.

The two methods of energy determination described in (b) and (c) above were compared with the method using central density (§2.8). For this comparison the energies of a number of isolated high energy γ-rays from the air were measured using each technique. The consistency between the methods was good and showed no systematic errors. The γ-ray energies are considered to have been determined to within 30%, this error arising mainly from uncertainties due to fluctuations in cascade developement.

No such independent check could be made on the track counting technique used for very low energy γ-rays, but for energies in the region of 200 Gev both counting and photometric methods could be employed and the agreement was within 30%.

(d) Total energy, ΣE_γ

The total energy radiated in an interaction in the graphite producing layer was estimated by summing the energies of the individual γ-rays. However the total energy could also be estimated by counting the total number of electron tracks inside a radius from the cascade axis, large enough that the lateral separations of the γ-rays were unimportant.

The photometer, with a 10μ wide slit, was used to measure the density of tracks at distances from the cascade axis ranging between 0 and 300 cos δ μ, where δ is the dip angle of the event. A numerical integration of these densities gives the number of electrons within a square of side 600 cos δ μ, which is very close to the number within a circle of radius 340 cos δ μ. The energy is then estimated from the theoretical curves shown in Fig 1.3.

This method must be applied with caution as the geometry and lateral separation of the γ-rays in some events render it inaccurate.

§ 2.12 Collecting Powers.

Collecting Powers were calculated in order to relate the number of events of a certain type detected to the rate of production of that type of event at the top of the atmosphere.

Let $N_i(E)$ be the number of events of the i^{th} type detected with energy greater than E; let λ_i be the interaction length (gm./cm.^{2}) in the production region considered. Let $R_i(E)$ be the production rate of events of the i^{th} type with

energy greater than E per gram of material at the top of the atmosphere; the units of $R_i(E)$ are number/gm.ster.sec. Then the collecting power, S_i, was defined by the equation

$$N_i = S_i \lambda_i R_i \qquad (2.9)$$

The units of S_i are $cm.^2$ ster.sec. S_i was computed for the 4 types of event - Nuclear Origins in the Detector, Nuclear Origins in the Graphite, γ-rays from the Atmosphere and γ-rays from the Graphite.

Fig. 2.10

(not to scale).

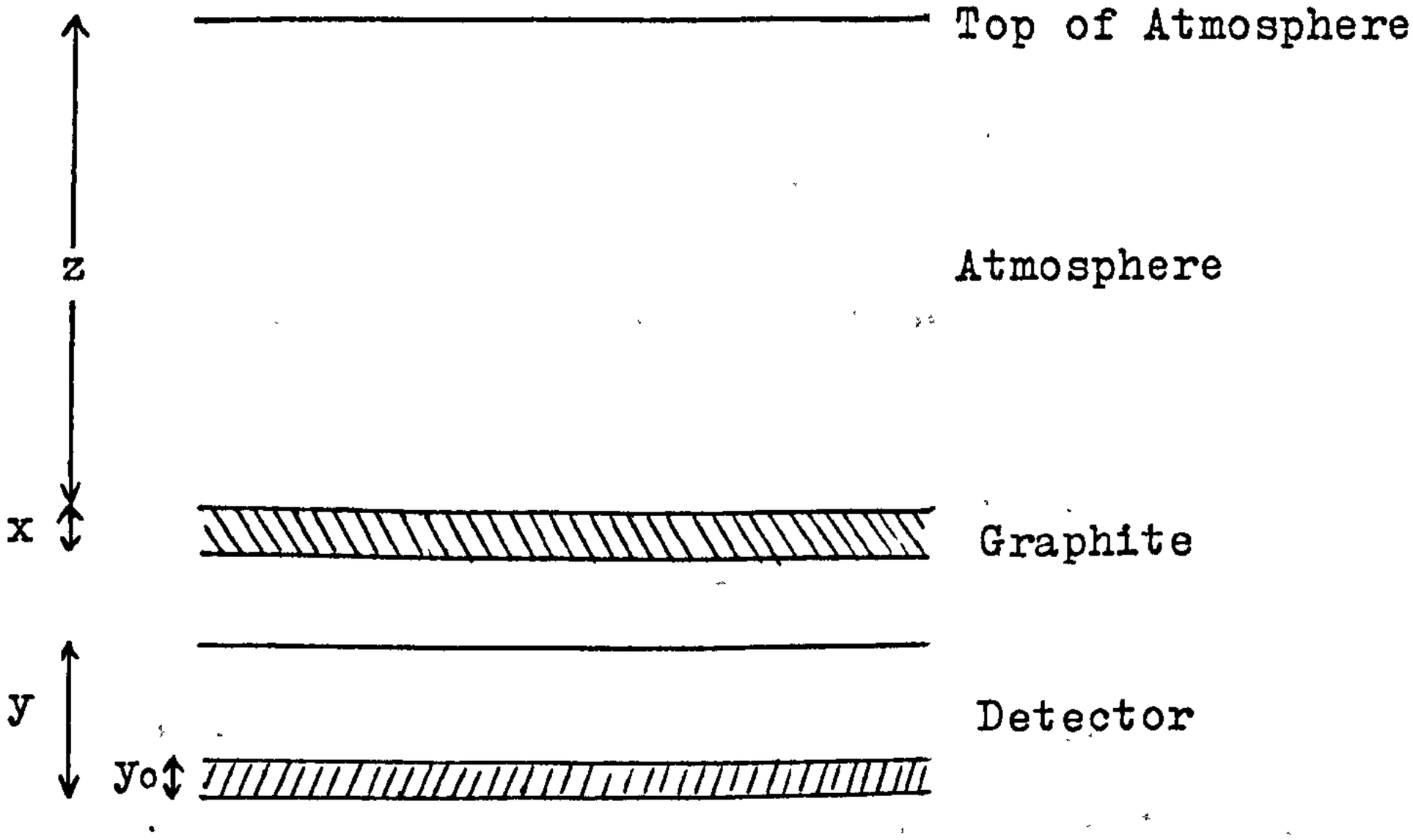

The computation of S_i involves an integration over the solid geometry of the assembly and over all the space angles allowed be the restrictions on dip angle, § 2.6. This integration was performed numerically on an electronic computor and the method is described in Appendix A. The expressions for the collecting powers in a simple one-dimensional case, Fig 2.10, are given below to illustrate the basic physical assumptions made. $\lambda_A, \lambda_C, \lambda_D$ are the interaction lengths of nuclear active particles (n.a.p.) in air, graphite and the detector respectively; z,x,y are the thicknesses of the air, graphite and detector respectively.

(a) Effect of the Atmosphere.

It was assumed that the flux of n.a.p., and hence the γ-ray source strength, is attenuated exponentially in the atmosphere with an attenuation length, Duthie et al (1962), of

$$\Lambda = 125 \text{ gm./cm.}^2$$

The flux of γ-rays at a depth z is then given by

$$F_\gamma(z) = R_\gamma \int_{z'=0}^{z} e^{-z'/\Lambda} \, dz' f(z', z) \qquad (2.10)$$

where f(z',z) describes the attenuation of γ-rays between their production at a depth z' and their detection at a depth z. The stationary solutions to the cascade equations in one-dimension were described in § 1.8. In particular equation (1.17) gives the fluxes of γ-rays and electrons at a depth t

for the case when the flux at t = 0 consisted of γ-rays and/or electrons with power law spectra of exponent s. If we apply the boundary condition that the flux at t = 0 consist only of γ-rays (i.e. $a_1 = -a_2$) then the conbined flux at a depth t is

$$\gamma(E,t) + \pi(E,t) = p(s)e^{\lambda_1(s)t} + q(s)e^{\lambda_2(s)t} \qquad (2.11)$$

p(s), q(s) are easily obtained from the tabulated values in Rossi (1952).

We can equate f(z',z) to this function, with t = z - z', provided that,

(i) The production spectrum is a power law.

(ii) The exponent of this spectrum does not change with depth in the atmosphere.

Substituting the stationary solution for f(z',z) in equation (2.10) and integrating we obtain:

$$F_\gamma(z) = R_\gamma \left[Ge^{\lambda_1(s)z} + He^{\lambda_2(s)z} - (G + H)e^{-z/\Lambda} \right] \qquad (2.12)$$

where
$$\left.\begin{aligned} G &= \frac{1}{1 + \Lambda\lambda_1(s)} \cdot \frac{(C(s) + \mu_o + \lambda_1(s))(\mu_o + \lambda_2(s))}{C(s)(\lambda_2(s) - \lambda_1(s))} \\ H &= \frac{1}{1 + \Lambda\lambda_2(s)} \cdot \frac{(C(s) + \mu_o + \lambda_2(s))(\mu_o + \lambda_1(s))}{C(s)(\lambda_2(s) - \lambda_1(s))} \end{aligned}\right\} \qquad (2.13)$$

It should be remembered that $\lambda_1(s)$ and $\lambda_2(s)$ are negative. This expression for $F_\gamma(z)$ is very insensitive to the value of the exponent s. Averaged over the range of depths applicable in this experiment, $25 \lesssim z \lesssim 75$, then $F_\gamma(z)$ changes by only ±4% for values of s in the range $s = 2.0 \pm 0.5$.

The spectrum of electromagnetic events observed in this exposure, Fowler (1963), is a good approximation to a power law with exponent ≈ 1.8 over the energy range $300 < E_\gamma < 10^4$Gev. Comparing this value with that obtained in previous measurrements at balloon and aircraft altitudes, Kaddoura (1961) and Duthie et al (1961,1962), it seems possible that the spectrum does steepen slowly with increasing depth in the atmosphere. However, in computing collecting powers, this effect may be completely neglected since all significant contributions to $F_\gamma(z)$ come from points less than an interaction length above in the atmosphere. It is therefore valid to use this solution in computing the collecting power; the errors introduced in assuming the spectrum to be a perfect power law will be at most a few percent.

(b) Effect of the Graphite Layer.

The probability of a n.a.p. interacting in the graphite layer is $(1 - e^{-x/\lambda_c})$ and therefore the shielding of the detector by the graphite is given by e^{-x/λ_c}. Occasionally (§ 2.4) an interaction in the graphite which radiates little energy is followed by a stronger interaction in the detector. Theoretically therefore the value of λ_c used should be a little greater than the interaction length but this effect

is negligible. In computing the production rate of individual γ-rays in the graphite layer the above expression was replaced by $\frac{\Lambda}{\lambda_c}(1 - e^{-x/\Lambda})$ where Λ is the attenuation length in graphite; this small correction (≈4%) is to allow for the effect of secondary interactions in the graphite layer.

The effect of the graphite layer on the flux of γ-rays from the overlying atmosphere is completely negligible.

(c) Probability of Detection.

For a nuclear active particle incident upon the detector, the probability of detection is equal to the probability that it interacts with sufficient length of detector available after the interaction for its electromagnetic cascade to develop. The detection probability is therefore

$$\begin{aligned} P &= (1 - e^{-\frac{y-y_o}{\lambda_D}}) \quad \text{for } y > y_o \\ P &= 0 \quad \text{for } y < y_o \end{aligned} \qquad (2.14)$$

For γ-rays incident upon the detector the probability would be obtained by replacing λ_D in the above expression by the conversion length of γ-rays in the detector. However the thickness of the detector in this experiment was such that this probability was unity.

In the simple one-dimensional case, Fig 2.10, the collecting powers may therefore be written as

(i) Nuclear Events in Detector

$$S_1 = e^{-z/\Lambda} \cdot e^{-x/\lambda_c} \cdot (1 - e^{-\frac{y-y_o}{\lambda_D}}) \qquad (2.15)$$

(ii) Nuclear Events in Graphite

$$S_2 = e^{-z/\Lambda} \cdot (1 - e^{-x/\lambda_c}) \qquad (2.16)$$

(iii) γ-rays from the Atmosphere

$$S_3 = \frac{\lambda_A}{\Lambda} F_\gamma(z) \qquad (2.17)$$

(iv) γ-rays from the Graphite

$$S_4 = e^{-z/\Lambda} \frac{\Lambda}{\lambda_D}(1 - e^{-x/\Lambda}) \qquad (2.18)$$

The programme used to compute the collecting powers in the general 3-dimensional case is given in Appendix A. The collecting powers were computed for various ranges of the dip angle, δ, corresponding to the geometrical selection criteria (§ 2.6); the values obtained are shown in Table 2.4. In performing these computations the following values of the constants were used:

(a) λ_A, λ_C were taken as the geometrical interaction lengths in air and graphite, 80 gm/cm^2. and 74 gm/cm.^{2} respectively.

(b) λ_D was taken as 15 cm (§ 2.2).

(c) The exponent s in equations (2.11) - (2.13) was taken as 2.0.

(d) The attenuation length in graphite was taken to be equal to that in air, 125 gm/cm.^{2}.

It should be noted that the expression for R_i, (equation (2.9)), depends only on the product $\lambda_i S_i$. Since the

thicknesses of graphite and detector, x and y, are considerably less than the respective interaction lengths, λ_c and λ_D, then the product $\lambda_i S_i$ is, to a first order, independent of the value of λ_i used.

Table 2.4.

Collecting Powers s_i (cm.^{2} ster.sec.)

	$0.15<\sin\delta<0.51$	$0.51<\sin\delta<0.92$
Nuclear Events in Graphite	240×10^5	393×10^5
Nuclear Events in Detector	679×10^5	505×10^5
γ-rays from Atmosphere	698×10^5	1912×10^5
γ-rays from Graphite	250×10^5	399×10^5

§ 2.13 Rates of Production of Events.

From these collecting powers and the numbers of events seen, Table 2.2, the rate of production of events in each class was calculated, using equation (2.9). Table 2.5. presents the rate of production of events per gram of material at the top of the atmosphere.

The errors quoted are statistical errors, allowance having been made for the fact that some single events contribute many γ-rays (§ 2.7).

A comparison of these rates yields information on the nature of the production process. This comparison is made in the next chapter when the production of γ-rays in graphite is discussed.

Table 2.5.

Rates of Production at Top of Atmosphere.

(no. of events/gm.ster.sec) x 10^9.

Class of Event	Energy (Gev)	Production Rate
γ-rays from Graphite	$E_\gamma \geqslant 1200$	5.0 ± 2.5
γ-rays from Air	$E_\gamma \geqslant 1200$	2.7 ± 1.0
γ-rays from Air + Graphite	$300 \leqslant E_\gamma < 1200$	23.0 ± 2.7
Nuclears in Graphite	$\Sigma E_\gamma \geqslant 1200$	5.4 ± 1.3
Nuclears in Detector	$\Sigma E_\gamma > 1200$	1.9 ± 0.4
Nuclears in Detector	$300 \leqslant \Sigma E_\gamma < 1200$	15.3 ± 2.2

CHAPTER III.

Graphite Interactions.

§ 3.1 Introduction.

In this Chapter a detailed discussion is given of the analysis of 25 nuclear interactions in the graphite producing layer, in each of which at least 1200 Gev was radiated as γ-rays. The energy and angle of every γ-ray within certain fiducal limits were measured; the distribution of these quantities and of the transverse momenta are studied and a critical account is given of the effect on the final analysis of the fiducal limits. The data was examined for possible correlations between these quantities and for any variation between individual events or with increasing energy. In the final three sections, § 3.8 - 3.10, the data is analysed in terms of a simple model of meson production.

§ 3.2 Experimental Details.

The 1900 events found by naked-eye scanning were examined under the microscope. Within the limits of dip angle, $0.15 < \sin \delta < 0.92$, 66 events possessing several almost parallel γ-ray cores were found. Each of these events was examined in many emulsion layers and the relative positions of its γ-ray cores accurately measured. An event was accepted as being of graphitic origin only if these measurements showed its cores to be converging to a point in the graphite layer. Four events of low energy, probably γ-rays which had bred in the air several hundred meters above the

Plates 1 and 2.

Photomicrographs of the γ-rays from two of the high energy graphite interactions. Plate 1 shows various stages in the developement of a highly multiple event (K 14) in which 13,000 Gev was radiated as γ-rays. Plate 2 shows an event (K 45) in which 2 γ-rays from the decay of a π^{o}-meson of energy 5,000 Gev carry most of the radiated energy.

The scale in both plates is in units of 10μ.

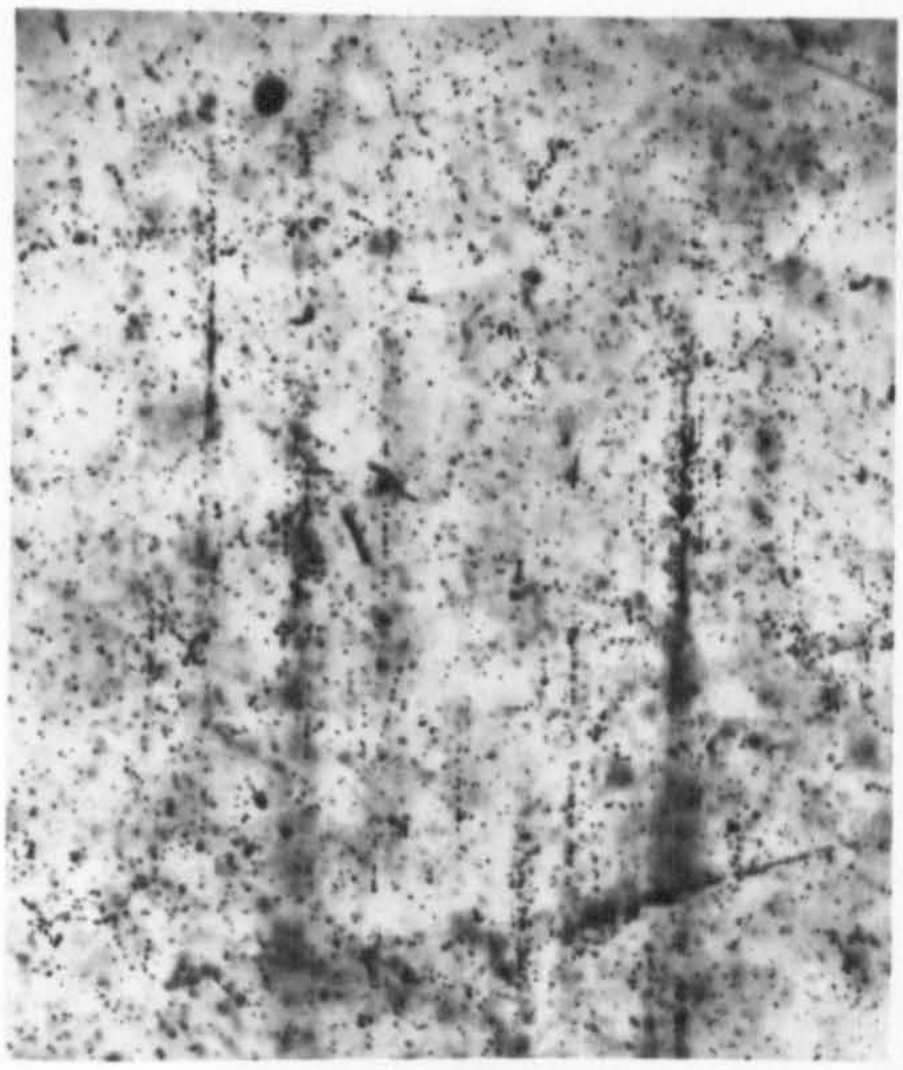

2 RADIATION LENGTHS

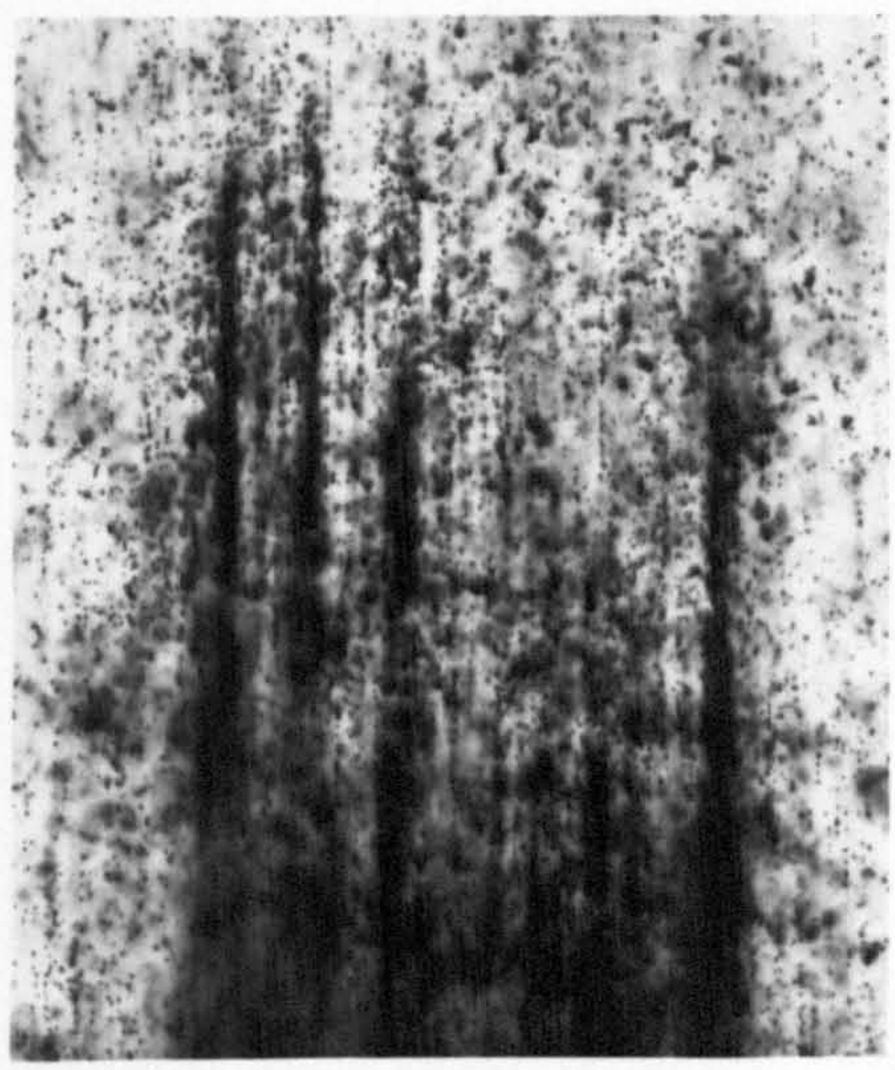

4 RADIATION LENGTHS

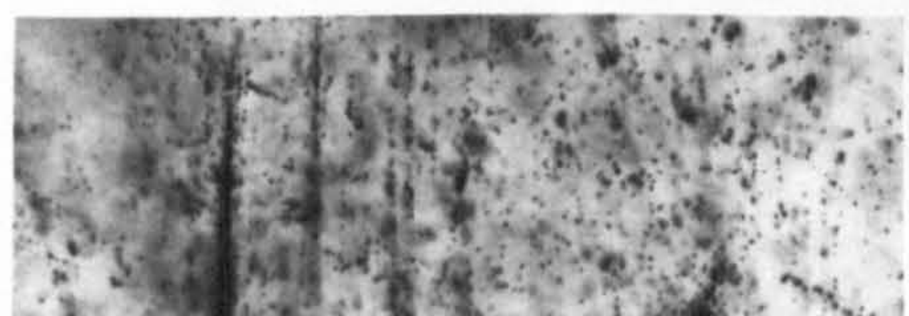

3 RADIATION LENGTHS

5 RADIATION LENGTHS

Plate 1.

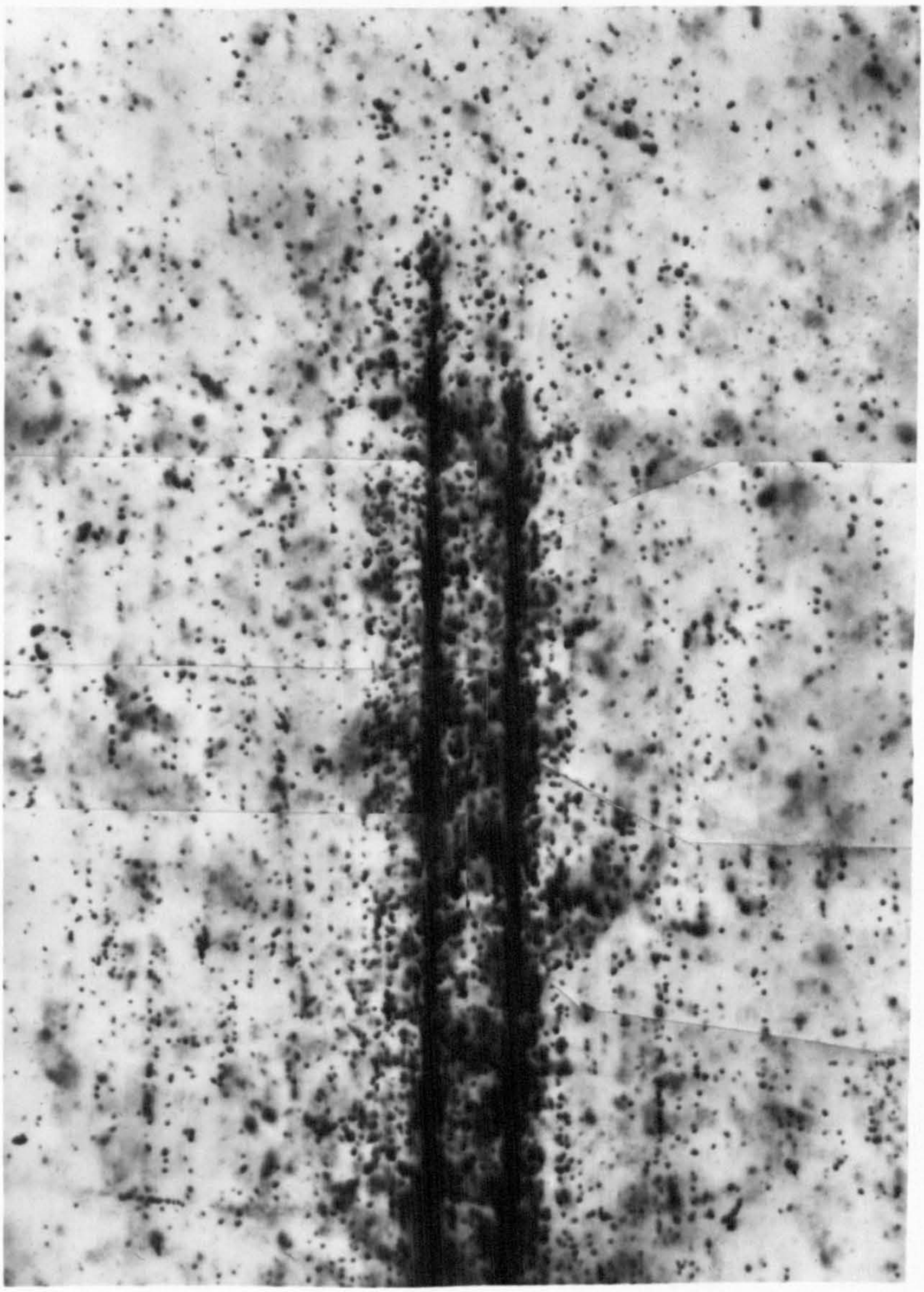

Plate 2.

assembly, were rejected as not satisfying this criterion.

Previously (§ 2.6) it has been shown that efficiency with which graphite events are detected and recognised is high for $\Sigma E_\gamma \geq 1200$ Gev but falls for lower energies. Of the remaining 62 events, 25 satisfied the criterion $\Sigma E_\gamma \geq 1200$ Gev; in order to obtain an unbiased sample, the analysis of individual graphite interactions was restricted to these 25 events.

The photometric methods adopted for measuring the energies of individual γ-rays have been described in the previous Chapter. In each event the energies of all the high energy (i.e. $E_\gamma > 200$ Gev) γ-rays were first measured. If the total energy of the event seemed likely to be 1000 Gev or more, a careful scan was made for low energy γ-rays. This scan was performed at depths of approximately 1.5 and 2.5 γ-ray conversion lengths from the point of entry of the event into the detector, and out to an angle of 10^{-2} radians from the axis of the event. The scan was made on a Cooke M4000 microscope using a x25 oil immersion objective. A γ-ray of 50 Gev between 1 and 3 radiation lengths from its point of origin should have 5 or more electrons within a radius of 15μ and should therefore be easily detectable in such a scan. The coordinates of each γ-ray found were noted and it was then traced through successive emulsion layers from its conversion until it reached maturity. The energies of all γ-rays within 10^{-2} radians were determined. Only those γ-rays with energies grater than 50 Gev were used in the final analysis since

below this energy the scanning may become inefficient and since at about 30 Gev the energy estimate is seriously influenced by the effects of cascade fluctuations.

The lateral position (x_i, y_i) of each γ-ray was recorded with respect to a prominent γ-ray near the centre of the event. The true position of the axis of the event is unknown; it was estimated as having a coordinate (a,b) with respect to the reference γ-ray:

$$a = \frac{\Sigma E_i^2 x_i}{\Sigma E_i^2} \quad ; \quad b = \frac{\Sigma E_i^2 y_i}{\Sigma E_i^2} \qquad (3.1)$$

where E_i, x_i, y_i are the energy and position coordinates of the i^{th} γ-ray and the summation is taken over all γ-rays with energies $E_\gamma \geq 50$ Gev and angles $\theta < 10^{-2}$ radians. The above axis is not the centre of momentum of the γ-rays; it is that axis which minimises the sum of their transverse momenta squared, $\sum_i P_{T_i}^2$. It was chosen as being less liable to fluctuate from the true axis of the event.

The space angle, θ_i, in radians, of every γ-ray was then calculated with respect to this axis. The finite thickness of the graphite, and the corresponding uncertainty in the distance of the orig$^{in}_{\Lambda}$ from the detector, led to an error of ± 10% in this angle.

For convenience in the analysis which follows the 25 graphite events have been divided into two groups.

(i) High Energy Group - 12 events, in each of which the total radiated energy, ΣE_γ, exceeded 3000 Gev.

(ii) Low Energy Group - 11 events, in each of which $3000 > \Sigma E_\gamma \geqslant 1200$ Gev.

There remain two events in which the presence of multiply charged particles among the cascades indicated that the event was caused by the interaction of a heavy primary nucleus in the graphite. In both of these events the high multiplicity, the low individual γ-ray energies and the angular distribution of the observed fragments, indicated that at least 3 or 4 nucleons had participated in the interaction. Therefore one of these events, with a total energy of 4500 Gev, was nevertheless, added to the Low Energy Group. The other event, which had a total energy of 1800 Gev and a highest individual γ-ray energy of 140 Gev, was not included in either group and is not considered in the rest of this analysis.

Figs 3.1 - 3.4 present the measured data. Every γ-ray within the limits $E_\gamma \geqslant 50$ Gev and $\theta < 10^{-2}$ rad. has been presented here; no attempt has been made to pair off γ-rays as π^0-mesons since this process is unreliable even at low multiplicities. Figs 3.1(a) and (b) show the individual γ-ray energies, E_γ, the total radiated energy, ΣE_γ, and the number of γ-rays within the above criteria for each event in the high and low energy groups respectively. Figs 3.2(a) and (b) show the laboratory angle of each γ-ray. The median angle of each event is also indicated; this was estimated by assuming the radiated energy, ΣE_γ, to be ten percent of the primary energy. Figs 3.3(a) and (b) show the transverse momentum, $P_T = E_\gamma \sin\theta$, of each γ-ray. The mean transverse momenta of

Figs 3.1 - 3.4.

These figures present the measured energies, angles and transverse momenta of all γ-rays observed from the high energy interactions in the graphite layer.

(a) High Energy Group, $\Sigma E_\gamma \geqslant 3000$ Gev.

(b) Low Energy Group, $3000 > \Sigma E_\gamma \leqslant 1200$ Gev.

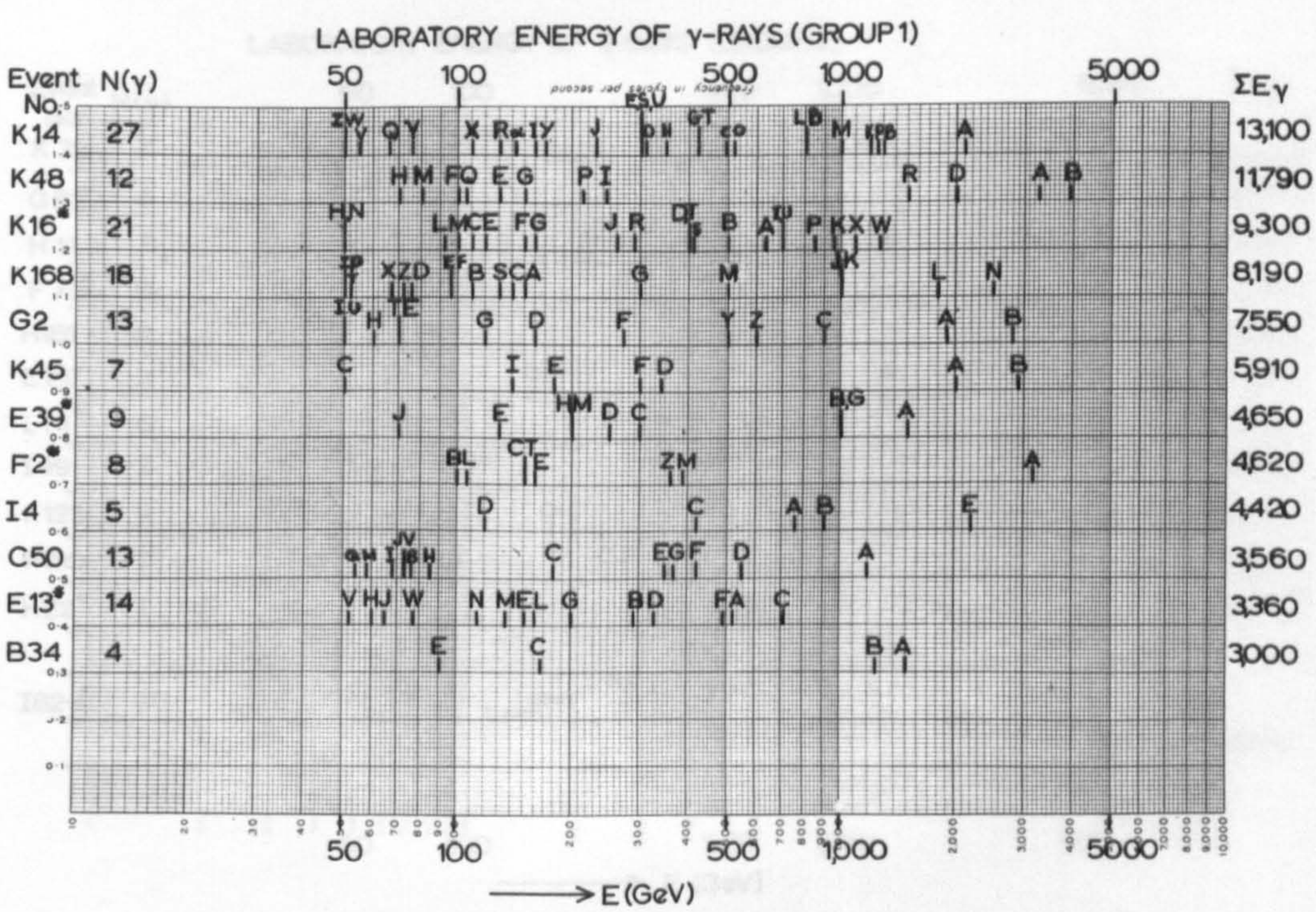
LABORATORY ENERGY OF γ-RAYS (GROUP 1)
Event No.
N(γ)
ΣEγ
50
100
500
1000
5000
K14 27 13,100
K48 12 11,790
K16 21 9,300
K168 18 8,190
G2 13 7,550
K45 7 5,910
E39 9 4,650
F2 8 4,620
I4 5 4,420
C50 13 3,560
E13 14 3,360
B34 4 3,000
E
C
B
A
E(GeV)

Fig 3.1 (a)

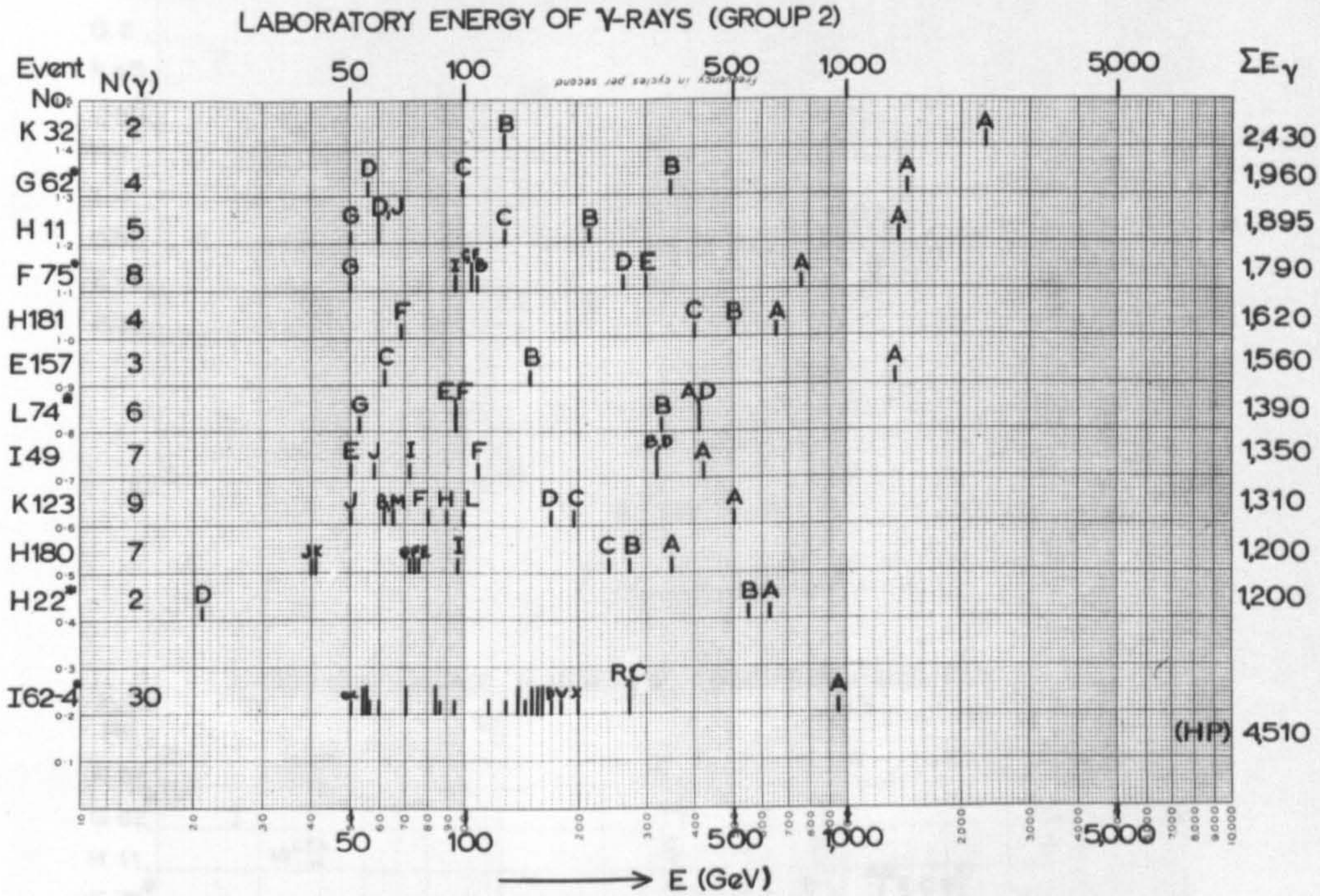
LABORATORY ENERGY OF γ-RAYS (GROUP 2)
Event No.
N(γ)
50
100
500
1,000
5,000
ΣEγ
K 32 2 2,430
G 62* 4 1,960
H 11 5 1,895
F 75* 8 1,790
H181 4 1,620
E157 3 1,560
L 74* 6 1,390
I 49 7 1,350
K123 9 1,310
H180 7 1,200
H22* 2 1,200
I62-4 30
RC
(HP) 4510
E (GeV)

Fig 3.1 (b)

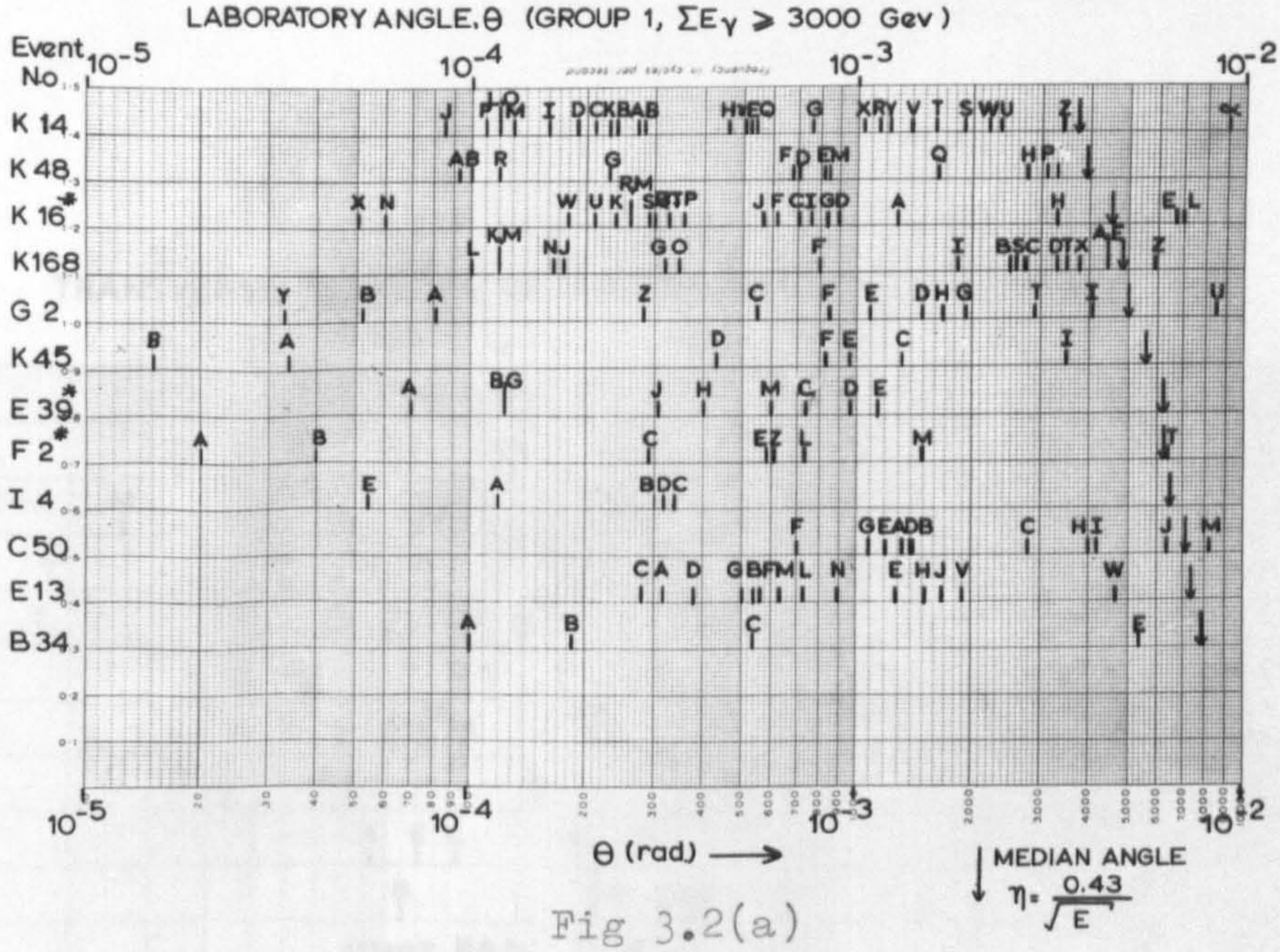

Fig 3.2(a)

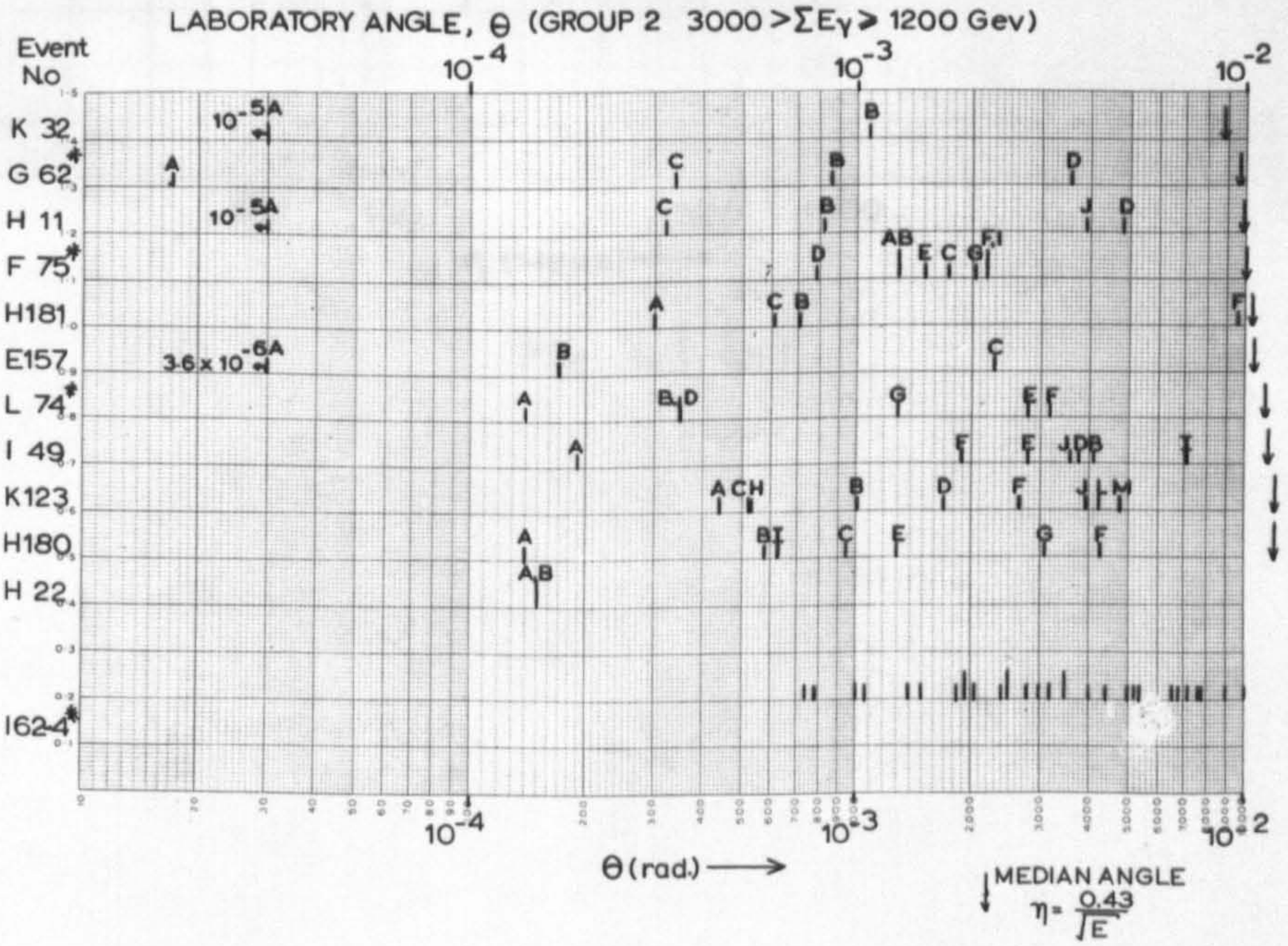

Fig 3.2(b)

TRANSVERSE MOMENTA OF γ-RAYS (GROUP 1, $\Sigma E_\gamma \geq 3000$ Gev)

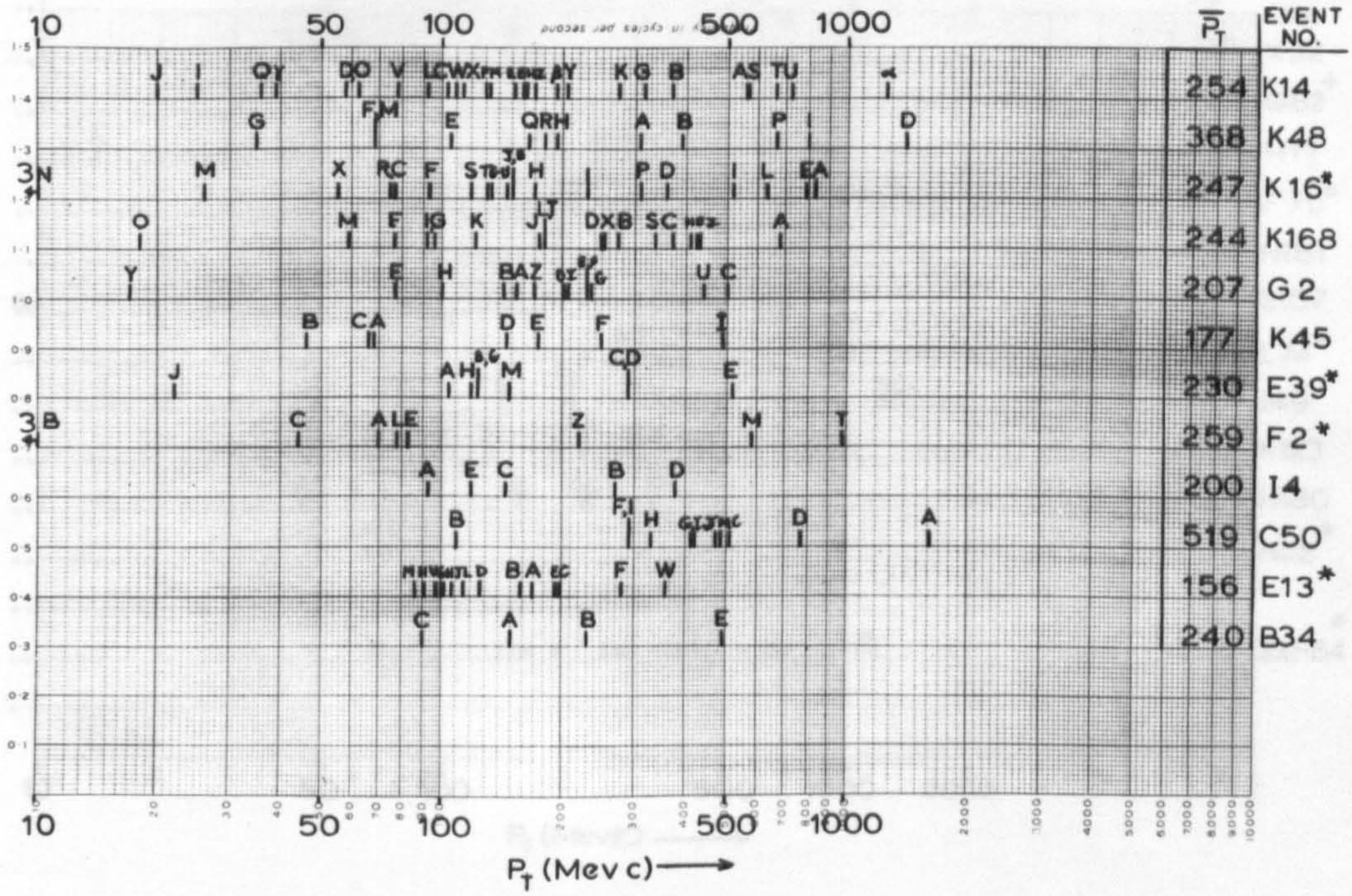

Fig 3.3 (a)

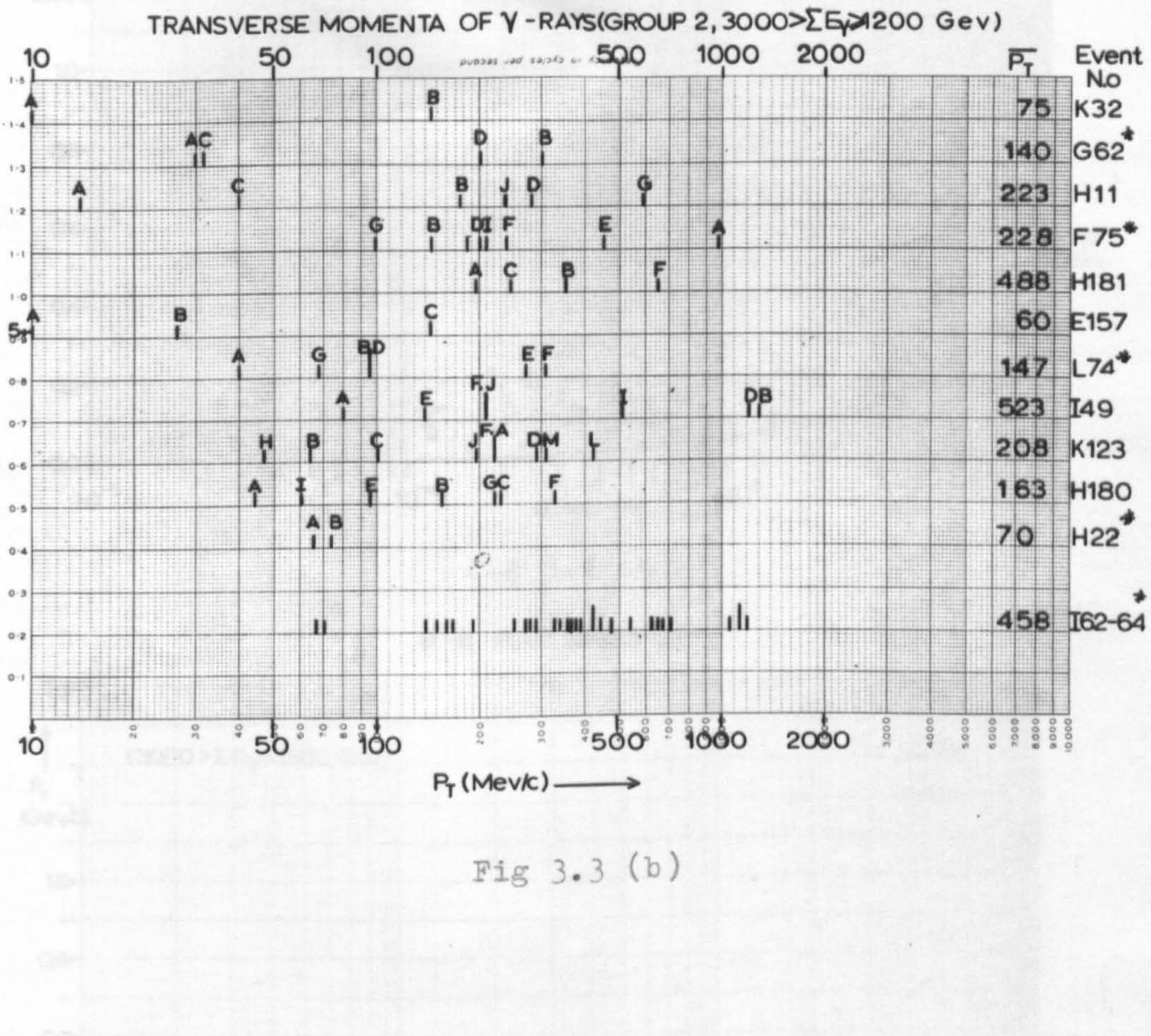
TRANSVERSE MOMENTA OF γ-RAYS(GROUP 2, 3000>ΣEγ≥1200 Gev)
10
50
100
500
1000
2000
P_T
Event No
75 K32
140 G62*
223 H11
228 F75*
488 H181
60 E157
147 L74*
523 I49
208 K123
163 H180
70 H22*
458 I62-64*
P_T (Mev/c)

Fig 3.3 (b)

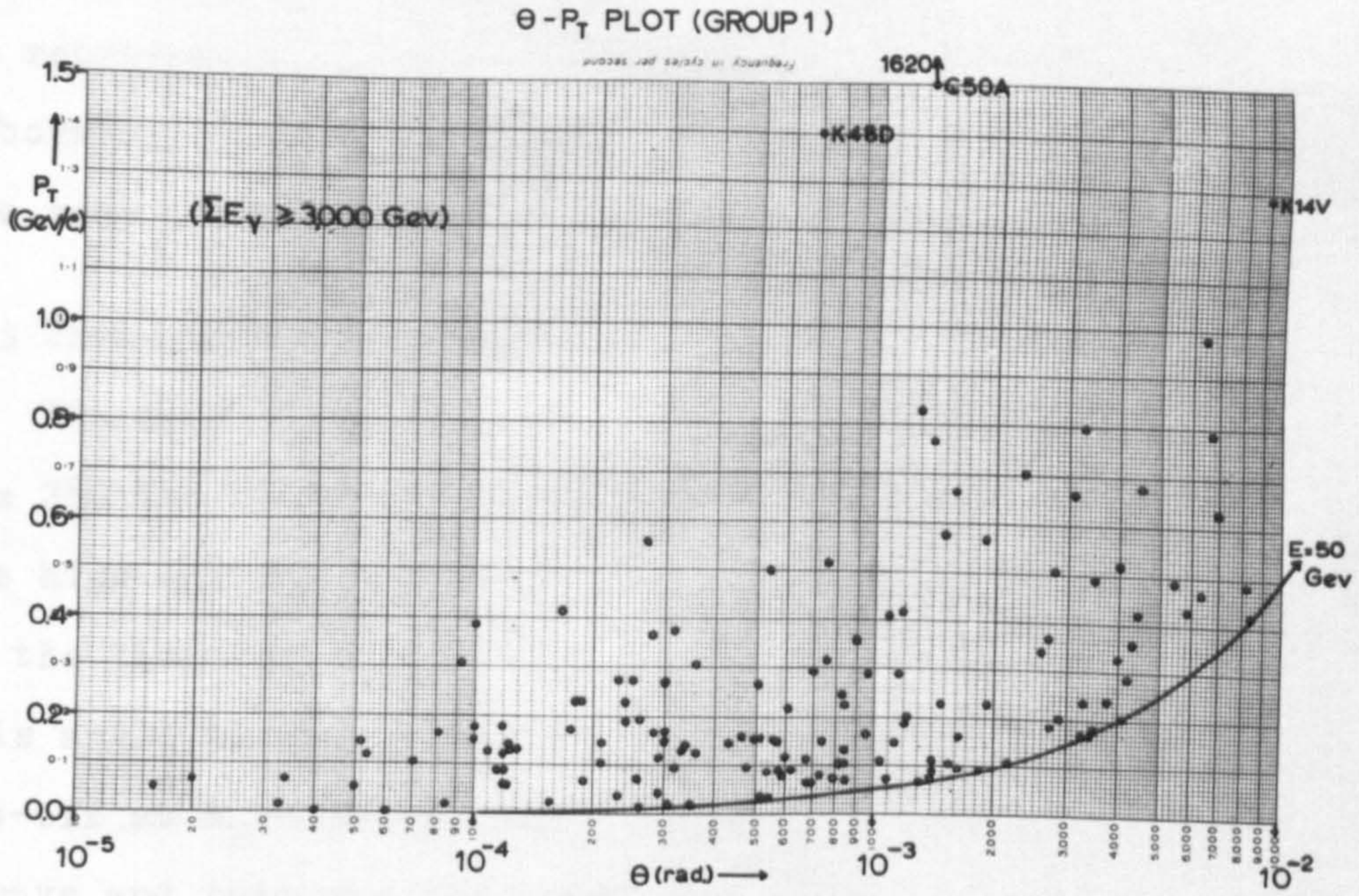

Fig 3.4 (a)

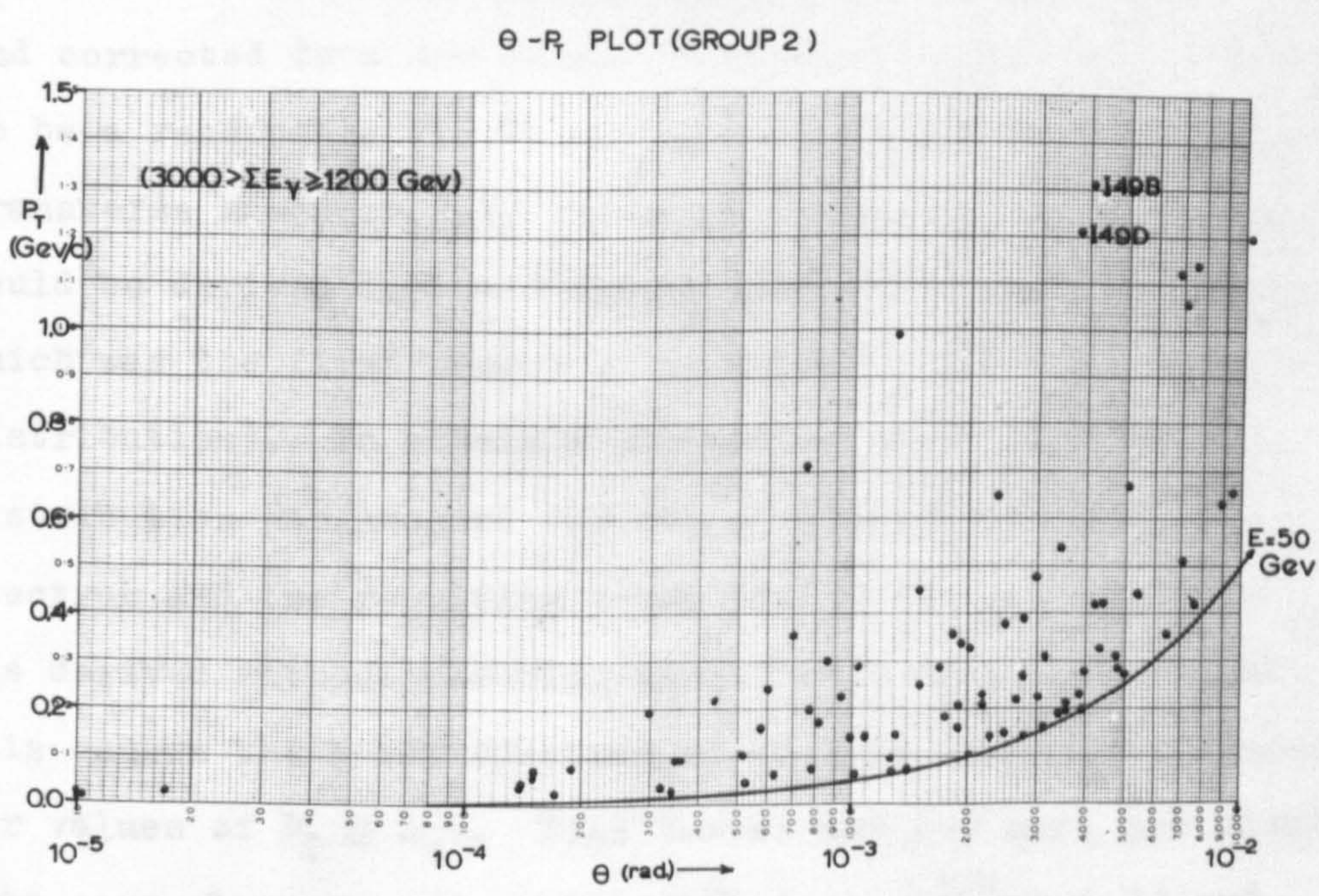

Fig 3.4 (b)

each event is given. Figs 3.4(a) and (b) show the combined distributions of transverse momenta and angles; each event is represented by one point. The curve corresponds to a laboratory energy of 50 Gev and shows the effect of limiting the scan to γ-rays above this energy.

§ 3.3 Transverse Momentum.

The mean transverse momentum of all the 236 γ-rays observed was 280 Mev/c. There is no significant difference between the high and low energy groups. This mean is little effected by the limiting of the scan to angles within 10^{-2} radians, since this angle is approximately the median angle. However the cut-off at E_γ = 50 Gev will result in a shortage of low P_T γ-rays and this was corrected for. Fig 3.5 shows the integral p_T spectrum for all γ-rays in both groups; the uncorrected and corrected data are shown. The uncorrected data is seen to be a reasonable fit to an exponential spectrum of γ-ray transverse momentum. If the pion rest mass were zero, this would be derived from a π^o-meson transverse momentum spectrum which was the first moment of an exponential (i.e. Boltzmanns distribution). To obtain a correction such a Boltzmann distribution was assumed for the π^o transverse momentum spectrum and the resulting γ-ray transverse momentum spectrum was derived without assuming the π^o rest mass to be zero; this causes the γ-ray spectrum to deviate from an exponential for values of $P_T \lesssim m_\pi c$. Figs 3.4(a) and (b) were now divided into several ranges of angle, θ, ($\theta_2/\theta_1 = 10^{1/4} \approx 1.8$) and

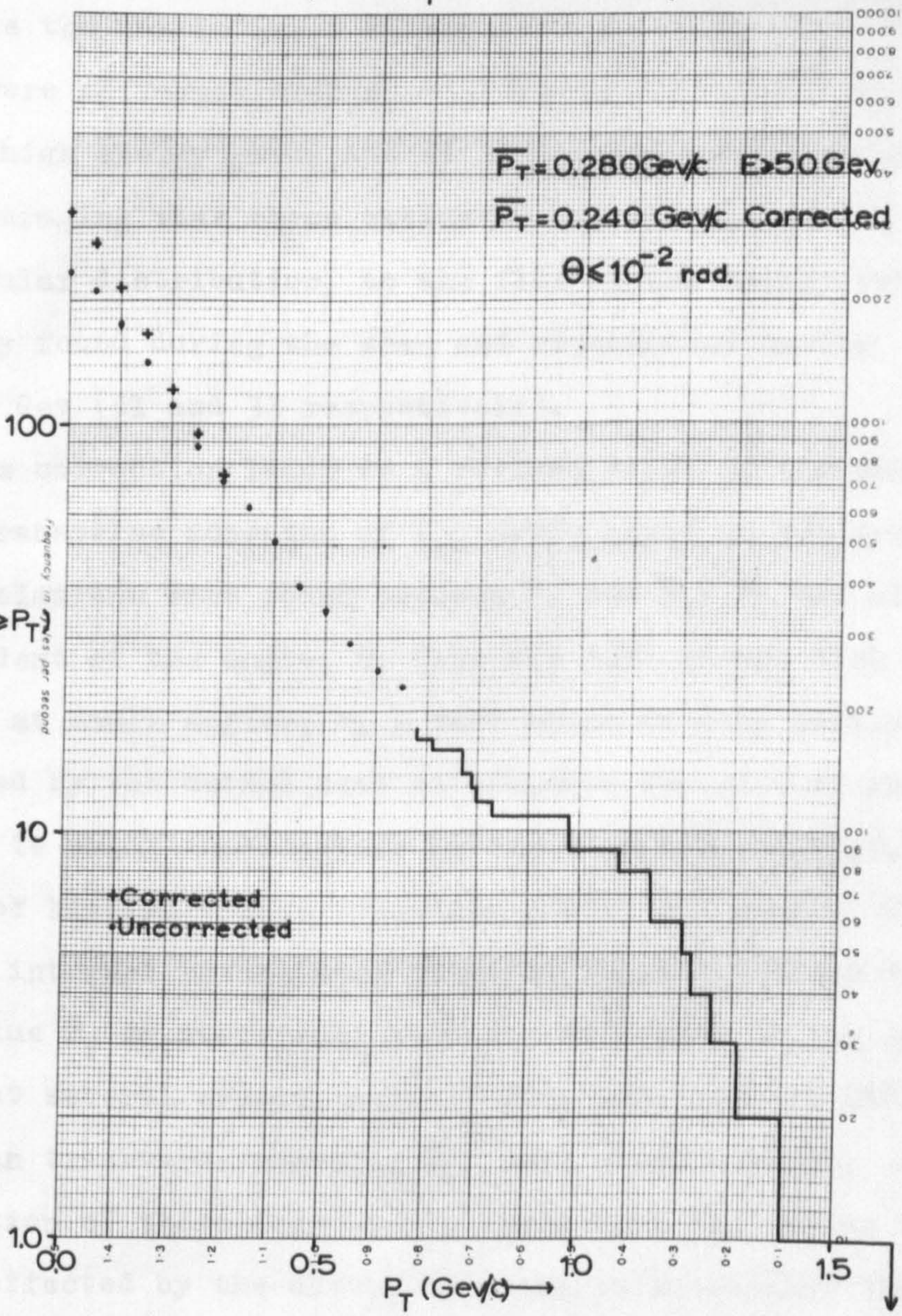
INTEGRAL γ-RAY P_T SPECTRUM(ΣE_γ>1200 Gev)
$\overline{P_T}$ = 0.280Gev/c E>50 Gev.
$\overline{P_T}$ = 0.240 Gev/c Corrected
θ≤10⁻² rad.
100
10
1.0
N(≥P_T)
frequency in cycles per second
+Corrected
•Uncorrected
0.0
0.5
1.0
1.5
P_T (Gev/c)

Fig 3.5.

in each angular interval the number of γ-rays above 50 Gev was used, in conjunction with the calculated spectrum, to estimate the number below 50 Gev. It was estimated that there were 48 γ-rays with E_γ < 50 Gev and $\theta < 10^{-2}$ radians in the high energy group and 46 in the low energy group. It is encouraging that these estimates are close, both in number and angular distribution, to the flux of low energy γ-rays actually found during the scan and rejected as having E_γ < 50 Gev (51 and 33 respectively).

This correction leads to a revised value of the mean γ-ray transverse momentum of 235 Mev/c based on 330 γ-rays. No correlations were found between P_T and E_γ; P_T was also independent of the angle, θ, (see Fig 3.4) except that P_T was low at small angles, θ, a fact which is only partly explained by the method used to estimate the axis of each event. It is of considerable interest to note, Fig 3.5, a tail of high P_T γ-rays extending out to 1.5 Gev/c. Of even greater interest is the wide range of values obtained for the mean value $\bar{P}_T$ in individual events. Reference to Fig 3.3 will show that several events, notably I49, C50, I62 and H181 have mean transverse momenta, $\bar{P}_T$, well above average. An examination of these four events shows this high value to be little effected by the choice of axis; in particular the axis of event I62 - 4 is well defined by the presence of an α-particle from the break-up of a heavy primary.

§ 3.4 Multiplicity of γ-rays.

In this section an estimate is made of the average total number of γ-rays produced in interactions at this energy and hence of the multiplicity of charged and neutral π-mesons. For the 12 events in the high energy group the mean number of γ-rays, of energy $E_\gamma \geqslant 50$ Gev, within the median angle, was 11.9 per interaction. The estimated number of low energy γ-rays within this angle is 2.5 per interaction. Therefore, assuming that all γ-rays result from the decay of π^o-mesons and that the production rate of mesons is charge independent and is the same in the foward and backward directions, the total pion multiplicity is:

$$N_{\pi_o}^{\pm} = 43 \pm 5 \text{ per interaction; } \Sigma E_\gamma \approx 6500 \text{ Gev.}$$

For the low energy group, excluding the interaction caused by a heavy primary in which several nucleons were believed to have interacted, the mean numbers of γ-rays within the median angle were 5.2 per interaction above 50 Gev, and an estimated 2.8 per interaction below 50 Gev, giving a total pion multiplicity of:

$$\overline{N_{\pi_o}^{\pm}} = 24 \pm 3 \text{ per interaction; } \overline{\Sigma E_\gamma} \approx 1500 \text{ Gev.}$$

Events caused by the interactions of heavy primaries in the graphite layer will usually have been recognized and were not considered in calculating these multiplicities. However α-particle interactions will be included in the above sample and the mean multiplicities in proton-light nucleus

collisions will be about 20% less than the values quoted. Also the events used were detected by means of their radiated γ-ray energy and, on account of the steeply sloping primary spectrum, the sample is likely to be biased towards high π^o inelasticities. It may be therefore that the sample is also biased towards events in which the fraction of neutral π-mesons is greater than $^1/3$. This effect is discussed in a later Chapter when the pionization process is examined; it is probably small. The two possible sources of overestimation mentioned will apply with equal force to both groups considered. Therefore the large, and remarkable, difference between the two multiplicities remains. It is of great interest to consider whether the increased number of γ-rays at high energies is due to a more copious production of low energy pions or if it is the result of the energy spectrum being modified at all energies. This will be examined in the next section where the partition of energy is discussed.

§ 3.5 Partition of Energy.

The fractional energy, f, of each γ-ray is defined to be $f = E_\gamma/\Sigma E_\gamma$ where the summation is made over all the γ-rays in the same event with $E_\gamma \geqslant 50$ Gev and $\theta < 10^{-2}$ radians. Figs 3.6(a) and (b) show the integral f-spectra for all γ-rays in the high and low energy groups respectively. Both spectra are seen to be good approximations to exponentials, e^{-f}/f_o, for values of $f > 0.1$. The value of the index f_o for the two groups is

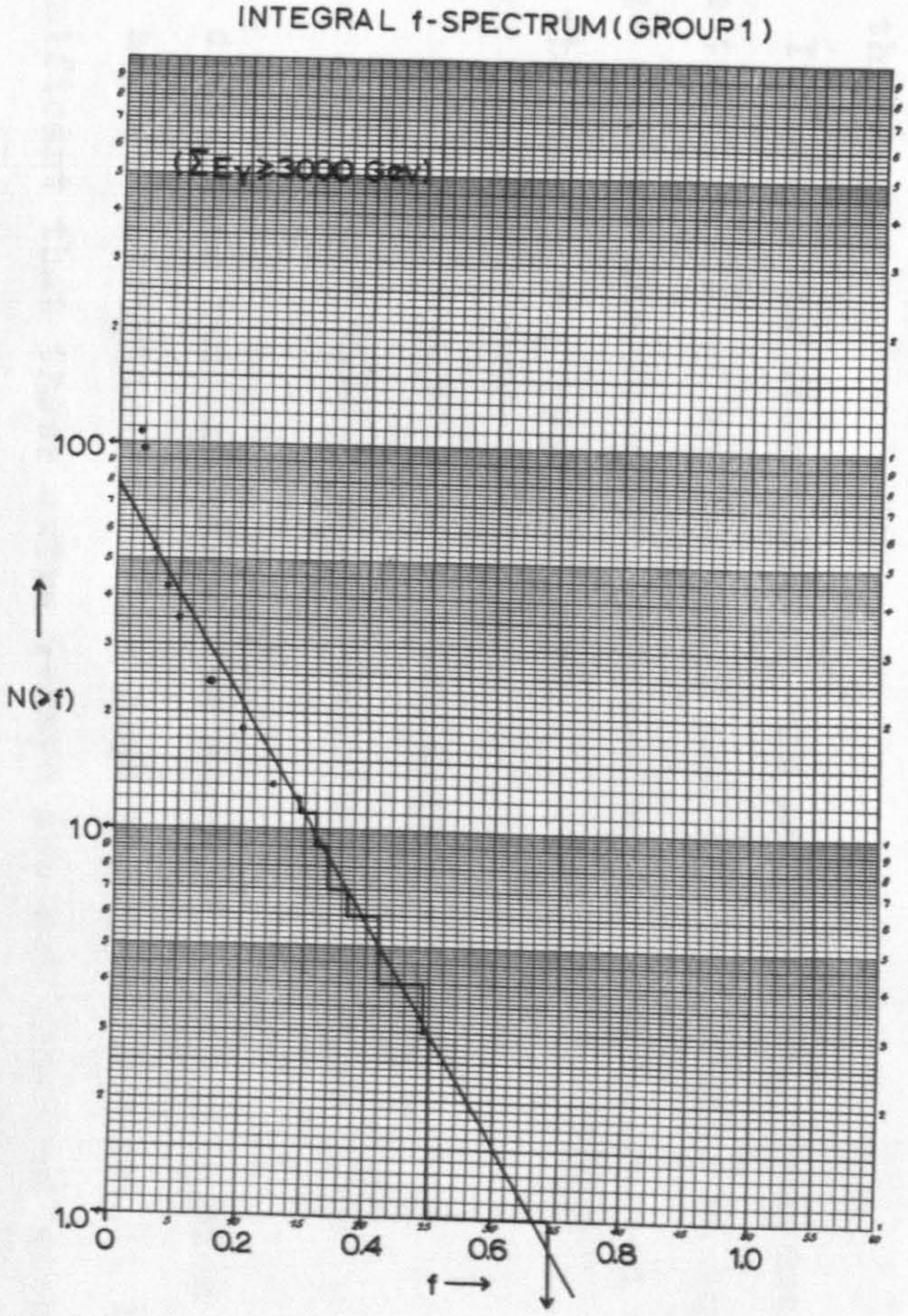

Fig 3.6 (a)

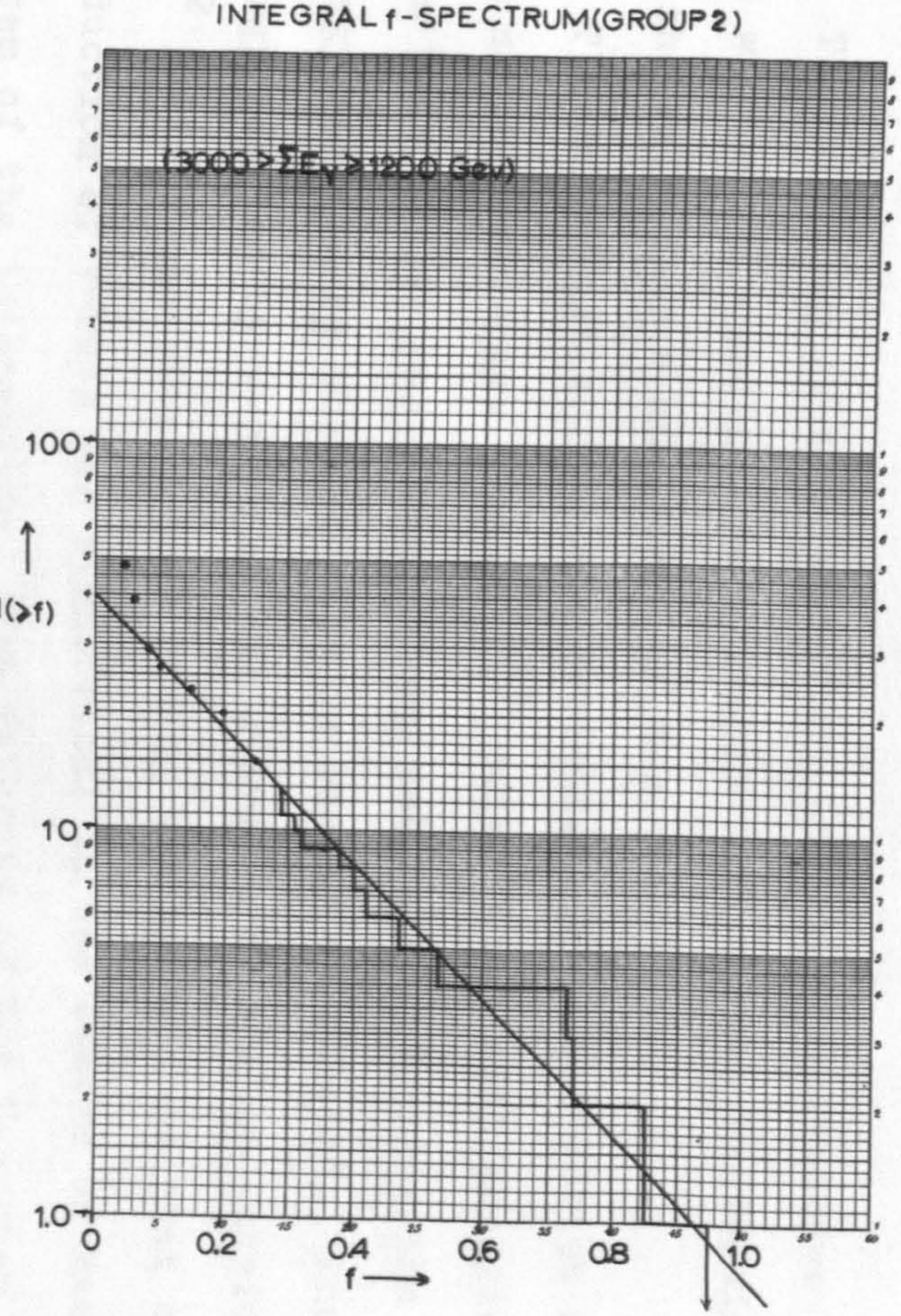

Fig 3.6 (b)

$f_o = 0.27$ for the low energy group.

$f_o = 0.16$ for the high energy group.

The limiting of the summation, ΣE_γ, to γ-rays above 50 Gev and within 10^{-2} radians will result in a slight overestimation of the values of f and hence of f_o.

The 'missing' energy was estimated and a correction applied. The number of γ-rays within 10^{-2} radians and with energies less than 50 Gev has already been estimated (§ 3.3); the energy carried by these γ-rays is easily calculated. The energy carried by γ-rays of all energies at angles outside 10^{-2} radians was obtained by making the assumption that the production of γ-rays was symmetrical in the Centre of Mass system of the interaction. The velocity of the C-system was calculated on the assumption that the energy radiated is 10% of the primary energy; the final answer is rather insensitive to this value.

It was calculated that, on the average, ΣE_γ underestimates the total radiated energy by 3% and 13% for events in the high and low energy groups respectively. The corrected values of the index, f_o, become

$f_o = 0.24 \pm 0.03$ Low Energy Group.

$f_o = 0.16 \pm \begin{matrix} 0.03 \\ 0.02 \end{matrix}$ High Energy Group.

The difference between these two numbers is a reflection of the higher multiplicity in the high energy group but it is significant that these extra γ-rays are not produced with

trivial energies but rather they lead to a change in the shape of the entire spectrum. In five of the twelve low energy events, Fig 3.1(b), the highest energy γ-ray has three times the energy of the next best γ-ray. This occurs in only one of the 12 high energy events, Fig 3.1(a). In most of these the energy is shared between at least 2 γ-rays of comparable high energies. These features are consistent with a model of pionization in which, as the primary energy increases, a constant fraction of this energy is shared among an increasing number of mesons.

§ 3.6 Centre of Mass System.

It is of interest to examine the distribution of γ-rays in the C-system of the primary interaction. This transformation can be made only if the Lorentz factor, γ_c, of the cente of mass system is known. γ_c was estimated by assuming that the energy of the incident particle was $E_o = 10\ \Sigma E_\gamma$ and that the mass of the target was one nucleon mass. The assumption that the mean energy radiated as neutral pions is 10% was based on an extrapolation of the results of Guseva et al (1962) at energies ≈ 100 Gev, on a comparison of the spectrum of primary cosmic ray particles with the spectrum of observed nuclear cascades, Kaddoura (1961), and on a comparison between the attenuation and interaction lengths of nuclear particles in the atmosphere, Duthie et al (1961). It is unlikely that the value of γ_c so estimated will be out by a factor of 3 and usually it will be much better than this.

For each event a value of γ_c was calculated in this

manner and hence the transverse and longitudinal momenta of each γ-ray in the centre of mass system obtained. This data is presented in Figs 3.7 and 3.8 for the low and high energy groups respectively. In each figure a line corresponding to a laboratory energy of 50 Gev has been drawn to illustrate the effect of the scanning cut off at this energy. The numbers of γ-rays within this area have been estimated previously, § 3.3, and these numbers are shown in the figures.

The distribution of longitudinal momenta in the two groups is remarkably similar. Both spectra, Fig 3.12, approximate well to an exponential distribution at high $p_{\parallel}$ ($p_{\parallel}$ > 2 Gev/c) but are peaked at low values; this distribution is discussed later in § 3.9. The mean parallel momentum, $\bar{p}_{\parallel}$, of the 'high energy' γ-rays ($p_{\parallel}$ > 2 Gev/c) is the same for both groups, 4.3 Gev/c.

§ 3.7 Texas Lone Star.

A description will be given here of a single high energy interaction which occured in an earlier experiment. The event was observed in a stack of similar composition to that used in this experiment (B2 Stack of Duthie et al, 1962) which was exposed on a balloon for 8 hours at 25 gm/cm.^{2} pressure. The flight took place in Texas in April 1960 and because of its unique energy the event was referred to as the 'Texas Lone Star'. The interaction, in which an estimated 150,000 Gev was radiated as γ-rays, took place 35 cms. away from the detector in a 1 mm. thick Aluminium container. It therefore simulates the type of graphite interaction which

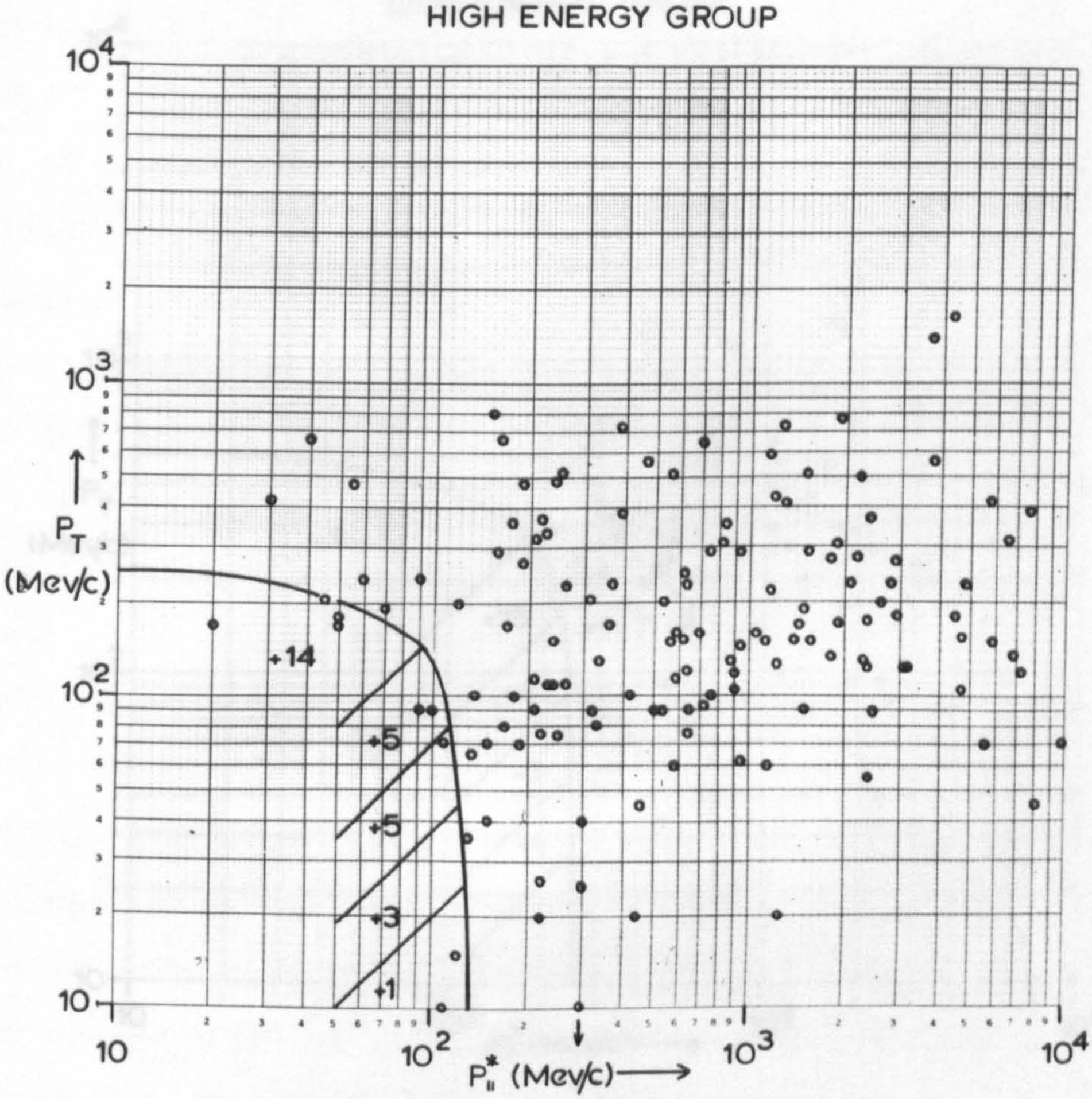

Fig 3.7.

Distribution of γ-ray Momenta in the C-System.

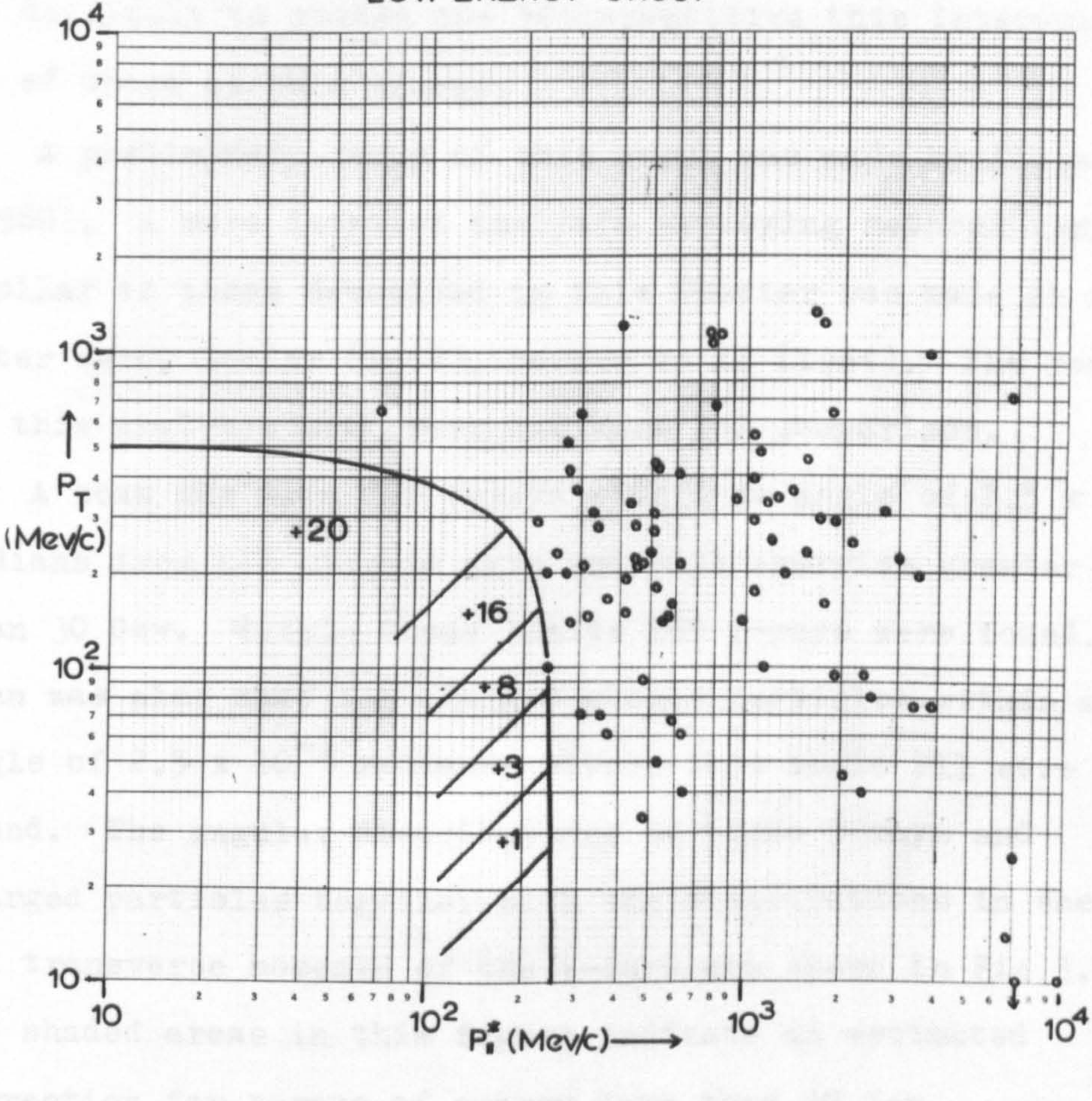

Fig 3.8.

Distribution of γ-ray Momenta in the C-System.

the present stack was designed to study and it is presented here as an example of an interaction with a light nucleus in which the energy radiated is an order of magnitude greater than that observed in the present experiment. It is difficult to assess how representitive this interaction is of those at this energy.

A preliminary study of this event was made by Ali et al (1960). A more detailed analysis employing methods very similar to those described in this Chapter was made at a later date, Bowler (1962), Bowler et al (1964). The results of this analysis are presented here for comparison.

A scan was made for γ-rays within an angle of 1.5×10^{-2} radians from the cascade axis and with energies greater than 30 Gev. Within these limits 195 γ-rays were found. A scan was also made for charged shower particles within an angle of 2.5×10^{-3} radians; within this angle 211 were found. The angular distributions of these γ-rays and charged particles together with the distributions in energy and transverse momenta of the γ-rays are shown in Fig 3.9. The shaded areas in this figure indicate an estimated correction for γ-rays of energy less than 30 Gev.

Assuming charge independence of the created particles, it was estimated that the total multiplicity was $\approx$ 500, of which about 80% were π^- mesons. The total energy radiated as γ-rays was 150,000 Gev and, in view of the similar angular distributions of γ-rays and charged particles, it seems plausible that the total radiated energy was

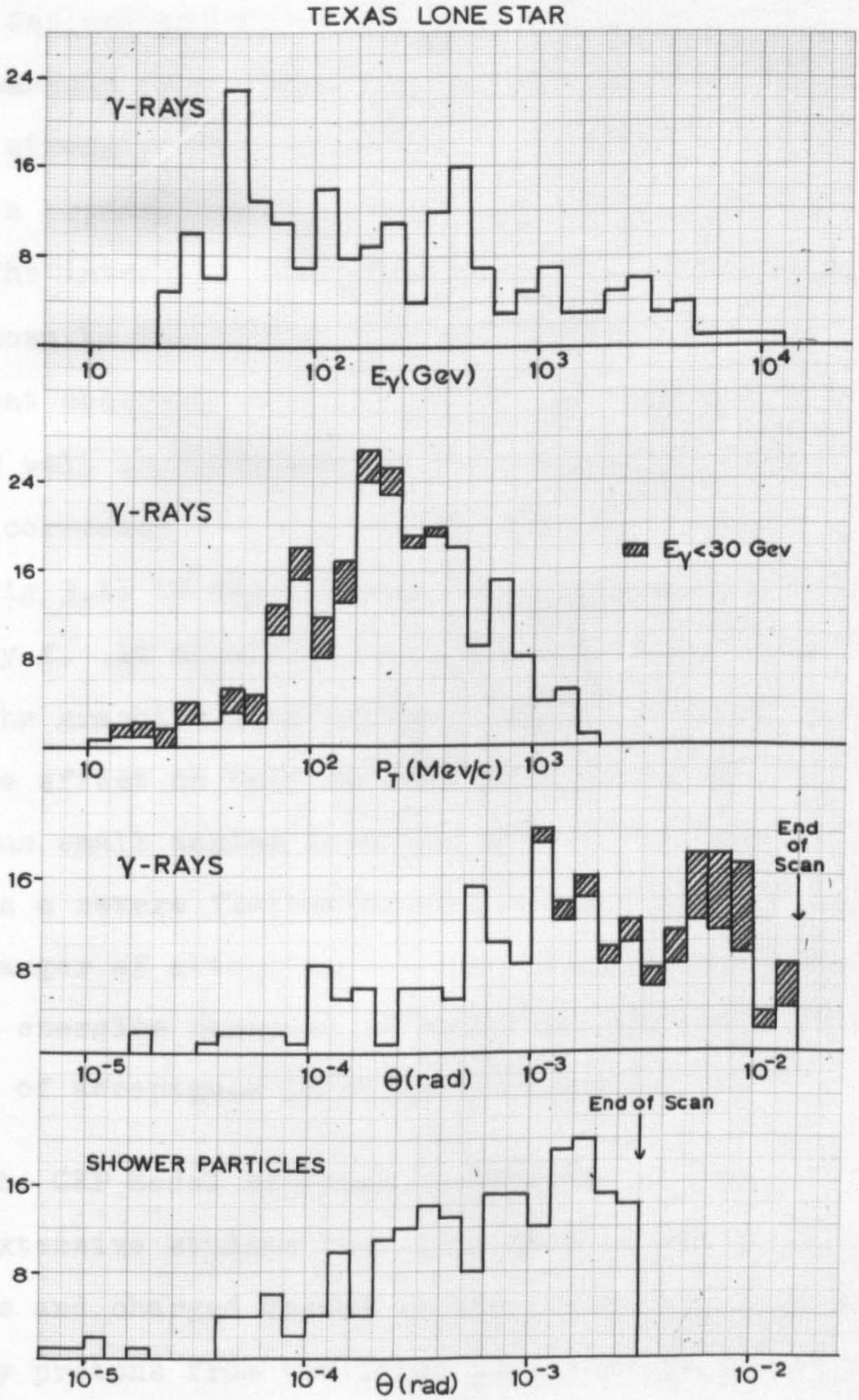
TEXAS LONE STAR
γ-RAYS
24
16
8
10
10²
Eγ(Gev)
10³
10⁴
γ-RAYS
Eγ<30 Gev
PT (Mev/c)
End of Scan
θ(rad)
10⁻⁵
10⁻⁴
10⁻³
10⁻²
SHOWER PARTICLES

Fig 3.9.

≈ 500,000 Gev. The position of the median angle was not well defined but was taken as 1.45 x 10^{-3} radians, which corresponds to a C-system Lorentz factor of 700. The absence of a strongly collimated core of shower particles suggested that a primary lighter than a Carbon was involved.

The integral transverse momentum spectrum of the γ-rays is shown in Fig 3.10. This distribution is similar in shape to that observed in the graphite interactions, Fig 3.5, being well approximated by an exponential distribution. The mean corrected transverse momentum was 320 Mev/c.

Fig 3.11 is the spectrum of the integral fractional energy f. It should be compared with Figs 3.6(a) and (b) for the graphite interactions. Also indicated in Fig 3.11 is the effect on this spectra of limiting the scan to various small angles from the axis of the event. This causes a severe flattening of the spectrum and illustrates the danger of attaching too much importance to the spectra of γ-ray energies observed in large air families, where the angle of acceptance is often very small.

§ 3.8 The CKP Model of Meson Production.

Extensive studies have been made on the production of γ-rays and charged mesons in the interactions of high energy protons from the large accelerators at the CERN and Brookhaven laboratories. Fiddecaro et al (1961) measured the energy spectra of γ-rays produced in the interactions of 23 Gev protons with liquid hydrogen; these measurements were made at a range of angles between 2° and 30° from the

Fig 3.10.

The Integral Transverse Momentum Spectrum of γ-rays in the Texas Lone Star.

Fig 3.11.

The integral spectrum of the fractional γ-ray energy $f = {}^{E_\gamma}/_{\Sigma E_\gamma}$ is shown for the Texas Lone Star. The different curves show the effect of limiting the scan to those γ-rays inside the angle indicated.

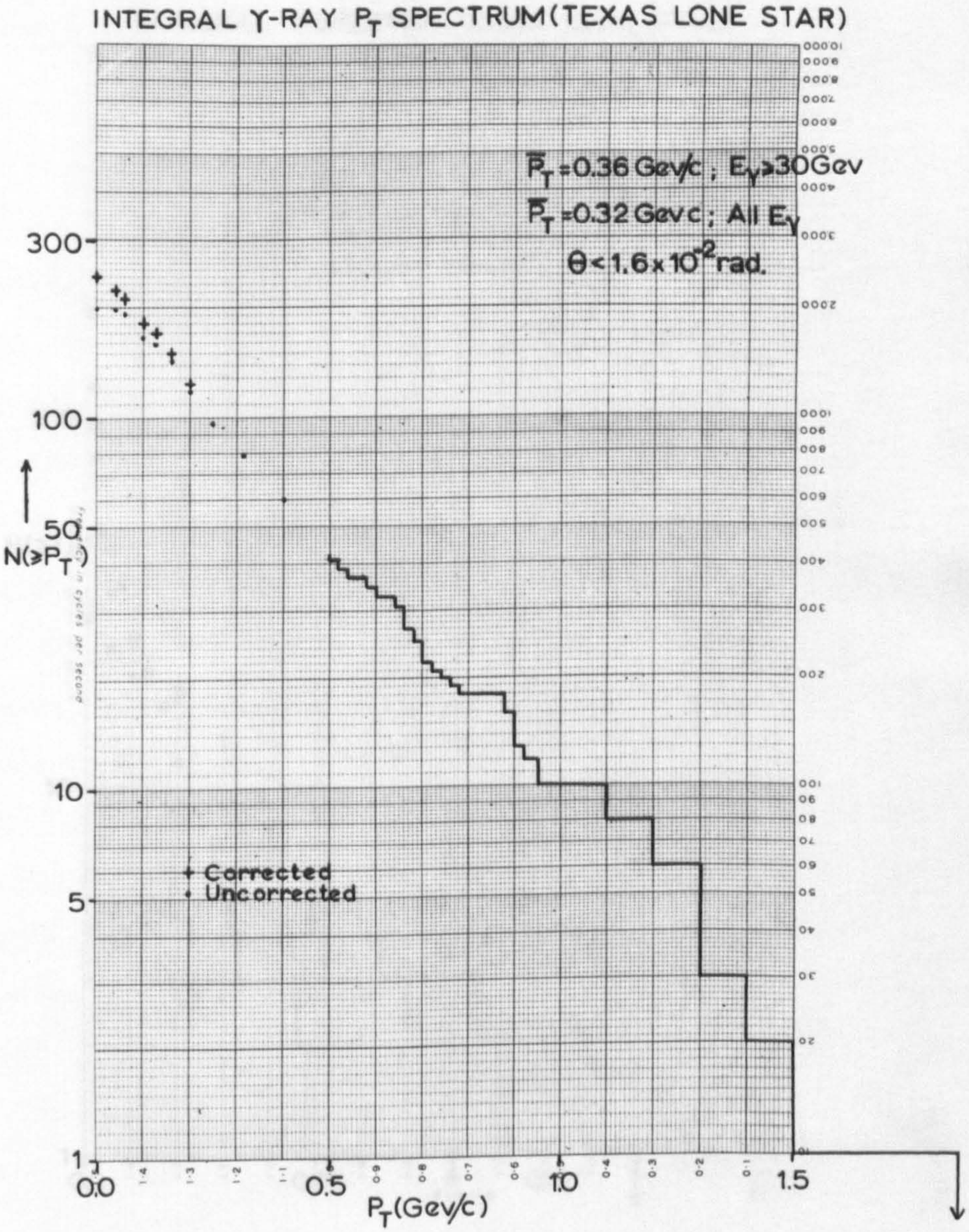
INTEGRAL γ-RAY P_T SPECTRUM(TEXAS LONE STAR)
$\bar{P}_T$=0.36 Gev/c ; E_γ>30Gev
$\bar{P}_T$=0.32 Gev c ; All E_γ
θ<1.6x10^{-2}rad.
300
100
50
10
5
1
N(≥P_T)
+ Corrected
• Uncorrected
0.0
0.5
1.0
1.5
P_T(Gev/c)

Fig 3.10.

INTEGRAL f-SPECTRA(TEXAS LONE STAR)

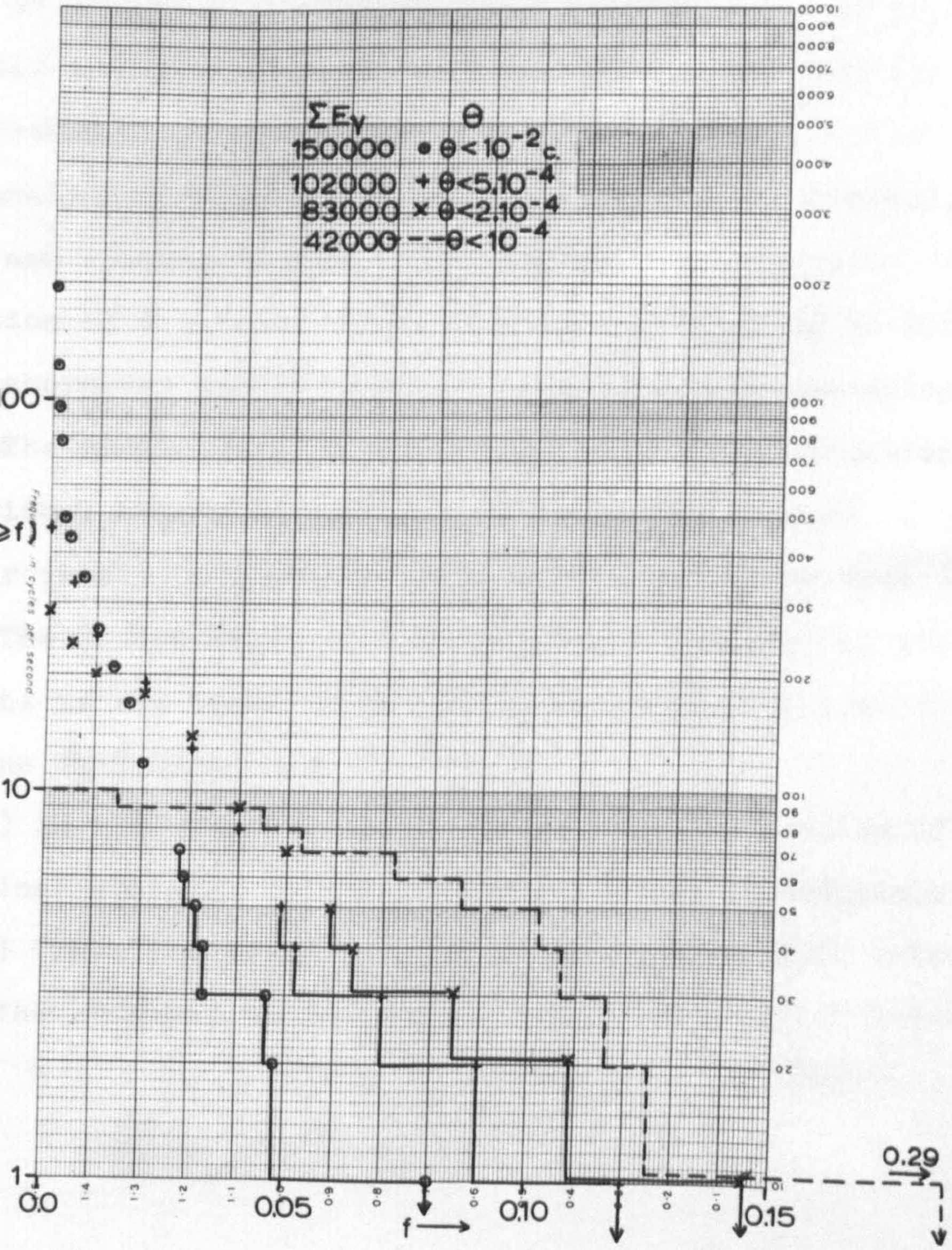

Fig 3.11.

incident direction. Baker et al (1961) studied the spectra of charged secondary particles from interactions in internal targets of Al and Be. They employed beam energies of 10,20,25 and 29 Gev and studied angles between 5° and 20° from the beam direction.

An analysis of these results has been made by Cocconi, Koester and Perkins (1961). They showed that a good description of π - meson production at angles of up to 20° in the laboratory can be provided by a simple phenomenological model. The model makes no attempt to describe fluctuations in individual events but only to describe the average behaviour in all collisions. The basic assumptions are:

(i) The distribution in the transverse momentum of the π - mesons is the first moment of an exponential , i.e. Boltzmanns distribution.

(iia) In the centre of mass system the distribution of longitudinal momentum of the π - mesons is an exponential.

(iii) These distributions are independent of each other so that the combined distribution is given by their product

$$\frac{\partial^2 N}{\partial P_{\parallel} \partial P_T} = A \frac{e^{-P_{\parallel}/P_o}}{P_o} \frac{P_T e^{-P_T/\pi}}{\pi^2} \qquad (3.2)$$

A is the multiplicity of π - mesons emitted in the foward hemisphere; P_o, π are constants. A, P_o and π may be functions of the primary energy.

Cocconi and his collaborators also considered an alternative assumption to (iia), namely

(iib) In the laboratory system the distribution of the energy of the π -mesons is an exponential.
The exponent of this exponential is $T \approx 2\gamma_c P_o$ and the model differs from (3.2) by a factor of approximately $(1 + 2 \tan^2 \phi/2)$ where ϕ is the angle of emission in the centre of mass system; this difference is small for $\phi \lesssim 30°$. This alternative approach is sometimes more convenient when the laboratory system is being considered.

Using values of $A = 3.0$, $P_o = 0.4$ Gev/c, $\pi = 0.18$ Gev/c, Cocconi, Koester and Perkins found that the model gave a good description of the CERN and Brookhaven results. These values correspond to a mean inelasticity of 0.4.

Bowler (1962) applied the CKP model to the results of Dodd et al (1961) on the interactions of 24 Gev/c protons in a hydrogen bubble chamber and to the results of the group at the P.N. Lebedev Institute, Moscow (Grigorov et al (1960); Dobrotin and Slavatinski (1960); Guseva et al (1961)) who studied the interactions of cosmic ray nucleons at energies of several hundred Gev using a cloud chamber together with a total absorption calorimeter. These comparisons were good; to avoid lengthy repitition their results will not be further described here.

§ 3.9 The CKP Model at High Energies.

In view of the excellent agreement of the results at lower energies with the CKP model, it will be of interest to examine the data on γ-ray production described in this Chapter in the light of this model. The model describes

the meson momentum spectra averaged over all types of interaction for a given unique primary energy. The two groups of graphite events represent averages over many events within a narrow band of radiated γ-ray energy but of unknown primary energy. However the range of primary energy involved will be small and the parameters A, P_o and π of expression (3.2) are known to vary only slowly with primary energy so that it is meaningful to compare the predictions of the model with the observed distributions.

Assuming that the γ-rays observed were all derived from the decay of π^o- mesons (other possible sources are mentioned in Chapter 4) the momentum distributions for γ-rays in the centre of mass system can easily be derived from equation (3.2). In making this derivation the transverse momentum of a γ-ray with respect to the direction of motion of its parent π^o- meson, at most $\frac{1}{2}m_\pi c$ ($\approx$ 70 Mev/c), was neglected. The error introduced by this assumption is negligible at the γ-ray momenta considered in this comparison, see Figs 3.7 and 3.8. The derived γ-ray momentum distribution is

$$\frac{\partial^2 N_\gamma}{\partial P_{II}\,\partial P_T} = 2A \frac{P_T\left(1 + \frac{P_T}{\pi} + \frac{P_{II}}{P_o}\right)}{\pi^2 P_o \left(\frac{P_T}{\pi} + \frac{P_{II}}{P_o}\right)^2} e^{-\frac{P_T}{\pi}} e^{-\frac{P_{II}}{P_o}} \qquad (3.3)$$

This distribution no longer possesses the feature that the values of P_T and P_{II} are independent. However several simple predictions may be obtained from equation (3.3)

(i) The distribution in γ-ray transverse momentum, averaged over all longitudinal momenta, is

$$\frac{\partial N_\gamma}{\partial P_T} = \frac{2A}{\pi} \; e^{-P_T/\pi} \qquad (3.4)$$

(ii) The distribution in γ-ray longitudinal momentum, averaged over all transverse momenta, is

$$\frac{\partial N_\gamma}{\partial P_{\parallel}} = \frac{2A}{P_o} \int_{P_{\parallel}/P_o}^{\infty} \frac{e^{-x}dx}{x} = \frac{2A}{P_o} \cdot Ei(-P_{\parallel}/P_o) \qquad (3.5)$$

Ei is the well known exponential integral.

(iii) The mean transverse momentum is a slowly varying function of longitudinal momentum.

$$\bar{P}_T\ (P_{\parallel}) = 2\pi \left\{ \frac{e^{-P_{\parallel}/P_o}}{\int_{P_{\parallel}/P_o}^{\infty} \frac{e^{-x}dx}{x}} - \frac{P_{\parallel}}{P_o} \right\} = 2\pi \left\{ - \frac{e^{-P_{\parallel}/P_o}}{Ei(^{-P_{\parallel}}/P_o)} - \frac{P_{\parallel}}{P_o} \right\} \qquad (3.6)$$

$\bar{P}_T = \pi$ at $P_{\parallel} \approx 0.3\ P_o$. For higher values of $P_{\parallel}$, $\bar{P}_T$ slowly increases to its asymptotic value of $\bar{P}_T(\infty) = 2\pi$, while for lower values of $P_{\parallel}$; $\bar{P}_T$ tends to zero.

Let us now compare the γ-ray production spectra observed in the two groups of graphite events and in the Texas Lone Star with those predicted above.

(i) The combined transverse momentum spectra for the

graphite events has already been presented, Fig 3.5, there being no significant difference between the two groups. The transverse momentum spectrum for the Texas Lone Star was shown in Fig 3.10. The closeness of both of these spectra to the exponential distribution, equation (3.4), has already been remarked upon. Both are extremely good fits over the entire range of P_T with values of the exponent:

π = 0.24 Gev/c Graphite Events

π = 0.32 Gev/c Texas Lone Star.

(ii) Fig 3.12(a), (b) and (c) present the centre of mass longitudinal momentum spectra for γ-rays in the low and high energy graphite groups and in the Texas Lone Star respectively. An attempt has been made to fit each spectra with a curve of the form of equation (3.5). It can be seen, Fig 3.12, that the fit is very reasonable in the case of the high energy graphite events and the Texas Lone Star but not quite so good for the low energy graphite events. The best values of the parameter P_o are

P_o = 2.1 Gev/c Low Energy Graphite Events

P_o = 2.6 Gev/c High Energy Graphite Events

P_o = 1.9 Gev/c Texas Lone Star.

It is a little surprising that P_o for the Texas Lone Star is lower than for the graphite events but it should be remembered that this is just one high energy event which may not be representative.

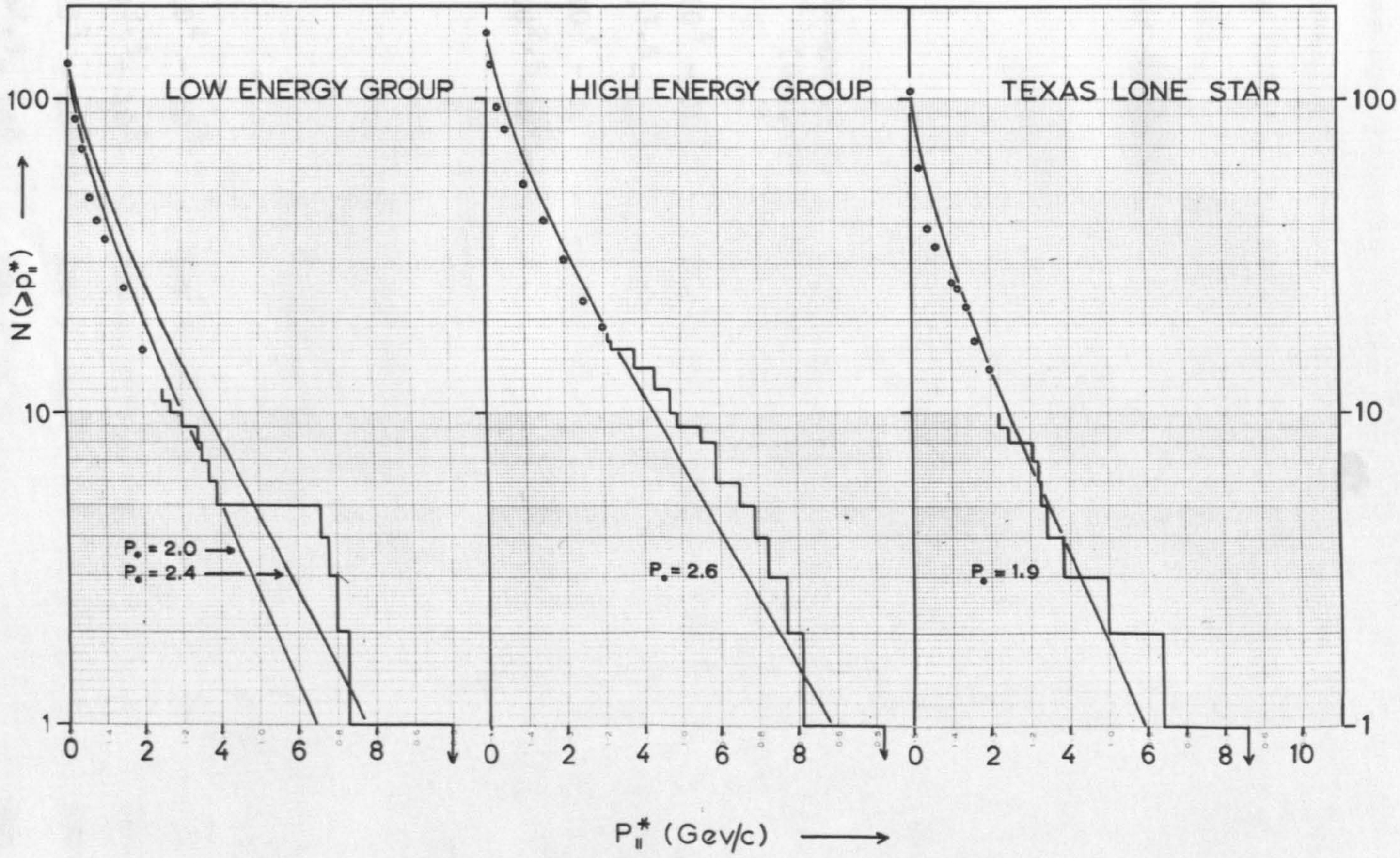
INTEGRAL C-SYSTEM MOMENTUM SPECTRA
LOW ENERGY GROUP
HIGH ENERGY GROUP
TEXAS LONE STAR
100
10
1
N(>p*∥)
P* = 2.0
P* = 2.4
P* = 2.6
P* = 1.9
0
2
4
6
8
10
P*∥ (Gev/c)

Fig 3.12.

(iii) Table 3.1 shows the mean transverse momenta of γ-rays for various ranges of longitudinal momentum. These values are compared with the expected values of equation (3.6). The results for the high energy graphite events and the Texas Lone Star are in excellent agreement but the expected variation of transverse momentum is not observed in the low energy graphite events.

Table 3.1.

Variation of P_T with $P_{\parallel}$

Graphite Interactions.

Range of $P_{\parallel}$ (Gev/c)	Observed $\bar{P}_T$ (Mev/c) Low Energy	Observed $\bar{P}_T$ (Mev/c) High Energy	Expected $\bar{P}_T$ (π =0.24, P_o=2.6)
$10^4 - 10^{3.5}$	230 ± 80	365 ± 90	380
$10^{3.5} - 10^3$	340 ± 65	255 ± 45	300
$10^3 - 10^{2.5}$	310 ± 50	200 ± 35	235
$10^{2.5} - 10^{2.1}$		205 ± 35	180

Texas Lone Star

	Observed $\bar{P}_T$ (Mev/c)	Expected $\bar{P}_T$ (π=0.32, P_o=1.9)
$10^4 - 10^{3.5}$	600 ± 180	545
$10^{3.5} - 10^3$	490 ± 80	460
$10^3 - 10^{2.5}$	320 ± 50	350
$10^{2.5} - 10^2$	250 ± 35	250
$10^2 - 0$	190 ± 25	165

§ 3.10 Conclusions.

It may be concluded from the above comparisons that the CKP model provides a very adequate phenomenological description of γ-ray production at these energies. The values of A, P_o and π needed to fit the data at various energies are summarized in Table 3.2 below. A here refers to the total number of π - mesons in the foward hemisphere.

Table 3.2

Type of Event	Estimated Primary Energy (Gev)	A	P_o (Gev/c)	π
Accelerator Results	30	3.0	0.40	0.18
Low Energy Graphite	1.5×10^4	12	2.1	0.24
High Energy Graphite	8×10^4	21	2.6	0.24
Texas Lone Star	5×10^5	200	1.9	0.32

The total energy carried by all particles in the centre of mass system may be found from the distributions (3.2) or (3.3). This energy is

$$E = 2A\, P_o c\, f(\alpha) \qquad (3.7a)$$

where $\alpha = \pi/P_o$ and $f(\alpha)$ may be expanded for $\alpha < 0.3$ as

$$f(\alpha) = 1 + \alpha^2 \left\{ 3 \ln\left(2 + \frac{2}{\alpha}\right) - 4 \right\} \qquad (3.7b)$$

For the events considered here α is small (0.1 - 0.2) and $f(\alpha)$ is close to unity. The energy available in the centre of mass system is $(2NE_p)^{\frac{1}{2}}$ where E_p is the laboratory energy

of the primary particle and N is the mass of the target particle which is at rest in the laboratory system. Hence, if K_{π^o} is the mean fractional energy radiated as π^o - mesons, then

$$K_{\pi^o} (2NE_p)^{\frac{1}{2}} = 2A\ p_o c\ f(\alpha) \qquad (3.8)$$

Perkins (1961) has given an extensive review of the known features of high energy interactions between 10^2 - 10^5 Gev. The evidence is that K_{π^o} is independent of energy in this range so that the product Ap_o must increase as the square root of the primary energy. Comparing the results at 30 Gev, Table 3.2, with those for the low energy graphite group, it will be seen that over this energy range, both A and p_o increase roughly as $Ep^{1/4}$. This is in agreement with the observed increase in the multiplicity of charged secondary particles as reported by Perkins (1961), Fowler and Perkins (1964) and other authors.

The rapid increase in A between the low and high energy graphite events has already been remarked upon, § 3.4; this trend is continued in the Texas Lone Star. It is difficult to imagine a production mechanism in which p_o decreases with increasing primary energy but these latter two groups of events would seem to indicate a rather rapid increase of A at very high energies with a corresponding saturation in the value of the mean centre of mass energy.

CHAPTER IV.

A Study of High Energy Interactions Occuring in Emulsions.

§4.1 Introduction.

In the previous Chapter the production of γ-rays in high energy interactions was studied and observed to be consistent with their having been produced by the decay of π^0 - mesons, the latter being distributed in energy according to a simple model. In this Chapter a study of the production of charged mesons is reported. The observations were made on interactions occuring in the photographic emulsion of the detector. These events, known in literature as 'jets', have been the object of intensive study in many laboratories over the last ten years. The information obtained from these studies has been limited since the energy of most of the secondary particles is much too high to be measured directly, and so only their angular coordinates can be obtained accurately.

In the analysis reported here the sample of jets was restricted in an attempt to include only proton-light nucleus collisions, see § 4.2. The angular distribution of the secondaries is compared with the CKP model, § 4.3, and found to be in good accord. Therefore an indirect method of determing the energy carried by the charged particles is evolved based on this model, this method is described in § 4.4. The ratio of the energy carried by charged and neutral particles is dependent on the manner in which the particles are produced. The distribution of this ratio is presented and used in § 4.5- 7 to obtain information on the possible parentage of the π-mesons

observed.

Finally, § 4.8, the possible production of pions via the decay of energetic hyperons is briefly discussed.

§ 4.2 Nuclear Interactions in Emulsion.

The following analysis includes every nuclear origin in emulsion detected both in the Indian Stack and in the other 7 assemblies of similar composition which had previously been exposed by the Bristol group. The details of each exposure, together with the number of such origins found, are summarized in Table 4.1. Each event was classified by 3 parameters, $(N_h + n_s.X)$. n_s is the number of fast charged particles produced (ionisation $g < 1.4\ g_{min}$), N_h is the number of slow particles ($g > 1.4\ g_{min}$) which result from the disintegration of the struck nucleus, and X describes the nature of the primary particle (p = proton; n = neutral; Li = Lithium nucleus etc.). In each event two measurements were made:

(i) The total energy radiated as γ-rays was determined using the methods which have been described previously, § 2.10.

(ii) The space angle θ of each of the shower particles was measured.

For tracks at very wide angles (> 0.2 radians) this measurement could be made with respect to the extropolated direction of the primary particle. However the majority of the tracks could only be resolved and measured at large distances from the interaction (i.e. > 0.5 mm.) where the extrapolated position of the primary was no longer known with sufficient accuracy. In most events there existed a narrow core of

Table 4.1.

Origins in Emulsion.

Detector	Composition	Height (gm/cm^2.)	Time (hrs)	No. Events.
C1	Em - Pb	220	840	5
C2	Em - Pb	220	580	20
W	Em - W	220	250	24
B1	Em - Pb	30	5	12
B2	Em - W	20	9	6
B3	Em - W	5	17	12
B4	Em - W	12	8	19
Indian	Em - W	20	30	36
Total				134

(Em = Emulsion; Pb = Lead; W = Tungsten-Nickel Alloy).

particles in the very foward direction. This core was taken as defining the axis of the event and the angles of particles outside the core were measured with respect to this axis. The angles of the particles within the core (typically 2 - 5 in number) were measured with respect to their own centroid. The true position of the axis within the core is not known so that the angles of these latter particles are only really known to be within an upper limit defined by the dimensions of the core.

The 134 events in the sample will include the interactions of primaries of all types with both the light and heavy nuclei in the photographic emulsion. In order to restrict the analysis to interactions between nucleons and light nuclei, two criteria were aplied:

(i) Only events with neutral or singly charged primaries were accepted; 19 events, mainly with α-particle primaries were rejected for this reason.

(ii) Only events with $N_h \leqslant 6$ were accepted.

Powell, Fowler and Perkins (1959) give a distribution of N_h values for 770 disintegrations in emulsion produced by heavy relativistic primary particles. They deduce that all collisions with $N_h > 6$ occur in heavy nuclei (Ag or Br), that most of the events with $2 \leqslant N_h < 6$ occur in light nuclei (C, N or O) and that of the remaining events with $N_h = 0,1$ about one half occur in hydrogen and the other half are due to glancing or peripheral collisions with light or heavy nuclei. Thus the acceptance criteria $N_h \leqslant 6$ should restrict the sample to collisions with hydrogen and light nuclei plus a few peripheral interactions with heavy nuclei. 53 events with $N_h > 6$ were rejected. Of the remaining 62 events, 5 could not be analysed because the primary interacted a short distance from the edge of a metal sheet, leaving insufficient emulsion for the angles of all the secondary tracks to be determined.

Thus the original sample of 134 events was reduced to 57 interactions between primaries of charge Z = 0 or 1 and light nuclei in the emulsion. These 57 events had cascade energies

ΣE_γ distributed from 150 Gev to 10^4 Gev as follows

	ΣE_γ < 500 Gev	17 events
500 <	ΣE_γ < 2000 Gev	27 events
2,000 <	ΣE_γ	13 events

This sample will be called sample A; to increase statistics sample B was obtained consiting of the above sample plus the published results of other groups. A further 59 events with $N_h \leqslant 6$ were obtained in this manner so that sample B contained 126 events. Whereas all of these additional events were found by scanning for the resulting cascade, their γ-ray energies were either not determined or else were determined using a different method to that described above. Consequently the enlarged sample, B, was only used in those parts of the following analysis in which a knowledge of the cascade energy was not needed.

The additional events were obtained from:

(i) The published data of the Chicago group, Barkow et al (1961) - 38 events.

(ii) The European section of the ICEF collaboration, von Lindern (1962) - 17 events.

(iii) A Bristol stack exposed prior to the use of sandwich stacks - 14 events.

As stated above the cascade energies of these events was not determined; their centre of mass Lorentz factors, see § 4.3, were distributed as follows:

$\gamma_c < 50$ 31 events

$50 < \gamma_c < 100$ 22 events

$100 < \gamma_c$ 16 events

The ranges of γ_c used here correspond approximately in primary energy to the ranges of ΣE_γ used above.

The observed distribution of charged multiplicity, n_s, for the 126 events in sample B is shown in Fig 4.1(a). It extends over a wide range of values, from 1 to 104, with a mean of 21. The curve shown is of the form

$$P_n = \frac{(1-r)^2}{r} n r^n \qquad (4.1)$$

The mean of this distribution is

$$\Sigma n P_n = \frac{1+r}{1-r}$$

and the parameter r was chosen to give the observed mean of 21. The curve is seen to give a reasonable fit to the data.

§ 4.3 Angular Distribution in the Centre of Mass System.

The Lorentz transformation relating the angles of emission of a particle in the laboratory and centre of mass systems is

$$\gamma_c \tan\theta = \frac{\sin\varphi}{\cos\varphi + \beta_c/\beta^*} \qquad (4.2)$$

θ = laboratory angle

φ = C-system angle

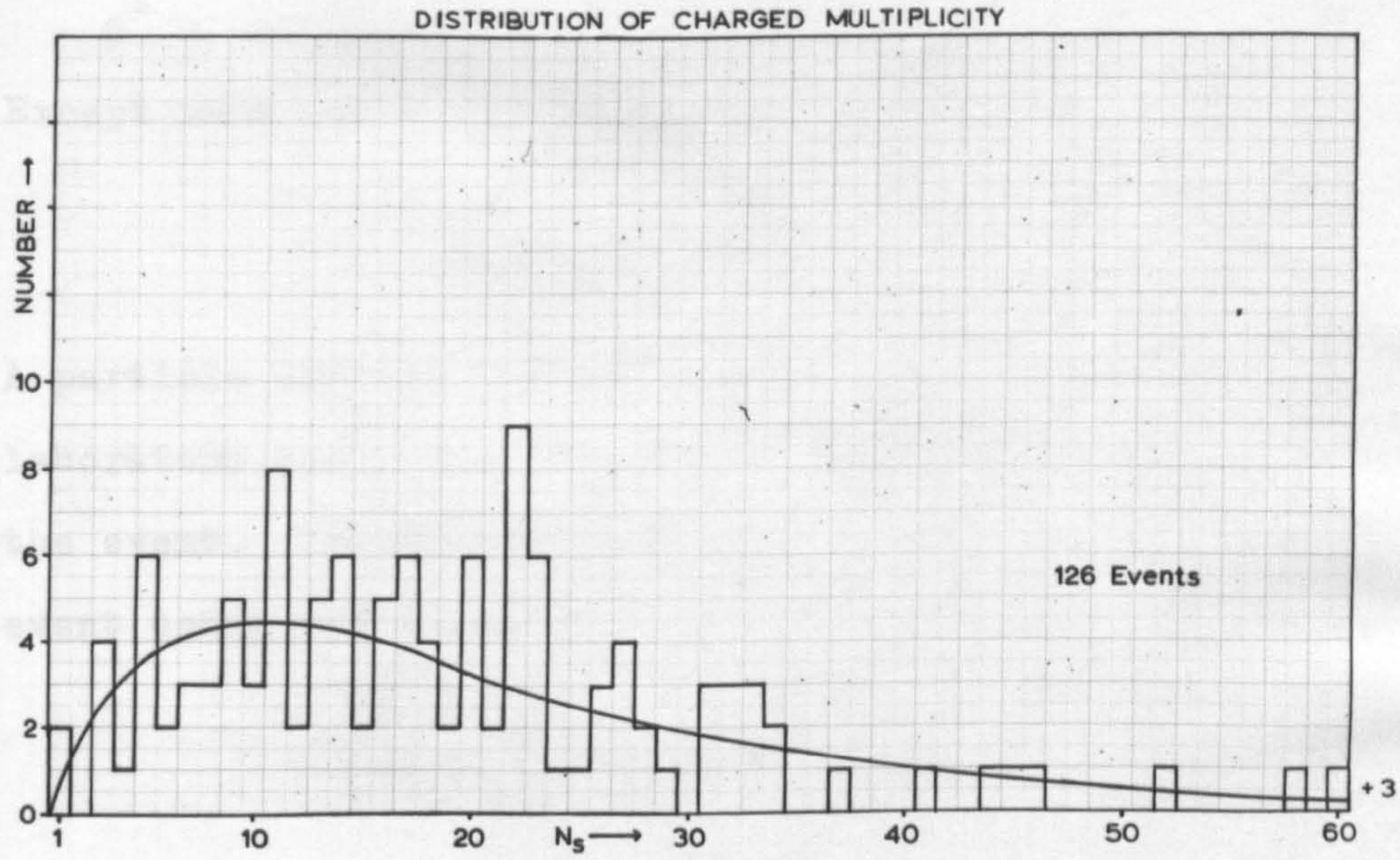

Fig 4.1 (a)

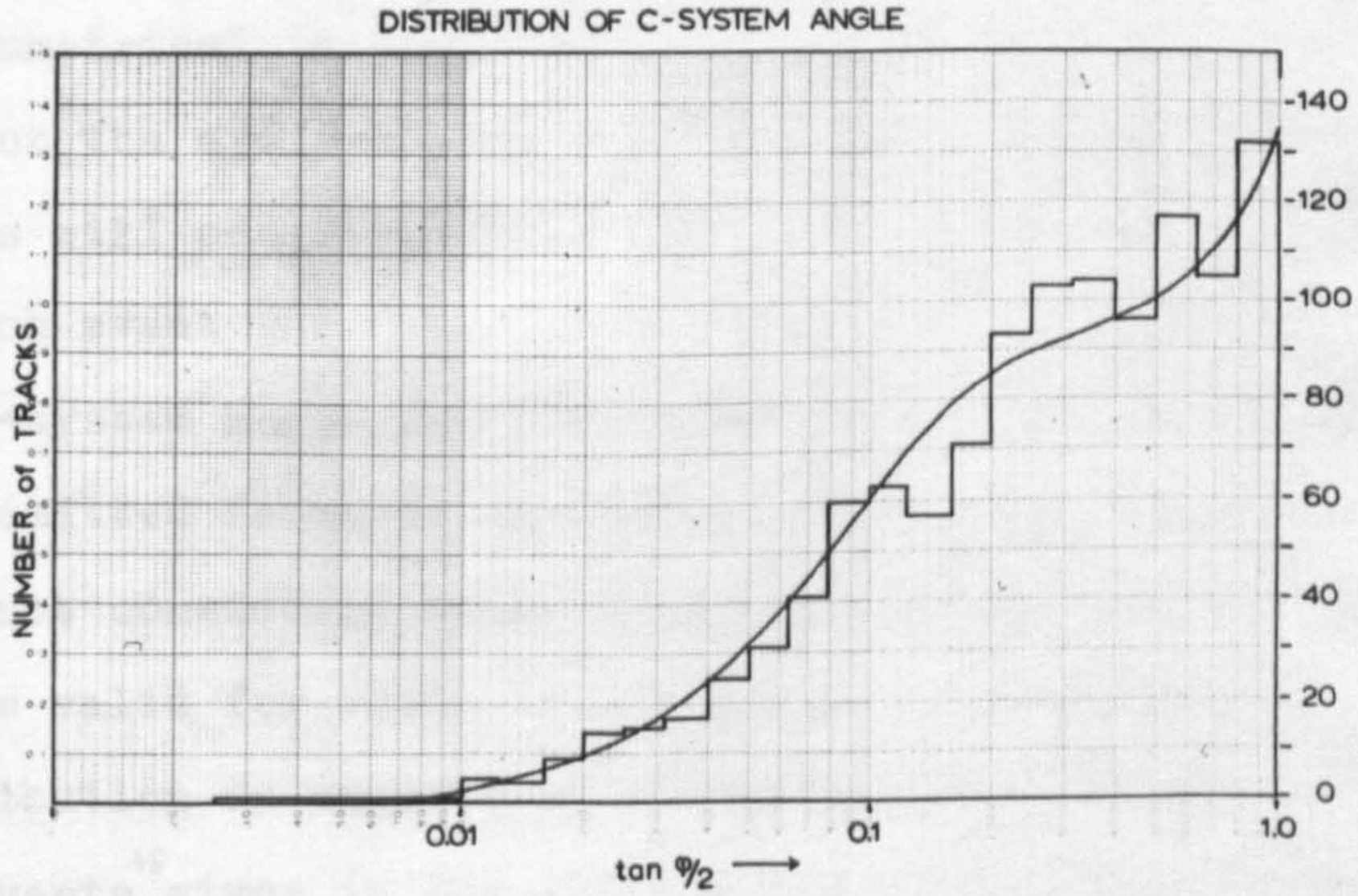

Fig 4.1 (b)

βc = velocity of C-system in the laboratory; $\gamma_c = (1-\beta c^2)^{-\frac{1}{2}}$

β^* = velocity of the particle in the C-system.

Except when $\cos \varphi \approx -1$ this is almost exactly

$$\gamma_c . \theta = \tan \varphi/2 \qquad (4.3)$$

A particle emitted at right angles in the C-system has a laboratory angle $\eta = 1/\gamma_c$; η is called the median angle of the event. The Lorentz factor γ_c was estimated for each event using the formula proposed by Castagnoli et al (1953)

$$\log \gamma_c = - \frac{1}{n_s} \sum_i \log \tan \theta_i \qquad (4.4)$$

the summation being made over all particles. The formula is derived from the assumption that the emission of particles is symmetrical in the C-system. While this is certainly true on the average, the values of γ_c estimated for individual events will occasionally be wrong by a factor of 3 or more. In each event the transformation (4.3) was used to estimate the C-system angle for all tracks within the median angle, i.e. emitted forwards in the C-system. The backward tracks were not considered since the approximation $\beta c = \beta^*$ is not always valid for these tracks and β^* is unknown. The combined distribution in angle φ of all the forward tracks from the 126 events is given in Fig 4.1(b); the histogram contains 1179 tracks.

The differential momentum distribution predicted by the CKP model, equation (3.2), may be re-written in terms of

variables p (C-system total momentum) and φ:

$$\frac{\partial^2 N}{\partial p \partial \varphi} = \frac{A}{\pi^2 p_o} \; e^{-p\left(\frac{\sin\varphi}{\pi} + \frac{\cos\varphi}{p_o}\right)} \; p^3 \sin\varphi \qquad (4.5)$$

Integrating over all momenta, p:

$$\frac{\partial N}{\partial \varphi} = 2A \frac{\pi}{p_o} \cdot \frac{\tan\varphi \sec^2\varphi}{\left(\frac{\pi}{p_o} + \tan\varphi\right)^3} \qquad (4.6)$$

This predicted distribution is plotted as the solid line in Fig 4.1(b). A was chosen so as to normalize the distribution (A=1179) and the ratio π/p_o was chosen to give a good fit to the data ($\pi/p_o = 0.2$). Despite the uncertainty in γ_c and the range of primary energies involved, the predicted distribution is in excellent accord with the data. The value of π/p_o used is greater than that observed in the graphite interactions, see Table 3.2, but many of the events in sample B are of much lower energy than those in the samples of graphite interactions and so this increase is to be expected.

§4.4 Energy Carried by the Charges Particles.

The ratio of the energies radiated as charged and neutral pions in high energy interactions is a quantity of great interest. However, whereas the energy in neutral pions is readily obtainable from measurements on the resulting

electromagnetic cascade, the energy in charged pions cannot be directly obtained at high energies. Most authors adopt the method of Edwards et al (1958) in which the charged energy is computed as $\bar{P}_T \Sigma$ cosec θ_i, where $\bar{P}_T$ is the mean transverse momentum of all the particles. As was realized by the proposers of this method it suffers from the severe disadvantages that $\bar{P}_T$ is not independent of angle θ and, more important, that very large contributions are obtained from tracks at the smallest angles, i.e. just those tracks whose angles are not at all well known (§ 4.2). An alternative method is therefore used in this thesis which was evolved in an attempt to overcome these limitations.

Let us assume that the distribution of charged pions in the C-system is described by the distribution function (4.5). This assumption is made plausible by the facts that this function has been shown to describe the production of π^o - mesons (§ 3.9) and that the integral of this function, equation (4.6), has been shown to describe the angular distribution of charged particles. The mean transverse momentum of particles emitted at a C-system angle φ is

$$\bar{P}_T(\varphi) = \frac{\int_o^\infty p \sin\varphi \frac{\partial^2 N}{\partial p \partial \varphi} dp}{\int_o^\infty \frac{\partial^2 N}{\partial p \partial \varphi} dp} = 3\pi \frac{\tan\varphi}{\frac{\pi}{p_o} + \tan\varphi} \qquad (4.7)$$

The fraction of particles emitted within an angle φ is

$$F(<\varphi) = \frac{1}{A} \int_0^{\varphi} \frac{\partial^2 N}{\partial p \partial \varphi'} d\varphi' = \left\{ \frac{\tan \varphi}{\frac{\pi}{p_o} + \tan \varphi} \right\}^2 \qquad (4.8)$$

so that

$$\bar{P}_T (\varphi) = 3\pi F^{\frac{1}{2}} \qquad (4.9)$$

The mean transverse momentum of all particles is $\bar{P}_T = 2\pi$ and hence the mean energy $\bar{E}$ carried in the laboratory by a particle emitted at an angle θ is

$$\bar{E} = \frac{1.5\ \bar{P}_T\ F^{\frac{1}{2}}}{\theta} \qquad (4.10)$$

where F is the fraction of those particles within the median angle which are also within the angle θ.

The total energy carried by all particles inside a given angle, θ_o, is

$$\Sigma E = \int_0^{F(\theta_o)} \frac{1.5 \bar{P}_T}{\theta} F^{\frac{1}{2}} dF = \frac{1}{2} \frac{\bar{P}_T}{\theta_o} F^{3/2} \frac{3-2F^{\frac{1}{2}}}{1-F^{\frac{1}{2}}} \qquad (4.11)$$

In integrating equation (4.11) the approximation $\tan \varphi = 2 \tan \varphi/2$ was used, which is certainly valid for the small angles considered here.

The energy carried by charged pions in each event was estimated as follows:

(i) The energies of tracks outside the narrow central core were estimated using equation (4.10). θ is well defined for these tracks and a value of F was computed for each track by dividing the number of tracks inside the angle considered by the total number inside the median angle. The energies of tracks outside the median angle, usually small, were estimated in a similar manner.

(ii) The total energy carried by tracks within the central core was estimated using equation (4.11). θ_o was taken as the upper limit on their angles and F as the fraction of tracks within this limit. The method therefore attempts to overcome both of the limitations in the usually employed method.

Various estimates have been made of the percentage of pions among the secondaries of high energy interactions. These results are summarized by Perkins (1961). Pions form about 80% of the total numbers of particles produced between 10 and 10^6 Gev primary energy, the remaining 20% being mainly K-mesons and nucleon pairs. Assuming that two-thirds of the pions and one-half of the other particles are charged, it follows that on the average 85% of the created charged particles are pions. The energy carried by charged π-mesons was therefore taken to be 85% of the total energy as computed above.

The incident primary nucleon is expected to emerge from most collisions at a very small angle, see below. This nucleon will exist as a charged state in approximately half

of the events seen. To make allowance for this nucleon, in every event the number of tracks within the central core was reduced by half a track.

The above process was used to calculate the energy carried by charged π-mesons in each of the 57 events of sample A. The value of $\bar{P}_T$ used was 0.5 Gev/c. Using the known cascade energy a value was then computed for R, the ratio of the energy carried by charged π-mesons to that carried by neutral π-mesons. The differential distribution of the values obtained is shown in Fig 4.2(a). The integral distribution, normalized to unity, is shown in Fig 4.2(b). The significance of the theoretical curves shown will be discussed later. The mean value of R is 1.8. No correlation is observed between R and n_s; the mean multiplicity in the ten events with $R \geq 3.0$ is 24 compared with 21 for the entire sample.

If we had observed all the interactions of a mono-energetic beam then R would be distributed about a mean of 2. However the events were detected by means of their electromagnetic cascades and were caused by primary particles with a steeply sloping energy spectrum so that large biases will exist in favour of events in which a large fraction of the energy radiated is in the form of π^0-mesons. The distribution of R is a reflection of the manner in which energy is partitioned amongst the secondary particles; its significance is discussed in the next section.

Fig 4.2.

(a) and (b) show the differential and integral distributions respectively of R, the ratio of the energies carried by charged and neutral π-mesons. The curves are the results of theoretical calculations referred to in the text.

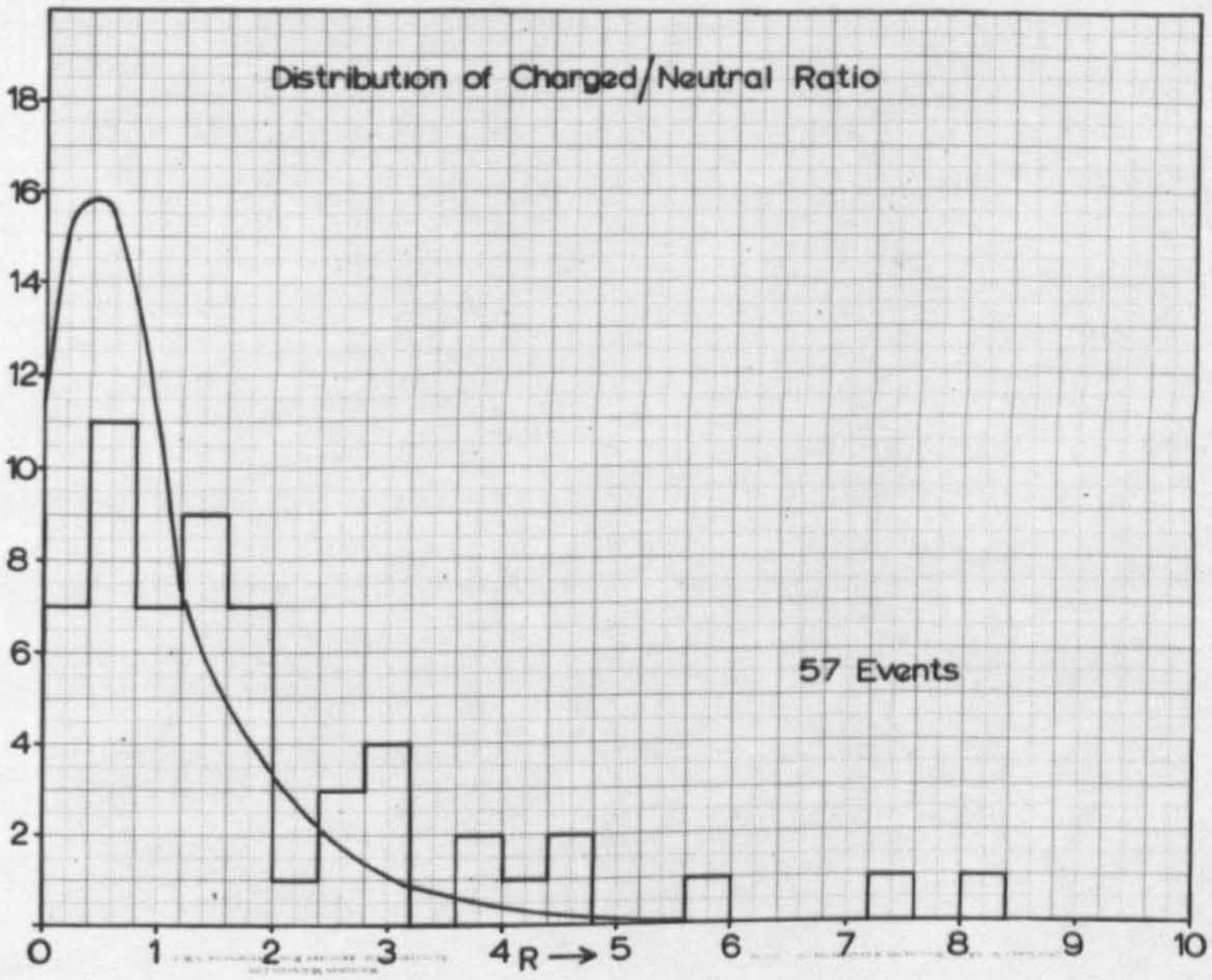

Fig 4.2 (a)

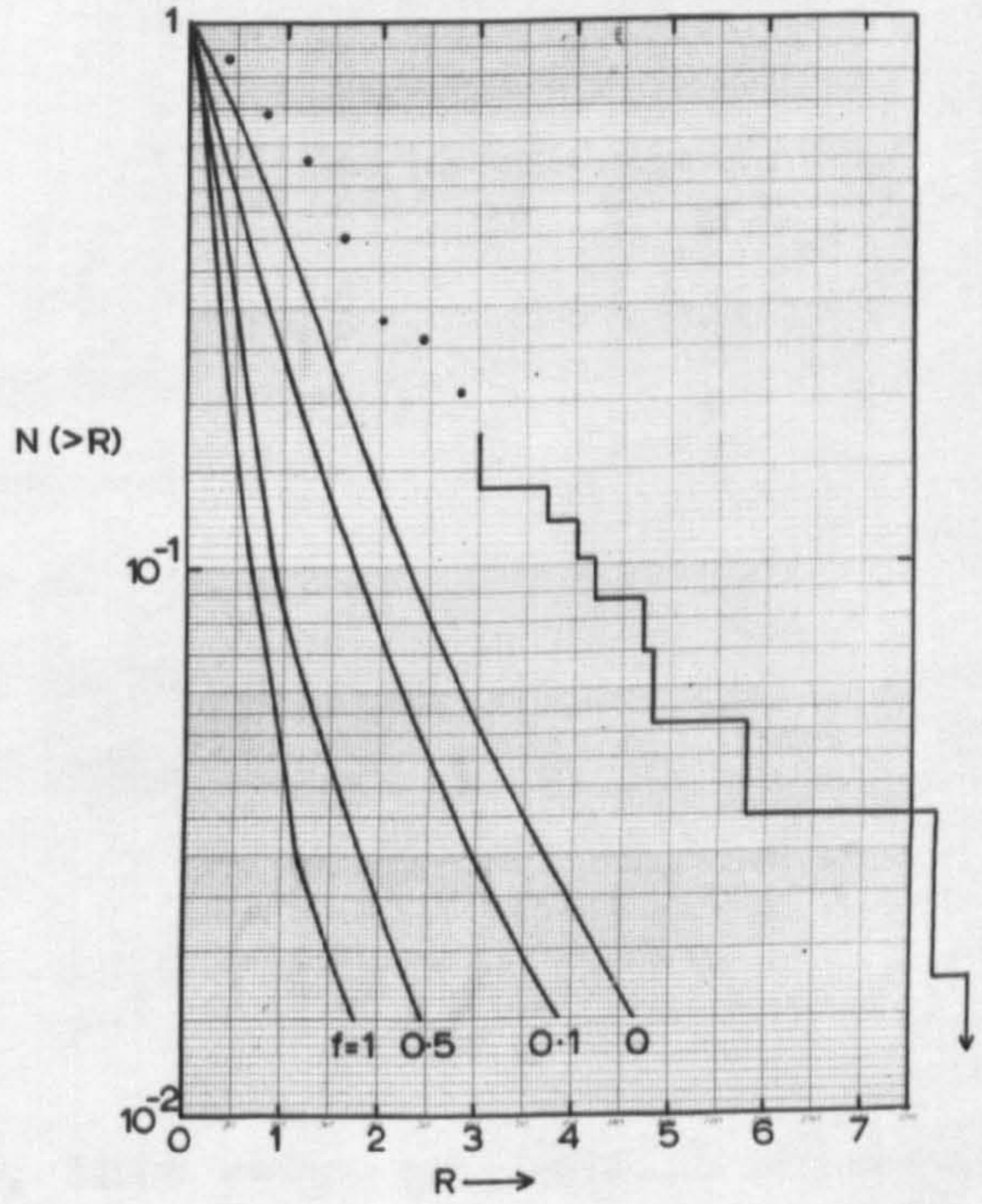

Fig 4.2 (b)

§4.5 The Pionization Process.

In what follows the term pionization is taken to include all modes of production of π-mesons, irrespective of whether these are produced directly in the primary interaction or indirectly via the decay of short lived mesons (η,ω, ρ), heavier mesonic fireballs, hyperons or nucleon isobars.

An established feature of high energy interactions is the retention of a large fraction of the primary energy by a few particles. This is deduced from the attenuation length, Λ, of the nuclear active component of the cosmic rays in the atmosphere, which is considerably greater than their interaction length, λ_i. These lengths are related by

$$\Lambda = \frac{\lambda_i}{1 - \sum_j f_j^{\gamma}} \qquad (4.12)$$

where f_j is the fraction of the primary energy given to the j^{th} secondary particle and γ is the index of the integral primary energy spectrum (assumed constant). The summation is made over all secondary particles capable of further interactions in the atmosphere. Taking Λ = 125 gm./cm.^{2} from Duthie et al (1962) and λ_i = 80 gm./cm.^{2} (geometrical value) then

$$\sum_j f_j^{\gamma} = 0.36 \qquad (4.13)$$

With $\gamma \approx 1.7$, this value can only be obtained if one particle carries about 50% of the primary energy, or if two particles between them share 70 - 80%.

This result is usually interpreted as the re-emergence of the incident nucleon with a high fraction of its former energy. However Peters (1962,1964) has suggested that this energetic particle may frequently be an excited state such as a hyperon or a nucleon isobar. The pions from the decay of such a particle would have energies much higher than those from other processes and, emphasized by the steeply sloping primary spectrum, would dominate the production processes. The mode of production via hyperons is no longer accepted as important; nevertheless further evidence against it is presented briefly in § 4.8.

The experimental data presented above on the production of charged and neutral pions shows no evidence for the division of the produced mesons into two groups of high and low energies. The analysis of Cocconi, Koester and Perkins at accelerator energies and the similar analysis given here use all the observed pions. Therefore it can be concluded that, if pions are produced via the decay of nucleon isobars, then this is part of one continuous production mechanism and does not constitute a separate dominant process.

The expected distribution of the ratio R was computed firstly from the standpoint of the CKP model of pionization and secondly from the same model with the additional hypothesis that fast isobars are also produced.

§ 4.6 Calculation of R Distribution from Pionization.

It was assumed that:

(i) The differential energy spectrum of the pions in the laboratory system is, see § 3.8,

$$dN = a\, e^{-E/T}\, \frac{dE}{T} \qquad (4.14)$$

a is taken as the number of pions within the median angle; pions outside this angle are assumed to carry a negligible fraction of the laboratory energy. The total energy radiated is $E_\pi = aT$.

(ii) For a given pionization energy, E_π, the forward pion multiplicity has a distribution, f(a), similar in form to that for charged shower particles, equation (4.1). The mean value of a was taken as 12; this was deduced from the mean number of charged particles, 21, on the assumption that 80% of the particles produced are pions.

(iii) The number, b, of π^o-mesons is given by the binomial probability

$$\frac{a!\left(\frac{1}{3}\right)^b\left(\frac{2}{3}\right)^{a-b}}{b!(a-b)!} \qquad (4.15)$$

and the probability that these b π^o-mesons carry a total energy E_n is given from equation (4.14) as

$$dN = \frac{\left(\frac{E_n}{T}\right)^{b-1} e^{-E_n/T}}{(b-1)!} \quad \frac{dE_n}{T} \qquad (4.16)$$

A similar equation pertains to the energy, E_c, carried by the remaining (a-b) charged pions.

(iv) The mean inelasticity of an interaction does not change with primary energy so that the values of the total pionization energy, E_π, are distributed according to a power law spectrum with the same index, γ, as the primary spectrum.

We may now write down the combined probability that the pionization process should simultaneously produce π^o-mesons with total energy in the range (E_n, dE_n) and $\pi\pm$-mesons with total energy in the range (E_c, dE_c)

$$d^2N = \int_{\varepsilon_\pi} \sum_a \sum_b \frac{\gamma dE_\pi}{E_\pi^{\gamma+1}} \cdot \frac{f(a)a!\left(\frac{1}{3}\right)^b\left(\frac{2}{3}\right)^{a-b}}{b!(a-b)!} \cdot \frac{\left(\frac{E_n}{T}\right)^{b-1} e^{-E_n/T} \frac{dE_n}{T}}{(b-1)!}$$

$$\cdot \frac{\left(\frac{E_c}{T}\right)^{a-b-1} e^{-E_c/T} \frac{dE_c}{T}}{(a-b-1)!}$$

This expression may be simplified by writing $E_c = RE_n$, $T = E_\pi/a$ and by performing the integration over all E_π. We obtain

$$\frac{dN/dR}{dE_n/E_n} = \frac{\gamma}{R(1+R)^{\gamma}} \sum_{a=2}^{\infty} \frac{f(a)a!(2R)^a}{a^{\gamma}(3+3R)^a} (a+\gamma-1)! \sum_{b=1}^{a-1} \cdot \frac{b(a-b)}{(2R)^b(b!(a-b)!)^2} \qquad (4.17)$$

This expression was evaluated numerically on an electronic computor, using a value of 2.0 for the exponent γ. The result is plotted as the solid curve in Fig 4.2(a) and as the curve designated f=0 in Fig 4.2(b). Reference to these figures will show that the observed values of R are considerably higher than would be expected from this theory. The observed mean of R is 1.8 which is so close to the value of 2.0 which would be expected if fluctuations were not present that it is difficult to concieve of any model of direct pionization which includes fluctuations and is able to explain these results. Therefore before examining other hypotheses the possibility that the energies carried by charged particles have been systematically overestimated by a factor 1.5 - 2.0 must be considered. This could occur firstly if the value used for the pions mean transverse momentum was too high or secondly if the fraction of the charged energy carried by pions is less than that assumed.

The corrected mean transverse momentum of all the γ-rays observed in the interactions in graphite was 235 Mev/c. There is no evidence that the transverse momenta of the charged

pions should differ from the neutral pions; the best value of the pion mean transverse momentum is therefore 0.47 Gev/c. A value of 0.50 Gev/c was used in the computation of R, but this difference is too small to be significant.

While it is known that pions form 80% of the total number of particles produced, and 85% of the charged particles, their relative energy content is not so well known. Wolfendale (1963) reporting at the Bristol Conference, described evidence that the ratio of the energies carried by charged K- and π-mesons is less than 0.3 over a wide range of pion energies, 1 - 10^4 Gev. At low energies this figure is obtained from the polarization of μ-mesons at sea level (measured from the angular distribution of their decay electrons), at intermediate energies from a comparison of the vertical and near horizontal fluxes of μ-mesons at sea level (as determined by a magnetic spectrometer) and at high energies from a comparison between the μ-meson spectrum at sea level and the γ-ray spectrum at high altitudes, Duthie et al (1962).

In the computation of R, 15% of the charged particle energy was assumed to be carried by K-mesons and nucleons. While this figure may well be correct it cannot be excluded on the present evidence that K-mesons may carry up to 25% of the total charged energy. In this case the energy carried by the pions would be considerably less than 85% and the discrepancy between the observed and expected values of R would be largely resolved.

As is shown later any production of fast nucleon isobars in addition to the process of pionization considered above leads to an even greater discrepancy. However the indirect production of pions via the decay of other mesons or fireballs would improve the agreement between theory and observation in two ways:

(i) By reducing the effect of fluctuations since an energetic π^0-meson will often be accompanied by energetic $\pi\pm$-mesons from the decay of their common parent body. The theoretical values of R would therefore be increased.

(ii) By increasing the fraction of the energy carried by K-mesons. Some of the short-lived mesons and fireballs produced will have non-zero strangeness and will decay into K- and π-mesons. If the kinetic energy available in the rest system of this parent body is low then the K-mesons, on account of their larger mass, will have a higher mean laboratory energy than the π-mesons.

It may be noted in passing that the pseudo-scalar meson, η^0, is a prolific producer of γ-rays, having a branching ratio of 70% into modes consisting entirely of γ-rays or π^0-mesons. However it is an isotopic singlet state and is therefore likely on statistical grounds to be produced relatively infrequently compared with triplet states such as the π- and ρ-mesons.

§4.7 The Isobar Model.

As has been remarked upon above, a model in which pions from isobar decay form a separate dominant group is inconsistent with the observed production of γ-rays in high energy interactions (Chapter III). The model is therefore considered here only briefly in order to show that its predictions concerning the charged/neutral energy ratio R are very different from what is observed.

The assumptions made are of general nature but the result does not depend strongly on these assumptions;

(i) In addition to the above process of pionization a fast isobar of energy KE_π is produced in a fraction f of the interactions.

(ii) The isobar decays by a cascade process to a nucleon and two pions

$$N^{**} \rightarrow N^{*} + \pi$$
$$\hookrightarrow N + \pi$$

Both pions have a $^1/_3$ probability of being in a neutral state; therefore at least one neutral pion is produced in $^5/_9$ of the isobar decays. The masses of the isobars, N^{**} and N^{*}, were taken as being 2 and 1.4 respectively in units of the nucleon mass. Isobars with large masses can be excluded since they would lead to large γ-ray transverse momenta. Similarly an isobar decaying into many pions is excluded since it is not then possible to satisfy the restriction on the elasticity expressed in equation (4.13).

Thus in this model most of the pions are produced via direct pionization but, if an isobar is produced, its pions contribute nearly all of the energy. The method of selecting events by their γ-ray energies, emphasized by the steepness of the primary spectrum, will result in nearly all of the events detected being of the type in which at least one, and often two, neutral pions from isobar decay are present. When both pions from the isobar are neutral then the charged/neutral energy ratio observed is very small. When one is neutral and one is charged then R is in fact about unity but, in the method used to compute R, the single charged pion from isobar decay will not be recognized as such but will be wrongly included as one of the low energy pions from pionization. Hence even in this case a small value of R is obtained.

The expected distribution in R was computed for various values of K and f, putting in the kinematics of the isobar decays. These results are shown in Fig 4.2(b) for the case K = 4. This value of K is reasonable if the elasticity of the surviving nucleon is to satisfy equation (4.13). As was explained above cases with frequent isobar production give distributions peaked at very small values of R. The process of direct pionization only becomes important at low values of f.

In view of the discrepancy between the observed values and the curve for direct pionization only (f = 0) it is difficult to estimate a quantitative upper limit for isobar

production. If isobars were produced in only 20% of the interactions it would be very difficult to reconcile the expected distribution with that actually observed.

§ 4.8 Production of Energetic Hyperons.

Peters (1961,1962) has suggested that in a high proportion of cases the persistent baryon, see § 4.5, from a nuclear interaction may be a hyperon. Subsequent decay of this hyperon would provide a source of delayed pions carrying up to 20% of the primary energy. It was suggested that the frequent production of such hyperons could account for the observed increasing slope of the γ-ray spectrum and for other phenomena occuring in Extensive Air Showers. This hypothesis was examined by Bowler et al (1962) and Bowler (1962) and shown to be inconsistent with their data. It is re-examined here in terms of the rates of production of γ-rays observed in the Indian Stack and reported above.

The mean decay length of hyperons energetic enough to produce γ-rays of energy 10^3 Gev is several hundred meters. The average distance traversed by an event between the graphite layer and the detector is about 30 cms and so, apart from the fast decay $\Sigma^\circ \rightarrow \Lambda + \gamma$, the measured production rate of γ-rays from the graphite interactions will not include those produced via hyperon decays. However this decay length is much less than the interaction length of nuclear particles in the rarified atmosphere at this altitude and so the flux of γ-rays incident upon the detector from the atmosphere will include a contribution from hyperons, if

these are produced.

As was described in § 2.6, the region of production of all γ-rays observed with energies $E_\gamma \geqslant 1200$ Gev is known with confidence. Hence a comparison of the rates of production of γ-rays above this energy from the graphite and from the atmosphere will enable the frequency of hyperon production to be estimated.

The kinematics of the hyperon-pion decay scheme is worked out in Appendix B. An expression is computed, equation (B.4), for the mean probability that a hyperon produced in the atmosphere should decay before reaching the detector. The contributions to the flux of produced γ-rays are worked out, both for direct pionization and for the direct and delayed production of γ-rays via hyperons. These calculations are summarized in equations (B.9) and (B.7). From these two equations the expected ratio of the production rate of γ-rays in the atmosphere (from direct and delayed pions) to the production rate in the graphite layer (direct pions only) is

$$\frac{R_A}{R_C} = \frac{0.041(1-C)^p + 0.013\ q\ C^p}{0.041(1-C)^p + 0.0025\ q\ C^p}$$

$$= \frac{1 + 0.32\ q\ \left(\frac{C}{1-C}\right)^p}{1 + 0.061\ q\ \left(\frac{C}{1-C}\right)^p}$$

where $p = 1.7$ is the index of the primary energy spectrum, q is the fraction of interactions in which a fast hyperon is

produced and C is the mean fraction of the primary energy retained by the persistent baryon (hyperon or nucleon). If $q = 0$ then $R_A = R_C$ but if $q > 0$ then R_A is expected to be greater than R_C.

The observed production rates, Table 2.5, are

$$R_A = 2.7 \pm 1.0$$

$$R_C = 5.0 \pm 2.5$$

The units are 10^{-9} events per steradian per second per gram of material placed at the top of the atmosphere. It can be seen that R_C is in fact greater than R_A, although this difference is not significant.

In view of these values it is very unlikely that hyperons play an important role in γ-ray production. The results are consistent with $q = 0$. Taking the extreme values of the production rates within the error ($R_A = 3.7$, $R_C = 2.5$) then we obtain an upper limit for q

$$q \lesssim 2.1\left(\frac{1-C}{C}\right)^p$$

This limit is sensitive to the value of C. C is restricted by equation (4.13) to values of the order 0.6 - 0.8. Taking $C = 0.7$ and $p = 1.7$ then

$$q \lesssim 0.5$$

This is an upper limit; the evidence suggests that q is much less than this, probably close to zero.

CHAPTER V.

Theories of High Energy Interactions.

§ 5.1 Introduction.

In this final Chapter a brief survey is presented of the theory of high energy interactions. This survey makes no pretence to being complete or authoratitive but it attempts to indicate the lines of reasoning being employed and where fuller details may be found.

Initial attempts to find a theory of high energy inelastic processes were based on statistical theory. The failure of these models to provide a complete description, at a time when the field theory of strong interactions had not yet developed enough to provide any alternative, left a gap which was filled by several phenomenological models. Finally in the last few years theories employing dispersion relations have had some degree of success.

§ 5.2 Statistical Theories.

Different versions of the model were proposed; essentially they assume that the cross sections for any particular process are mainly governed by the corresponding phase space available.

Fermi (1950,1951) suggested that at the moment of impact the energy of the colliding nucleons is transferred to the meson field and the region of space originally occupied by the nucleons is thereby loaded with a large amount of energy. In this region the produced particles may interact many times before they fly apart and a thermodynamic

equilibrium is reached. When the gas begins to expand the particles cease to interact and fly out freely in all directions. The predictions of the model may be summarized as:

(i) The multiplicity is proportional to the fourth root of the primary energy.

(ii) At high primary energies (> 10^4 Gev) the number of nucleons and anti-nucleons produced is greater than the number of pions.

(iii) The mean transverse momentum is about 3 Gev/c and it increases as $E_p^{1/4}$.

(iv) The inelasticity is of the order of unity.

(v) As a result of the thermodynamic equilibrium the energy spectrum of the produced particles in the C-system will be given by Planck's distribution law.

Landau (1953) proposed a modification of Fermi's theory in which the interactions of the particles continue during the expansion of the gas until their mean free path is of the order of the dimensions of the interaction volume. The final break up occurs at a lower temperature than previously and hence the pions, on account of their small rest mass, form a higher proportion of the produced particles. Different parts of the interacting gas break up at different times and the final form of the C-system energy distribution is $^{dE}/E$ plus a slow logarithmic term. In Landau's original theory the mean transverse momentum was high ($\approx$ 4 Gev/c) but in an improved version, Rozenthal (1957), the mean was

0.4 Gev/c, compatible with that observed. However the overall agreement was still not good, Losty (1959). The angular distributions of most jets were in better agreement with the original than with the revised theory.

Other statistical models were proposed by Heisenberg (1952), Takagi (1952), Kraushaar and Marks (1954) and others. However none of these theories could provide a satisfactory description of high energy interactions.

§5.3 Phenomenological Models.

The 'Two Centre' model of meson production was proposed by Cocconi (1958) and Ciok et al (1958). They assumed that, after impact, there are four 'units' in the C-system. Firstly the two nucleons which can carry a large fraction of the primary energy and secondly two slowly moving fireballs or meson clouds which decay by the isotropic emission of mesons, mainly pions. The mean momentum of the pions is assumed to be $\approx$ 1 Gev/c in order to explain the low observed values of transverse momenta. A small fraction of observed jets, typically those with small n_s and N_h, do exhibit a double structure in their angular distributions as is predicted by this model, see for example Gierula et al (1961). However it offers no explanation of the many events which do not exhibit such a structure and is of rather limited use.

The Isobar Model of Peters (1964) differs from the above in that the two energetic units are assumed to be nucleon isobars which decay by the emission of one or two pions. The production mechanism of the low energy pions is not considered

in detail but their energies are assumed to be much less than those from isobar decay. This model has already been commented upon in an earlier Chapter.

The model proposed by Cocconi, Koester and Perkins (1961) has been discussed frequently in this thesis. It has no theoretical basis but attempts to describe the observed data in terms of simple distribution functions. Its success in doing this is encouraging but a model which explains why these distributions occur is clearly urgently needed.

§ 5.4 The Peripheral Model.

In the peripheral model two particles, A and B, interact by exchanging a single virtual quantum of a field E to give final states C and D. For elastic scattering C and D are equivalent to A and B but in inelastic processes the final states are groups of particles, see Fig 5.1(a). The cross section is assumed to be dominated by the process in which E is a quantum of the lightest field which can connect the vertices Ω and Ω'. In the case of NN and πN interactions this quantum is the pion. The model was developed by several authors, in particular Drell (1960), Salzman and Salzman (1960a,1961) and Selleri (1961).

Using the notation of Fig 5.1(a) then P_i $(i = 1,4)$ are the four-momenta of the incident particles and final states, m_i $(i = 1,4)$ are the masses of the incident particles and the total internal energy of the final states and (Δ,μ) is the four-momentum and mass of the exchanged quantum. A,B,C, and D are physical states and so

Fig 5.1.

These figures are Feynman diagrams representing the various field-theoretical models discussed in the text.

(a) The peripheral model of multi-particle production via the exchange of a single virtual boson.

(b) Single pion production on a similar model.

(c) One of the diagrams representing multi-particle production in the multi-peripheral model.

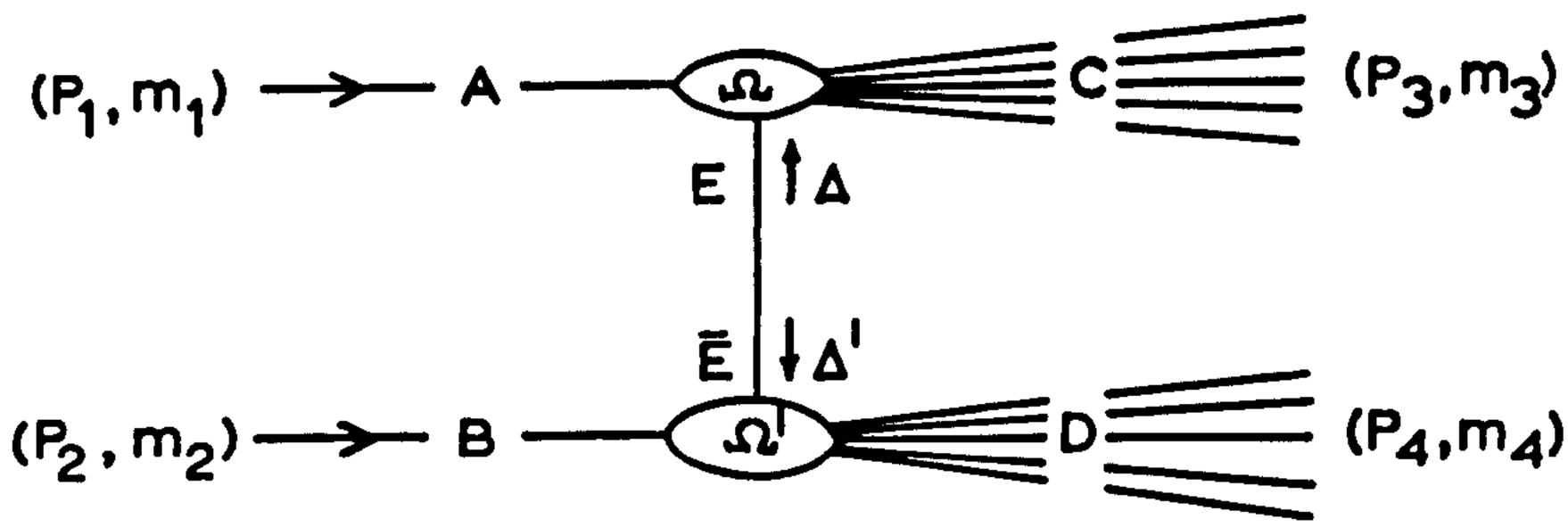
(P_1, m_1)
A
Ω
C
(P_3, m_3)
E
Δ
Ē
Δ'
(P_2, m_2)
B
Ω'
D
(P_4, m_4)

(a)

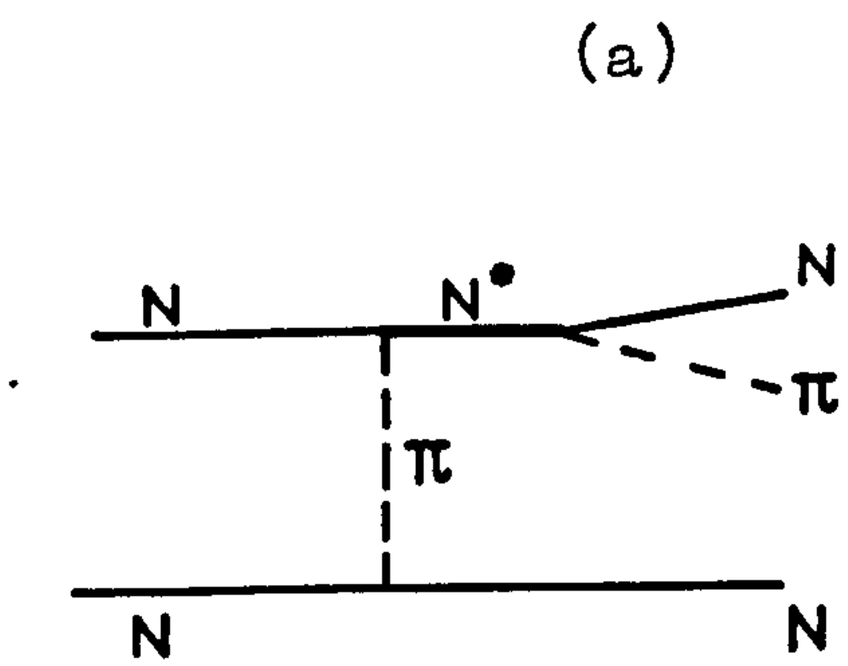
N
N*
N
π
π
N
N

(b)

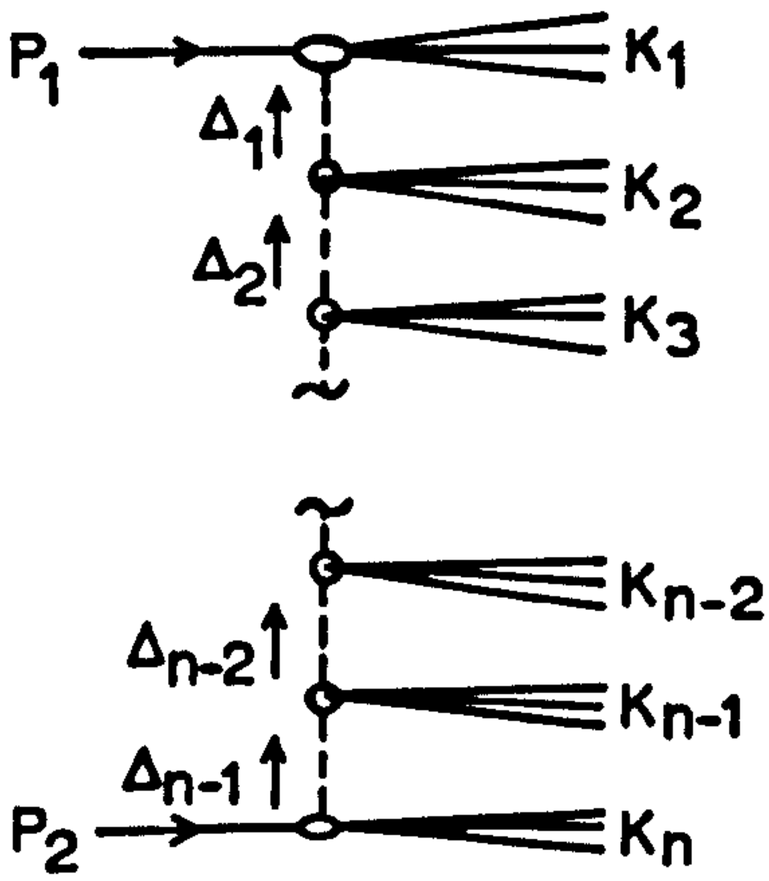
P_1
K_1
Δ_1
K_2
Δ_2
K_3
K_{n-2}
Δ_{n-2}
K_{n-1}
Δ_{n-1}
P_2
K_n

(c)

Fig 5.1.

$$P_i^2 + m_i^2 = 0; \quad i = 1,4.$$

but E is virtual and

$$\Delta^2 \neq -\mu^2$$

Δ^2 is positive for elastic scattering and is almost always positive for inelastic processes. The exchange of E between Ω and Ω' is equivalent to the exchange of its anti-particle $\bar{E}$ with opposite four-momentum between Ω' and Ω.

The cross section for the interaction A + B → C + D is computed as the product of three terms, one describing the transfer of E and the others its interaction at the two vertices. The first term is called the propagator and, in one-pion exchange, it has the form $(\Delta^2 + \mu^2)^{-2}$ and so large values of Δ^2 are severely damped. The latter terms involve the strength of the field coupling and the size of the four-momenta. The computations at the vertices are usually made with the assumption that the exchanged particle is real and are therefore strictly valid only for small Δ^2.

The model works well at low energies. Pion production in NN and πN interactions at 1-3 Gev is consistent with the exchange of a single pion followed by the excitation of one or both of the vertices into a nucleon or a pion isobar as shown in Fig 5.1(b). Measurements made at these energies have been described by many authors, for example Salzman and Salzman (1960b), Fickinger et al (1962), Pickup et al (1962), Drell (1961).

However the model is not adequate in order to explain the main features of high energy interactions, see Berestetski and Pomeranchuk (1960), Gribov (1960), and, for example, constant total cross sections are inconsistent with this model. Koba (1961) has pointed out that to explain many cosmic ray jets on this model very large four-momentum transfers would be needed, $\Delta^2 \approx 100\ m_\pi{}^2$.

§ 5.5 The Multi-peripheral Model.

Amati and Fubini (1961) and Goebel (1961) considered the validity of the one boson exchange model via the theory of dispersion relations and the Mandelstam representation. They showed, simultaneously, that the simple peripheral model is justified only if the energy at each of the vertices, m_3 and m_4, is low (a few Gev or less). At higher energies the boson exchange picture is still valid but each vertex or 'bubble' must be split into two others until the energy in all the bubbles is low. A high energy process is therefore considered as a succession of low energy interactions as indicated by Fig 5.1(c). This is the basis of the multi-peripheral model; it was first worked out in detail by Amati, Fubini and Stanghellini (1961a,1961b) and expanded by several other authors, for example Frautschi (1963).

It is assumed that

(i) processes at high energies are dominated by one-pion exchange and may be described by a series of low energy resonance interactions.

(ii) the amplitudes of these low energy interactions

can be calculated on the assumption that the interacting particles are real. The particles are assumed to interact by forming a resonant final state which then decays into a small number of particles by a characteristic low energy interaction.

The following notation is used below, see Fig 5.1(c).

P_1, P_2 are the four-momenta of the interacting particles.

$\Delta_i (i=1, n-1)$ are the four-momenta of the exchanged quanta.

$k_j (j=1, n)$ are the four-momenta of the final states.

μ is the mass of the pion.

$s = (P_1 + P_2)^2$ is the available energy in the C-system of the interacting particles and is proportional to the primary energy.

The laws of conservation of energy and three-momentum must hold at each vertex.

$$k_1 = P_1 + \Delta_1$$

$$k_i = \Delta_i - \Delta_{i-1} \quad (i=2, n-1)$$

$$k_n = P_2 - \Delta_{n-1}$$

The amplitude corresponding to the diagram with n vertices, Fig 5.1(c), is written as

$$A_n(P_1, P_2) = \frac{T(P_1 \Delta_1 ; k_1)\ T(\Delta_1 \Delta_2 ; k_2) \ldots\ldots T(\Delta_{n-1} P_2 ; k_n)}{(\Delta_1^2 + \mu^2)(\Delta_2^2 + \mu^2) \ldots\ldots\ldots\ldots\ldots (\Delta_{n-1}^2 + \mu^2)} \qquad (5.1)$$

The terms of the denominator are propagators describing the exchange of the virtual pions and the terms in the numerator

are the amplitudes describing the interactions at each vertex. As was stated above the amplitudes T were calculated on the assumption that the interacting particles are real, $\Delta_i^2 + \mu^2 = 0$ The total cross section at a given primary energy, s, is obtained by summing the expressions (5.1) for all values of n. The amplitude for any one graph, $A_n(s)$, is found to increase fairly rapidly above some threshold value of s, to reach a maximum, and then to decrease asymptotically as $\frac{1}{s}(\log s)^{n-2}$. At any energy s the contribution from one diagram, i.e. one value of n, will predominate over the others, although contributions from the neighbouring diagrams, with (n-1) vertices or (n-2) etc., may also be present. The mean value of n is calculated as increasing as log s.

Amati et al (1962b) arrive at the following conclusions.

(i) The mean elasticity is independent of energy s and of n. The elasticity is defined here as the fraction of the available energy radiated from the extreme vertices at the ends of the chain. (Frautschi derives the same result but adds that the spread in the elasticity values will be large).

(ii) Since the break up of the final states is a low energy process and is independent of the energy s at which they were formed then the fraction of pions among the produced particles will be high and independent of s.

(iii) Since high momentum transfers Δ are not favoured then the transverse momenta of the secondaries are determined mainly by the break up of these final states. Hence the

observed transverse momenta should be low and independent of s.

(iv) The predicted multiplicity of final states, and hence of secondary particles, increases as log s.

(v) The laboratory energy of the final states, excluding the two from the extreme vertices, has the distribution $^{dE}/_{E}$ providing E is not too large or too small.

Salzman (1963) has suggested that diagrams in which the final states from the extreme vertices are unexcited nucleons should be more important than diagrams in which these states are nucleon isobars, especially for low values of Δ.

It can be seen that many of the predictions of the multi-peripheral model are in good accord with the experimental evidence. While this is encouraging it should be remembered that it was derived with the experimental evidence in view. Also its predictions concerning the spectra of the produced particles are not exact enough to be checked in detail. The observed increase in multiplicity, see Perkins (1961), is $s^{1/4}$. Also it is not clear to the writer that the model can accomodate the observed large fluctuations in multiplicity at a given primary energy.

Appendix A.

Computation of Collecting Powers.

Take axes x and y in the plane of the emulsion-metal layers and z perpendicular to this plane; let a,b,c be the dimensions of the detector in these directions, the detector being bounded by the planes x=0, x=a, y=0, y=b, z=0 and z= -c. Fig A.1 is a projection on the top face of the detector (z=0) drawn for unique values of the space angles P and δ.

Fig A.1
(Not to scale).

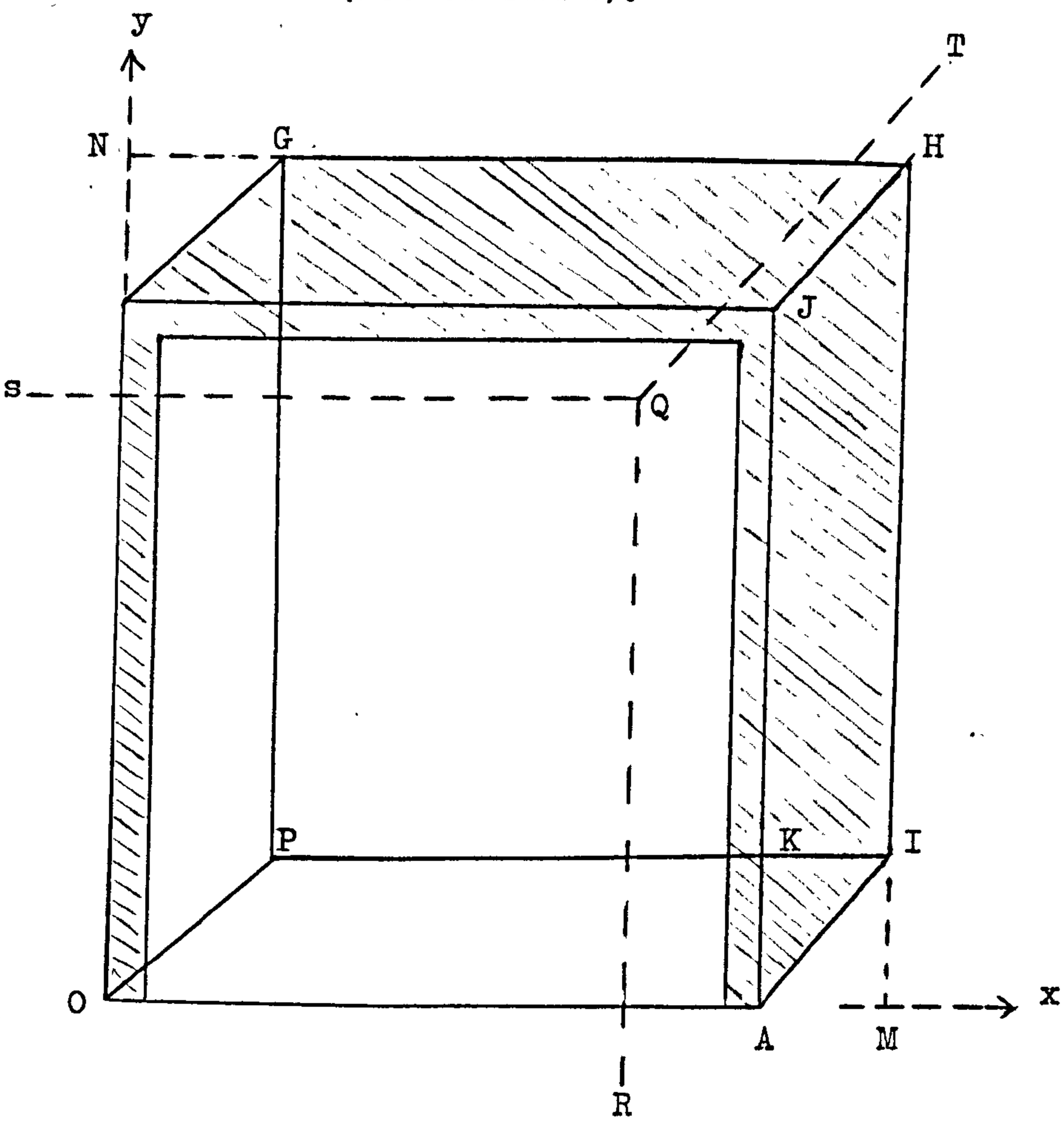

P = Angle between y-axis and the projected direction in the emulsion plane.

δ = Dip angle relative to this plane.

The direction cosines may be written in terms of these angles as:

$$\cos X = \sin P \cos \delta$$

$$\cos Y = \cos P \cos \delta$$

$$\cos Z = \sin \delta$$

Fig A.1 is particularly useful in determining the path taken through the detector of a particle incident from a direction defined by P and δ. E.g. Particles passing through the rectangle LJKP enter the detector through its z=0 plane and leave via z= -c; particles passing through KIA enter via x=a and leave via y=0 etc. The coordinates of the point P with respect to O are $x = c.\frac{\cos X}{\cos Z}$, $y = c.\frac{\cos Y}{\cos Z}$. The shaded area represents that part of the stack which is shielded by the metal frame supporting the emulsions.

The effect of the graphite layer is indicated by the three dashed lines passing through Q; particles traversing the z=0 plane within the lines SQ and QR have traversed the graphite plane which is perpendicular to the z-axis etc. The coordinates of the point Q with respect to O are $x=a+d-t\frac{\cos X}{\cos Z}$, $y=b+d-t\frac{\cos Y}{\cos Z}$ where d is the separation between the edge of the detector and the centre of the graphite layer in the x- and y-directions and t is the separation in the z-direction.

The computation of the collecting power now proceeds

as follows:

(i) Fix values of P and δ

(ii) Divide the area ONHM into a large number of small rectangles

(iii) Compute the position of each small rectangle with respect to the points, P,Q etc. and hence compute the lengths of detector and of graphite traversed by a particle passing through this small rectangle with space angles P and δ

(iv) Hence compute the collecting power of each small rectangle for each type of event using equations (2.15) - (2.18) with a value of the atmospheric depth

$$z = z_o \sec \delta \sec P$$

where z_o is the verticle depth of the assembly in the atmosphere. The collecting power is set equal to zero for those rectangles within BNG and AIM. The collecting powers for γ-rays from the air and nuclear events in the graphite is also zero for rectangles within the shaded area of Fig A.1 (that part of the detector shielded by metal frame). The collecting power for nuclear events in this shielded area was slightly amended from equation (2.15) since events were only accepted from this region if they traversed at least 4 r.l. of detector before interacting.

(v) Sum over all small rectangles to obtain the total collecting power of the detector for a beam of particles in the direction P, δ. This sum must be multiplied by the area presented to the beam by each small rectangle, i.e. $\sin \delta \, \Delta x \, \Delta y$, where Δx and Δy are the lengths of the sides.

(vi) The total solid angle, within the accepted limits of δ, was divided into many equal elements and the above computation was made for a value of P and δ in the centre of each element. The total collecting power is given by the sum of all these computations, multiplied by the element of solid angle, $\Delta P \Delta(\sin \delta)$.

The above computation was performed numerically using an IBM 1620 computor. The results have been presented in Table 2.4.

Appendix B.

The Production of γ-rays via Hyperons.

(i) Kinematics of Hyperon Decay

Assuming that the energy spectrum of the hyperons is a power law, exponent p, then the spectrum of decay π^{o}-mesons is a power law with the same exponent. The intensity of mesons at a given energy is related to the intensity of hyperons at the same energy by their spectrum factor

$$S_{Y\pi} = \frac{B}{p+1} \quad \frac{R_2^{\,p+1} - R_1^{\,p+1}}{R_2 - R_1} \qquad (B.1)$$

B is the branching ratio into the decay mode considered and R_1, R_2 are the minimum and maximum fractions of the hyperon energy which the π-meson may obtain. These fractions are easily computed from the masses of the particles involved.

(ii) Probability of Decay in Atmosphere

The probability that a hyperon produced at a depth x should decay between (y, y + dy) is

$$P.dy = \left(\frac{x}{y}\right)^{m} e^{\frac{y-x}{\lambda_i}} \quad \frac{m\,dy}{y} \qquad (B.2)$$

where λ_i is their interaction length and m is the ratio of the scale height of the atmosphere, $^{RT}/_{Mg} \approx 6.4 \times 10^{5}$cm., to the hyperon decay length, γcτ.

The fraction of hyperons decaying before a depth z, averaged over an exponential source distribution, is

$$f = \frac{\int_0^z dx \int_x^z dy \; P_\circ e^{-x/\Lambda}}{\int_0^z dx_\circ e^{-x/\Lambda}}$$

For $z < \Lambda, \lambda_i$ this expression may be expanded as

$$f \approx \frac{m}{m+1}\left(1 - \frac{1}{2}\frac{z}{(m+2)} \circ \frac{\Lambda-\lambda_i}{\Lambda\lambda_i}\right) \qquad (B.3)$$

m is a function of the hyperon energy, $m = {}^{k}/E'$. The values of the constant k for the 4 hyperons of unit strangeness are given below

	k(Gev)
Λ	$0.9 \; .10^5$
Σ^+	$3.1 \; .10^5$
Σ^-	$1.6 \; .10^5$
Σ°	$\approx \; 10^{12}$

Finally the expression for f must be averaged over the hyperon production spectrum and the kinematics of the hyperon-pion decay.

$$\bar{f} = \frac{\int_{E/R_2}^{E/R_1} f \; \frac{p dE'}{E'^{p+1}} \; \frac{dE}{(R_2 - R_1)E'}}{\int_{E/R_2}^{E/R_1} \frac{p dE'}{E'^{p+1}} \; \frac{dE}{(R_2 - R_1)E'}}$$

E is the π^0 energy considered. For $E' < k$ we obtain

$$f \approx 1 - \frac{p+1}{p} \frac{E}{k} \frac{R_2^{\,p} - R_1^{\,p}}{R_2^{\,p+1} - R_1^{\,p+1}} \left(1 + \frac{1}{2} z \frac{\Lambda - \lambda}{\Lambda \lambda_i} i\right) = 1 - \frac{E}{E_o} \qquad (B.4)$$

Since $z < \Lambda, \lambda_i$ this expression is insensitive to the values used for these quantities; we take $z=50$, $\Lambda=125$, $\lambda_i=80$ gm./cm.^{2}. Taking $p=1.7$ and the relavent values for R_2 and R_1 we obtain E_o for each hyperon.

Hyperon	E_o (Gev)
Λ	$1.3 \cdot 10^4$
Σ^+	$6.2 \cdot 10^4$
Σ^-	$3.2 \cdot 10^4$
Σ^o	$\approx 5 \cdot 10^{10}$

We are considering the production of γ-rays with energies $E_\gamma \geq$ 1200 Gev. From the above expression for $\bar{f}$ it can be seen that, if hyperons capable of decaying into such γ-rays

are produced in the atmosphere, then they have a high probability of decaying before reaching the detector.

(iii) Contribution of Hyperons to the Flux of γ-rays.

Assume that a hyperon is produced in a fraction q of the interactions and that it carries a fraction C of the primary energy. Then the flux of hyperons at a particular energy is related to the flux of primary particles at the same energy by

$$\frac{N_Y}{N_p} = qC^p \qquad (B.5)$$

As before, p is the index of the integral primary energy spectrum.

Also assume that the hyperon has an equal probability of being in one of the four states of unit strangeness, i.e. $\Lambda, \Sigma^+, \Sigma^-$ or Σ°. The Σ^- hyperon cannot decay into a π° meson and is considered no further. The flux of γ-rays from the remaining three states is

$$\frac{N_\gamma}{N_Y} = \frac{1}{4} S_{\pi\gamma} \left(f_\Lambda S_{\Lambda\pi} + f_{\Sigma^+} S_{\Sigma^+\pi} + f_\Lambda S_{\Lambda\pi} S_{\Sigma^\circ\Lambda}\right) + \frac{1}{4} S_{\Sigma^\circ\gamma} \qquad (B.6)$$

The quantities S_{ij} refer to the spectrum factors as defined in equation (B.1). The f_i refer to the decay probabilities defined by equation (B.4); f is unity for the Σ° hyperon. The third term in the bracket refers to the indirect decay

chain $\Sigma^\circ \rightarrow \Lambda \rightarrow \pi^\circ$; the last term refers to the fast electromagnetic decay $\Sigma^\circ \rightarrow \gamma$. Evaluating (B.6), for a π°-meson energy E = 2000 Gev, and combining it with (B.5) we obtain

$$\frac{N_\gamma}{N_p} = q\ C^p(0.0105 + 0.0025) \qquad (B.7)$$

The first term in this expression refers to the delayed, weak decays of the hyperons, the second to the direct, fast decay of the Σ°.

(iv) Contribution from Direct Pionization.

The mean fraction of the primary energy given to the directly created particles is (1-C). Assume that $^3/_4$ of this is radiated as pions. Hence the mean fraction given to π°-mesons is $\frac{1}{4}(1-C)$. This is assumed to be shared between b particles according to an exponential spectrum. The number of γ-rays at a given energy E is therefore

$$N_\gamma(E) = S_{\pi\gamma} \int_{E'=0}^{\infty} N_p(E')dE'\ b\ e^{-E/T}\ \frac{dE}{T} \qquad (B.8)$$

where $bT = \frac{1}{4}(1-C)E'$.

Integrating over all primary energies, E', gives

$$\frac{N_\gamma(E)}{N_p(E)} = S_{\pi\gamma} \quad \frac{(1-C)^p \Gamma(p)}{4^p \; b^{p-1}}$$

Taking p=1.7 and b=4.0 (see § 4.6) we obtain

$$\frac{N_\gamma}{N_p} = 0.041 \; (1-C)^p \qquad \text{(B.9)}$$

Concluding Remarks.

This thesis has described studies made on the production of π-mesons in individual high energy interactions and, in particular, on the manner in which the radiated energy is shared amongst the mesons. The experimental data was shown to be remarkably consistent with a simple phenomenological model developed to describe meson production at accelerator energies. The spectrum of γ-ray transverse momenta was found, at all energies considered, to be well fitted by an exponential distribution, with a mean value increasing only very slowly with increasing primary energy. Between accelerator energies and the lowest energy cosmic ray events considered the mean multiplicity of pions was found to increase as the fourth root of primary energy, $E_p^{1/4}$. This rate of increase is similar to that observed by other authors. However at higher energies there is an indication that the rate of increase is more rapid and this indication is supported by the single high energy event observed. This change in the rate of increase of multiplicity occurs at a primary energy of about 2.10^4 Gev and is, if substantiated, of great interest. It corresponds to a limiting of the mean π-meson energy in the Centre of Mass system to about 3 Gev.

The results obtained in this thesis can be related both to the theoretical description of high energy interactions

and to studies of the propagation of cosmic rays in the atmosphere.

Several of the more successful theories of high energy interactions were reviewed in Chapter 5. If an adequate theory is to be developed, then it must be able to account for the simple energy and momentum spectra observed in this analysis. The cosmic rays provide at present the only source of nuclear particles above 30 Gev and several other groups are at present studying their individual interactions. The group in Moscow under the direction of Professor N.A.Dobrotin is engaged in a detailed study of the interactions of particles with several hundred Gev energy. The interactions occur in a LiH target and the primary and secondary particles, if charged, are observed in two expansion cloud chambers. The strength of the method, however, is derived from the measurement of the energy of the primary particle which is made in a total ionization calorimeter, many interaction lengths thick, placed beneath the lower cloud chamber. This enables the C-system velocity to be unambiguously determined and removes many of the uncertainties present in other work in this field. Their results were shown by Bowler (1962) to be consistent with the CKP model and the Moscow group has given a detailed analysis of the results. The apparatus is bulky so that measurements have had to be made at ground level or, with a smaller version, in an aircraft. Consequently the flux of nucleons is small and, even at these modest

energies, a period of years is needed to collect a large sample of events.

An analysis of γ-ray production at energies similar to those studied in this thesis is being undertaken by a combined Japanese and South American group. They employ composite detectors of emulsion and lead, the emulsion plane being horizontal. A large array is at present being exposed on Mt. Chacaltaya in the Andes and previous smaller arrays have been exposed at balloon and mountain altitudes. Their analysis of individual nuclear interactions is based on the observation of several γ-rays from a single nuclear interaction in the overlying air. The angle of acceptance of the apparatus is therefore small. As was demonstrated in the Texas Lone Star, Fig 3.11, the radiated energy may be spread over large angles and the limiting of the analysis to γ-rays within a small solid angle may yield an incorrect result. In the opinion of the author, while such an analysis of air families is of use, too much reliance should not be placed upon the results.

The propagation of cosmic rays through the atmosphere is studied at the highest energies via Extensive Air Showers and, at more moderate energies, by observing the fluxes of γ-rays and nuclear particles at various depths in the atmosphere. Such latter studies have been performed by many groups, in particular those in Japan, Moscow and Bristol, and a comparison of these fluxes yields indirect information

on the properties of nuclear interactions. Firstly a comparison between the spectrum of nuclear particles and the spectrum of primary particles, as deduced from EAS, gives the mean fraction of the primary energy radiated as γ-rays. The absolute value is not well determined due to uncertainties in normalization but the similar indices of the two spectra mean that the elasticity does not change significantly with primary energy.

Secondly the ratio of the fluxes of γ-rays and nuclear particles is dependent on the manner in which the radiated energy is subdivided. The Bristol group, Duthie et al (1961) report that the γ-ray spectrum is steeper than the nuclear spectrum and that this difference becomes more pronounced at γ-ray energies greater than 2.10^3 Gev. They interpret these results as being due to a meson multiplicity increasing as $E_p^{1/4}$ below this energy and increasing more rapidly above it. Such a behaviour is indicated in the present analysis. However the evidence from the other groups is conflicting. The Japanese report such a steepening only in some of their exposures, while two of the Russian experiments, at aircraft altitudes, report a flattening at about this energy. Several weaknesses in the methods of these groups should be mentioned here. In the Japanese work γ-rays and nuclear interactions in the detector cannot always be distinguished and so the γ-ray spectrum will contain a contamination of nuclear events. Also the highest energy points on their γ-ray spectrum are obtained from families of parallel cascades

which are interpreted as the "electromagnetic debris" of individual γ-rays of high energy which have bred in the atmosphere. The energy of this parent γ-ray is obtained by comparing the distributions of energy and position of the observed cascades with the predictions of cascade theory. This method involves the estimation of both the position of conversion and the energy of the parent γ-ray. Two objections to this method arise, (i) cascade fluctuations seriously influence the development near the origin and (ii) in our experience there is no way of ascertaining that the parent was in fact a single γ-ray. The Russian experiment was made with a counter array, not a visual technique, and the flattening in their energy spectrum may well be due to the simultaneous observation of several γ-rays from a single high energy interaction. In view of these uncertainties and the importance of the result, better measurements of the spectra are clearly needed together with further and better studies of individual interactions.

In an assembly being examined in Bristol at present, the graphite in the producing layer was interleaved with photographic emulsion sothat the primary and charged secondary particles could be observed as well as the γ-rays. If successful this will be a powerful extension to the present method. Other requirements are an extension of the analysis to higher primary energies, which can only be achieved by increasing the size of the detector or the exposure time,

and to lower energies, which would require a producing layer closer to the detector. Finally great thought should be given to finding a method of estimating the primary energy. Such an estimate would be of immeasureable value.

References.

Ali H.H., J.G.Duthie, A.Kaddoura, P.H.Fowler and D.H.Perkins; Proc.Rochester Conf., 829 (1960)

Amati D. and S.Fubini; Proc.CERN Conf.on High Energy Physics, 343 (1961)

Amati D., S.Fubini and A.Stanghellini; Phys.Letters, 1, 29 (1962a)

Amati D., S.Fubini and A.Stanghellini; Nuovo Cim., 26, 898 (1962b)

Baker W.F., R.L.Cool, E.W.Jenkins, T.F.Kycia, S.J.Lindenbaum, W.A.Lore, D.Lüers, J.A.Niederer, S.Ozaki, A.L.Read, J.J.Russell and L.C.L.Yuan; Phys.Rev.Letters, 7, 3 (1961)

Barkow A.G., B.Chamany, D.M.Haskin, P.L.Jain, E.Lohrmann, M.W.Teucher and M.Schein; Phys.Rev., 122, 617 (1961)

Berestetski V.B. and I.Ya.Pomeranchuk; Proc.Rochester Conf., 333 (1960)

Bethe H.A. and W.Heitler; Proc.Roy.Soc., A146, 83 (1934)

Bethe H.A. and L.C.Maximon; Phys.Rev., 93, 768 (1954)

Bhaba H.J.; Proc.Roy.Soc.; A154, 195 (1936)

Bowler M.G.; Ph. D. Thesis, Bristol (1962)

Bowler M.G., P.H.Fowler and D.H.Perkins; Nuovo Cim., 26, 1182 (1962)

Bowler M.G., P.H.Fowler and S.N.Tovey; To be published (1964)

Castagnoli C., G.Cortini, C.Franzinetti, A.Manfredini and D.Moreno; Nuovo Cim., 10, 1539 (1953)

Ciok P., T.Coghen, J.Gierula, R.Holynsky, A.Jurak, T.Samiewski, A.Miesowicz, O.Stanisz and J.Pernegr; Nuovo Cim., 8, 166 (1958)

Cocconi G.; Phys.Rev., 111, 1699 (1958)

Cocconi G.,L.J.Koester and D.H.Perkins; L.R.L.Internal Report U.C.I.D. 1444 (1961)

Dobrotin N.A. and S.A.Slavitinsky; Preprint (1962)

Dodd P.,M.Jobes, J.Kinson, B.Tallini, B.R.French, H.J.Sherman, I.O.Skillicorn, W.T.Davies, M.Derrick and D.Radojicic; Proc.Aix-en-Provence Conf., I, 433 (1961)

Drell S.; Phys.Rev.Letters, 5, 342 (1960)

Drell S.; Rev.Mod.Phys., 33, 458 (1961)

Duthie J.G.; Ph.D. Thesis, Bristol (1961)

Duthie J.G.,C.M.Fisher, P.H.Fowler, A.Kaddoura, D.H.Perkins, K.Pinkau and W.Wolter; Phil.Mag., 6, 89 (1961)

Duthie J.G.,P.H.Fowler, A.Kaddoura, D.H.Perkins, and K.Pinkau; Nuovo Cim., 24, 122 (1962)

Edwards B.,J.Losty, D.H.Perkins, K.Pinkau and J.Reynolds; Phil.Mag., 3, 237 (1958)

Fermi E.; Prog.Theor.Phys., 5, 570 (1950)

Fermi E.; Phys.Rev., 81, 683 (1951)

Fickinger W.J.,E.Pickup, D.K.Robinson and E.O.Salant; Phys.Rev., 125, 2082 (1962)

Fiddecaro M.,G.Finochiaro, G.Gatti, G.Giacomelli,W.C.Middelkoop and T.Yamagata; Proc.Aix-en-Provence Conf., I, 73 (1961)

Fowler P.H. and D.H.Perkins; Phil.Mag., 46, 587 (1955).

Fowler P.H. and D.H.Perkins; Proc.Roy.Soc. To be published (1964)

Gierula J.,D.M.Haskin and E.Lohrmann; Phys.Rev., 122, 626 (1961)

Goebel C.; Proc.CERN Conf. on High Energy Phys., 353 (1961)

Gribov V.N.; Proc. Rochester Conf., 340 (1960)

Grigorov N.L.,V.V.Guseva, N.A.Dobrotin, K.A.Kotelnikov, V.S.Murzin, S.V.Ryabikov and S.A.Slavatinsky; Proc. Moscow Cosmic Ray Conf., I, 143 (1960)

Guseva V.V.,N.A.Dobrotin, N.G.Zelevinskaya,K.A.Kotelnikov, A.M.Lebedev and S.A.Slavatinsky; Proc.Kyoto Conf. 1961. J.Phys.Soc.Japan, 17 Supp. A-III, 375 (1962)

Handel Davies,H.A.Bethe and L.C.Maximon; Phys.Rev., 93, 788 (1954)

Heisenberg W.; Zeit.fur Physik, 133, 65 (1952)

Kaddoura A.; Ph.D. Thesis, Bristol (1961)

Koba Z.; Proc.CERN Conf.on High Energy Phys., 296 (1961)

Klein O. and Y.Nishina; Zeit.fur Physik, 52, 853 (1929)

Kraushaar W. and L.Marks; Phys.Rev., 93, 326 (1954)

Landau L.; Dolk.Akad.Nauk.S.S.S.R., 12, 51 (1953)

Losty J.; Ph.D. Thesis, Bristol (1959)

Malamud E.; Phys.Rev., 115, 687 (1959)

Molière G.; Zeit.Naturforsh, 39, 1801 (1948)

Møller C.; Ann.der Physik, 14, 531 (1932)

Nishimura J.and K.Kamata; Prog.Theor.Phys., 7, 185 (1952)

Nishimura J.and K.Kamata; Prog.Theor.Phys., Supp.6, 93 (1958)

Nishimura J.and J.Kidd; Tables prepared for the I.C.E.F. Project. Privately circulated (1960)

Perkins D.H.; Proc.CERN Conf.on High Energy Phys., 99 (1961)

Peters B.; Proc.Kyoto Conf. 1961. J.Phys.Soc.Japan 17, Supp. A-III, 524 (1962)

Peters B.; Nuovo Cim., 23, 88 (1962)

Peters B.; Proc.Jaipur Conf. 1963. To be pulished (1964)

Pickup E.,D.K.Robinson and E.O.Salant; Phys.Rev., 125, 2091 (1962)

Pinkau K.; Ph.D. Thesis, Bristol (1958)

Pinkau K.; Preprint (1964). Submitted to Nuovo Cim.

Powell C.F.,P.H.Fowler and D.H.Perkins; "A Study of Elementary Particles by the Photographic Method." Pergamon Press (1960)

Rossi B.and K.Greisen; Rev.Mod.Phys., 13, 240 (1941)

Rossi B.; "High Energy Particles." Prentice-Hall (1952)

Rozenthal I.L.; J.E.T.P., 4, 217 (1957)

Salzman F.and G.Salzman; Phys.Rev.Letters, 5, 377 (1960a)

Salzman F.and G.Salzman; Phys.Rev., 120, 599 (1960b)

Salzman F.and G.Salzman; Proc.CERN Conf.on High Energy Phys., 283 (1961)

Salzman F.; Preprint (1963). Submitted to Phys.Rev.

Selleri F.; Phys.Rev.Letters, 6, 64 (1961)

Takagi S.; Prog.Theor.Phys., 7, 123 (1952)

von Lindern L.; Private communication (1962)

Wheeler J.A.and W.E.Lamb; Phys.Rev., 55, 858 (1939)

Williams E.J.; Proc.Roy.Soc., A169, 531 (1939)

Williams R.W.; Phys.Rev., 98, 1387 (1955)

Wolfendale A.W.; Report at Bristol Conf. 1963; published in Brit.J.Applied Physics, 14, 239 (1963)

Acknowledgements.

It is my great pleasure to thank Professor C.F.Powell, F.R.S., for the facilities of his laboratory and to thank all members of his staff, in particular Dr.P.H.Fowler and Dr.D.H.Perkins, for their continued advice, encouragement and interest during my entire stay at Bristol.

My thanks are also due to Mrs.B.Klein, who typed this thesis so conscientiously, to Mr.W.Harbour who prepared the figures with great care, to Mrs.N.Kaddoura, Mrs.B.Ellicott, Miss G.Mansfield and Mrs.B.Klein who performed the tedious work of scanning, to Mrs.M.Ward who drew some of the diagrams and to Mrs.P.Penney who read part of the manuscript.

I am indebted to the Department of Scientific and Industrial Research for a Research Studentship and to the University of Bristol for a Research Assistantship.

Memorandum.

I declare that I have submitted no part of the work described in this thesis for any higher degree at this or any other University.

During the past three years I have been engaged in the study of the high energy interactions of cosmic ray particles. The initial stages of the analysis of graphite interactions occuring in the Indian stack were performed by myself, the energy measurements were made in collaboration with Dr.P.H.Fowler and Dr.M.G.Bowler and the analysis of the results with Dr.P.H.Fowler. I also helped with the analysis of origins in the detector and was responsible for the computation of the collecting powers and rates of production of events. The measurements on all the jets in emulsion were made by myself; the subsequent analysis was made with the help of Dr.D.H.Perkins and Dr.P.H.Fowler.

In addition to the work described in this thesis I also took part in the analysis, with Miss V.M.Mayes and a group from the University of Kiel, of a stack designed to detect any flux of high energy primary γ-rays. The result was negative and forms part of Miss Mayes' thesis.

While on leave of absence I spent 3 months at the Brookhaven National Laboratory, New York, working mainly on the analysis of the annihilations of 2.7 Gev/c anti-protons in a hydrogen bubble chamber; this work is not reported here.

I have taken part in several balloon flying expeditions to Cardington and one prolonged expedition to Southern Italy.

Stuart Tovey

March 1964.